12-2022

Gate-Controlled Quantum Dots in Two-Dimensional Tungsten Diselenide and One-Dimensional Tellurium Nanowires

Shiva Davari Dolatabadi
University of Arkansas, Fayetteville

Gate-Controlled Quantum Dots in Two-Dimensional Tungsten Diselenide and One-Dimensional Tellurium Nanowires

A dissertation submitted in partial fulfillment
of the requirements for the degree of
Doctor of Philosophy in Physics

by

Shiva Davari Dolatabadi
University of Isfahan, Iran
Bachelor of Science in Physics, 2005
Shahid Beheshti University, Iran
Master of Science in Photonics, 2009

December 2022
University of Arkansas

This dissertation is approved for recommendation to the Graduate Council.

Hugh O. H. Churchill, Ph.D.
Dissertation Director

Jin Hu, Ph.D.
Committee Member

Salvador Barraza-Lopez, Ph.D.
Committee Member

Abstract

This work focuses on the investigation of gate-defined quantum dots in two-dimensional transition metal dichalcogenide tungsten diselenide (WSe_2) as a means to unravel mesoscopic physical phenomena such as valley-contrasting physics in WSe_2 flakes and its potential application as qubit, as well as realizing gate-controlled quantum dots based on elemental tellurium nanostructures which may unlock the topological nature of the host material carriers such as Weyl states in tellurium nanowires.The fabrication and characterization of gate-defined hole quantum dots in monolayer and bilayer WSe_2 are reported. The gate electrodes in the device design are located above and below the WSe_2 nanoflakes to accumulate a hole gas. For some devices we additionally used gates to deplete the gas to define the dot. Temperature dependence of Coulomb-blockade peak height complies with single-level transport and the small size of the dot leads to observation of excited states in the Coulomb diamond measurements. Further, magnetic field dependence of the excited states in the bilayer devices provides a lower bound for g factors. For the chiral crystals of elemental Te, the intriguing property of combining Weyl physics with a small semiconducting bandgap enables the creation of gate-tunable devices to probe and utilize the topological properties of Te. The formation of gate-defined quantum dots in Te would allow Coulomb blockade spectroscopy to provide information about the strength of exchange interaction, spin-orbit coupling, and g-factors associated with discrete quantum states in Te nanostructures. Using low-pressure physical vapor deposition, Te nanowires are grown that permits local control of carrier density using electrostatic gates. While atomically flat hexagonal boron nitride (hBN) gate dielectrics haves been widely used for high quality layered material devices, the relatively weak adhesion to Te nanowires makes hBN-insulated Te device assembly challenging. Therefore, the configuration of the device underwent a few iterations. The gate electrodes design and insulating strategy compare different methods involving more traditional dielectrics, as well as a hybrid approach that uses a global Si backgate and hBN-insulated local top gates for these Weyl semiconductor devices. Early measurements of Te devices demonstrate density

control in these devices. Future work must be aimed at quantum transport measurements in Te dots.

Acknowledgements

Many people have helped me on this journey, and I would like to briefly acknowledge some of them.

First, I would like to express my sincere gratitude to my advisor, *Dr. Hugh Churchill*, for his kindness, patience, and provision for an excellent academic ambience in which I could grow. His insight and immense knowledge were the beacon which enlightened my scientific path during the past seven years.

Next comes my parents for their affection and sacrifices to raise me and my siblings for always being supportive. My gratitude extends to my family in the physics department whom I learned from particularly *Dr. William Oliver III, Dr. Reeta Vyas, and Dr. Surendra Singh* as well as my dissertation committee members, *Dr. Salvador Barrraza-Lopez and Dr. Jin Hu* for their help and guidance throughout these years.

Finally, the entire Churchill's research group, particularly *Doha, Josh, Yomi, and Jeb* for their companionship which made my years at our lab delightful.

Dedication

To the valiant people of Iran who fight for

Woman Life Liberty,

Man Land Prosperity.

Table of Contents

List of Figures

List of Published Papers

Chapter 2

S. Davari, J. Stacy, A. M. Mercado, J. D. Hull, R. Basnet, K. Pandey, K. Watanabe, T. Taniguchi, M., J. Hu, and H. O. H. Churchill, "Gate-Defined Accumulation-Mode Quantum Dots in Monolayer and Bilayer WS_2", *Physical Review Applied* **13**, 054058 (2020).

Chapter 1

Introduction

1.1 Motivation and Objectives

The vast field of spintronics which benefits from controlling electron spin by magnetic fields through the spin magnetic moment, by electric fields through spin-orbit coupling, and by optical fields via spin optical selection rules for interband transitions, has extended interest in valley pseudospin as another internal quantum degree of freedom (DoF) for electrons [1]. Electrons in 2D crystals with a honeycomb lattice structure possess an extra DoF called valley in addition to the charge and spin degrees of freedom which forms the basis for a diverse range of applications from transistors and photodetectors to magnetic memory devices [2]. Electron valley DoF emerges as local extrema in the electronic band structures. Inequivalent valleys well-separated in the Brillouin zone (BZ) can be energetically degenerate due to the crystal symmetry and serve as novel information carriers controllable via external fields [3]. The valley DoF has made it possible to explore new physical phenomena and to envisage novel applications in electronics and optoelectronics [4]. Despite the early progress in examining valley degeneracy and intervalley coupling in two-dimensional electron gases (2DEGs) in silicon inversion layers [5–9] and generation of valley current and valley polarization in a number of material systems such as aluminum arsenide quantum wells [10–12] silicon heterostructures [13, 14], diamond [15] and bismuth [16]based on valley-dependent energy dispersion of the carriers owing to the mass anisotropy, the versatile control of valley pseudospin has been limited due to the lack of intrinsic physical properties representing valley occupancy [1].

1.2 Valley Degree of Freedom

The advent of graphene and transition metal dichalcogenides (TMDs) as two-dimensional (2D) materials with hexagonal lattice structures with valleys of energy-momentum dispersion

at the corners of the hexagonal BZ denoted by K and K$'$ points have significantly advanced the manipulation and the control of valley pseudospin by introducing well-defined physical quantities that distinguish the K and K$'$ valleys. Previously, the valley DoF had been accessed by applying strain and magnetic fields in non-TMD materials. Still, ultrathin semiconducting TMDs have allowed access to the valley DoF because of the emergence of valley-contrasting intrinsic physical properties in this class of materials and therefore, have attracted attention for the next-generation nanoelectronics due to their highly tunable optical and electronic properties and their potential for spin- and valleytronic applications [12, 17]. TMDs are now at the forefront of solid-state research due to their unique band structure featuring a large band gap with degenerate valleys and nonzero Berry curvature [1].

Group VIB transition metal dichalcogenides (TMDs) have a chemical formula of MX_2 where M is a transition metal atom such as molybdenum or tungsten, and X is a chalcogen atom from the oxygen column such as sulfur (S), selenium (Se), or tellurium (Te). A monolayer is defined as a hexagonally ordered plane of the transition metal atoms sandwiched by two hexagonally ordered planes of chalcogen atoms with a thickness of 6 - 7°A with strong in-plane covalent bonding and weak out-of-plane van der Waals (vdW) interactions. The weak vdW interactions between MX_2 layers facilitate the isolation of single layers through mechanical exfoliation or by chemical means [18–25].

Depending on the stacking order, the monolayer TMDs are found in two polytypes based on the position of the chalcogen atoms with respect to the metal element in the X - M - X structure [26]. The monolayer polytypes can be either trigonal prismatic (honeycomb motif), or octahedral (centered honeycomb motif), also known as 2H and 1T phases. Group VIB transition metal dichalcogenides (TMDs) with two d-electrons in the transition metal are primarily found in trigonal prismatic geometry. The half-filled d-orbitals in this group results in semiconducting behavior with decreasing band gap as the chalcogen atomic number increases, i.e., W = S, Se, Te [26, 27].

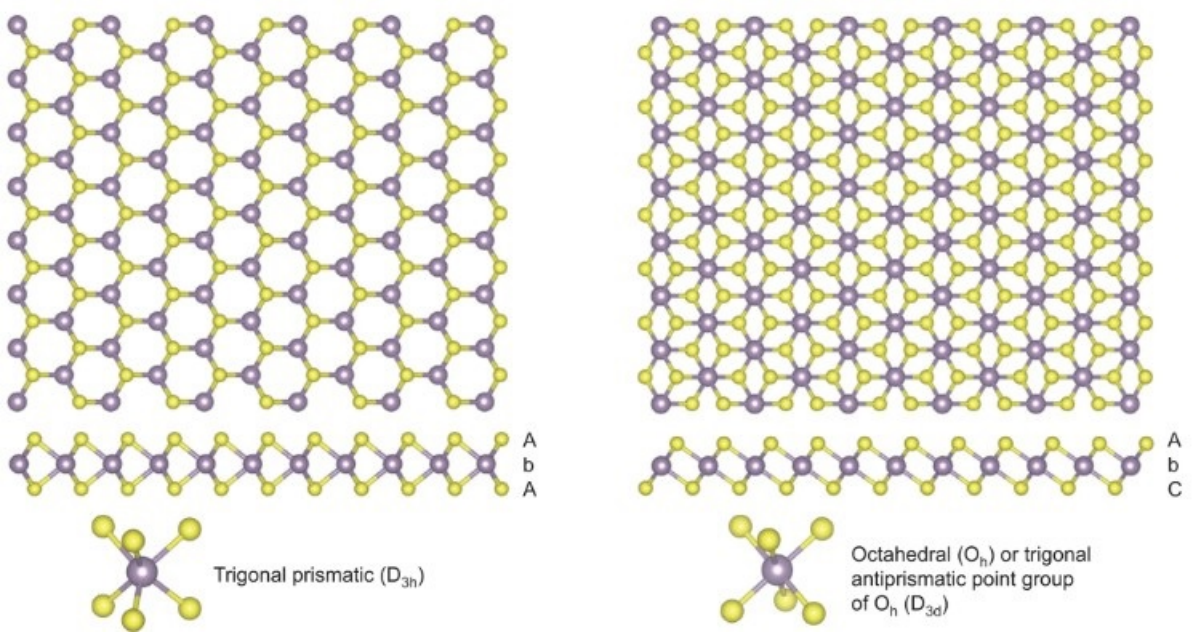

Figure 1.1: Two polytypes of single-layer TMDCs. Left pannel, the trigonal prismatic (1H). Right pannel, the octahedral (1T) [26].

Due to the broken sublattice symmetry, TMDs have a band gap [28]. Having an intrinsic band gap typically in the visible range of 1-2 eV, TMDs have overcome the main challenge of graphene which lacks band gap for the electronic applications [29–31]. Moreover, the electronic properties of the semiconducting TMDs depend on the number of layers. Many TMD band structures are similar in general features with widening band gap with decreasing the layers due to the quantum confinement effect [28, 32]. Most TMDs are expected to undergo a transition from an indirect band gap in the bulk material with the conduction band minimum located at halfway between Γ and K points in Brillouin zone and the valence band maximum located at Γ point to a direct band gap at the K point where the valence band maximum and the conduction band minimum coincide at the K point of the Brillouin zone as the semiconducting thickness is reduced to the monolayer [30, 31].

In particular, the bulk tungsten diselenide WSe_2 has an indirect band gap of 1.2 eV. In contrast, the monolayer WSe_2 has a direct band gap of 1.7 eV that results in enhanced photoluminescence, for example [31, 34]. Further, the optical transitions in thinned TMD

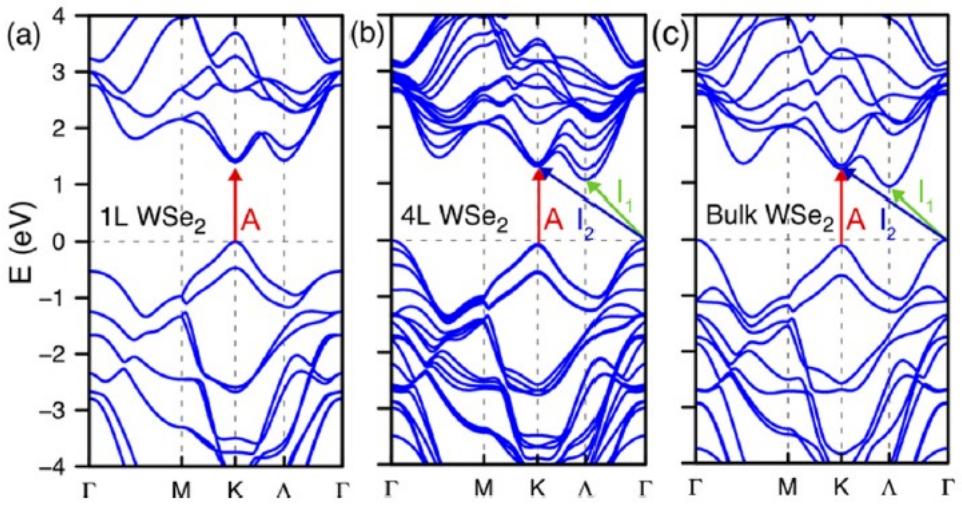

Figure 1.2: Theoretical calculation results of the energy band structures of (a) single-layer, (b) four-layer, and (c) bulk WSe2. Arrows represent the excitations, where A, I1, and I2 are the interband transitions from K to K, from to , and from to K, respectively [33].

samples are dominated by excitons rather than direct interband transitions. Figure 1.2 shows that as the thickness of the crystal decreases to a few layers and the indirect band gap increases monotonically, the direct excitonic energy does not change at the K point. In the 2D limit, the direct excitonic transition energy becomes larger than the indirect one resulting in the monolayer TMD becoming a direct band gap semiconductor [27]. Monolayer TMDs have a hexagonal lattice structure that lacks spatial inversion symmetry with the local extrema of both conduction and valence bands located at the corners of the first Brillouin zone which could be divided into two groups denoted by K and $K^{'}$ points related to one another by time-reversal symmetry forming two energetically degenerate but inequivalent valleys.

The electrons in the Bloch bands of monolayer TMDs with hexagonal crystal structure acquire Berry phase which is characterized by two physical quantities, the Berry curvature and the orbital magnetic moment. The valley-contrasting Berry curvature due to the broken inversion symmetry acts as an effective magnetic field in the momentum space and interacts with electric field which leads to an anomalous velocity for the electrons in the TMD materials. Moreover, when an in-plane external electric field is applied, the valley-contrasting Hall current can be observed giving rise to the valley Hall effect (VHE) in which carriers in

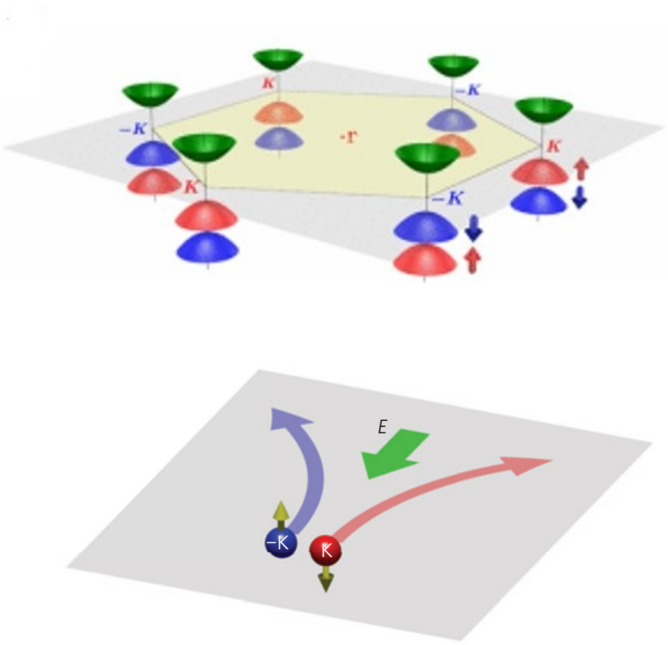

Figure 1.3: Upper panel; Schematic drawing of the band structure at the band edges located at the K points [28], Lower panel; Valley Hall effect [1].

different valleys flow in opposite transverse directions [2–4, 35–38]. The other physical quantity which is the orbital magnetic moment arises from the self-rotating motion of the electron wavepacket. Breaking inversion symmetry allows valley-contrasting orbital magnetic moment in the out-of-plane direction which interacts with external magnetic field leading to lift the valley degeneracy known as valley Zeeman effect (VZE) [39–43]. The valley-contrasting orbital magnetic moment also interacts with optical fields. The orbital magnetic moment is associated with a valley-dependent optical selection rule with circularly polarized light for the interband transition at each valley. The selectivity of the valleys by the handedness of the optical excitation allows the optical control and detection of the valley polarizations [28, 44, 45]. Furthermore, the conduction and the valence band edge at the K and K$'$ points are formed predominantly by d-orbitals of the heavy transition metal atoms where the strong spin-orbit coupling (SOC) results in spin splitting of the valence and the conduction bands in the out-of-plane direction for monolayer TMDs. The signature of this strong SOC can be observed in the optical absorption spectra where the A and B excitons are associated with

the two spin-split valence bands at each valleys with energy splitting of 400 meV in WSe_2, for example. Moreover, the splitting in the conduction band is small but finite (several tens of meV) and arises from the weak mixing of p-orbitals of the chalcogen atom coupled to the remote d-orbitals [28, 46–49].

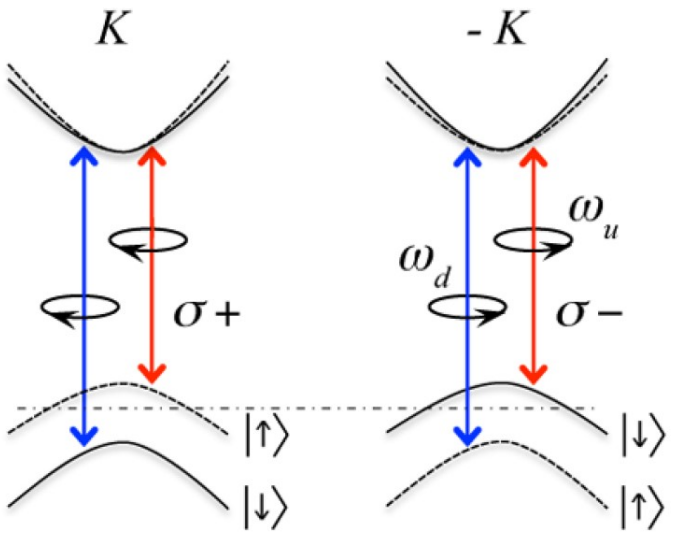

Figure 1.4: Valley and spin optical transition selection rules. The splitting in the conduction band is exaggerated. ω_u and ω_d are the transition frequencies from the two split valence-band tops to the conduction band bottom [28].

Nonetheless, the inversion symmetry is restored in the bilayer TMDs. By applying an out-of-plane electric field, the inversion symmetry in the bilayers breaks and the valley-contrasting Berry curvature, magnetic moments, and optical selection rules can be induced which opens up the possibility of tuning these properties with reversible electrical control [44, 45, 50]. These properties enable novel spintronic and valleytronic devices to be made with monolayer TMDs, and gate-controlled quantum valleytronic devices are possible in bilayer TMDs subject to external electric fields [50].

To wrap up this section, the remarkable properties such as the presence of a band gap that undergoes a transition from indirect in multilayers to direct band gap in monolayer TMDs have opened up possibilities in optoelectronics [51, 52]. Additional modalities include strong spin-orbit coupling and valley-dependent optical selection rules [28, 53–55]. The former is

the necessary condition for spintronics [56] and the latter allows access to the valley degree of freedom in TMDs and thus, the study of a variety of valley-dependent phenomena using an optical approach [57]. The unique band structure of atomically thin TMDs also offers new routes toward investigating quantum transport phenomena. Upon applying external magnetic fields, the valley Hall effect, the Shubnikov-de Haas oscillations, and the quantum Hall effect would allow investigation of the valley states [58–67]. Looking beyond these bulk phenomena, electrical confinement and manipulating the charge carriers in semiconducting TMDs are essential for realizing qubit systems [68–70]. From the aspect of quantum devices, semiconducting TMDs with presence of large band gaps are suitable platforms to form quantum dots using electric fields. Gate-defined quantum dots allows electrical access and manipulation of the valley degree of freedom in atomically thin TMDs, which is the main focus of this work.

1.3 Methods of Confinement

The strong interplay between spin and valley pseudospin is the epitome of the bulk TMD properties. The versatile control of these quantum degrees of freedom as potential carriers for quantum information processing requires exploiting a small number of particles confined in atomically thin TMDs known as quantum dot provided that the bulk properties of spin and valley pseudospin are inherited in the quantum confinement regime. In nanostructures, spatial confinement can cause intervalley coupling and valley hybridization that inhibits the robustness of the valley-spin states and renders the valley pseudospin to no longer be a good quantum number. However, in atomically layered TMDs, strong carrier confinement in one dimension can still preserve the bulk-like spin and valley properties in the two-dimensional plane [32]. Quantum dots can be defined by the confinement potentials realized by patterned electrodes on an extended TMD flake or by lateral heterostructures between monolayer TMDs of different band gaps with type II band alignment with the surroundings [71]. To find the

potential profile within the TMD layer in the gate geometry, one can use commercial finite element analysis simulation tool modeled by solving Poisson equation [72].

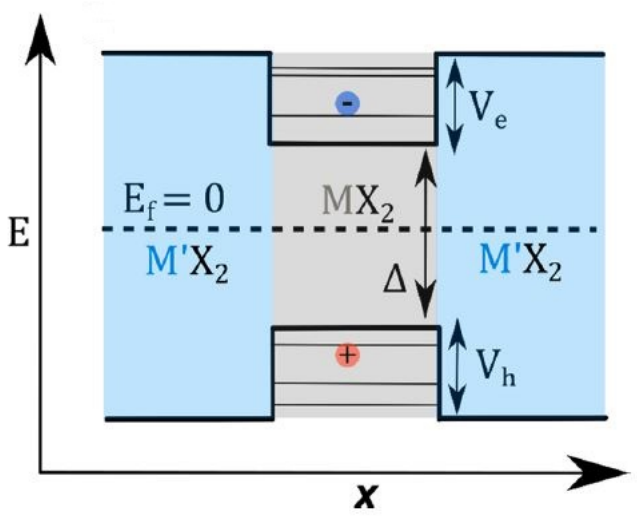

Figure 1.5: The band offsets between different monolayer TMDs create quantum wells for confining electrons and holes[71].

Therefore, the pivotal issue in this context is to identify the degree of valley hybridization due to the quantum confinement as the lateral confinement may result in strong intervalley coupling which could be detrimental to the bulk valley physics. Further, in quantum dots defined in 2D crystals, the intervalley coupling is proportional to the probability distribution of electrons at the quantum dot boundary where the translational invariance is lost. In monolayer TMDs, the intervalley coupling is generally weak due to the vanishing amplitude of electron wavefunction at the quantum dot boundary. The valley hybridization is quenched by the strong spin-valley coupling [73]. The following sections focus on self-assembled quantum dots followed by quantum dots formed by the localized defects, strain, and moiré patterns. Finally, the gate-defined quantum dots which are this study's main focus, are discussed.

1.3.1 Self-Assembled Quantum Dots

Confinement sufficient to address valley-spin states of a small number of particles is required to define a qubit. Coherent in-plane quantum confinement can be achieved in the vertical

self-assembled heterostructures. Optically active quantum dots that confine the motions of the charged carriers in regions of order of exciton Bohr radius, can be achieved by self-assembly through chemical synthesis, i.e., colloidal quantum dots [74] or epitaxial growth such as molecular beam epitaxy (MBE) or metal-organic chemical vapor deposition. The colloidal quantum dots with novel applications in the fields of optoelectronics and biomolecular tagging in biomedicine [75, 76] are impractical on the scope of solid-state devices due to the complex surface chemistry, unreliable spatial positioning, or lack of electrical and optical access [71]. Thus, the epitaxial growth using the strain-driven Stranski-Krastanov (SK) growth mode is the subject of this section [77]. Semiconductor self-assembled (SA) quantum dots which were first demonstrated for the InAs/GaAs system, are the product of SK growth process in the lattice-mismatched systems where the islands form spontaneously above a certain critical thickness as a result of mismatch strain relief [78]. Further, after the formation of a thin elastically strained epitaxial wetting layer, the island growth starts. The further growth of the wetting layer increases the film energy. Then, the nanometer-size islands take place to minimize the surface energy of the growing film which eventually transforms the islands into quantum dots by capping them with the larger band gap material. The result is the electron and hole states which represent energy quantization in islands of 2-5nm high and $\tilde{2}$0nm base width for the In(Ga)As dots in GaAs with delta function-like densities of states. This growth process can be applied to many strained-layer epitaxial systems including a large number of group III-V, II-VI, III-Nitrides, and group IV systems [78]. Due to the quantized electronic states and high radiative efficiencies, SA quantum dots have had favorable applications both in fundamental physics and in the fields of quantum information. The device applications can be categorized into two groups based on the properties of the large ensembles and the properties of the single dot. Light-emitting diodes [79, 80], high performance semiconductor lasers, and infrared detectors [81, 82] belong to the first category whereas single photon sources and two-level systems [83] are classified in the second group. The structural studies such as scanning tunneling microscopy (STM), energy-filtered transmission electron microscopy

(TEM), and grazing-angle x-ray diffraction can exhibit the composition profiles and the asymmetric shape of these quantum dots which result in breaking inversion symmetry, and thus leads to the presence of a permanent dipole moment which is defined as holes localized above electrons [84]. The small size of these quantum dots leads to enhancement of Coulomb interactions. The typical electrons (holes) charging spectra can be obtained by using Schottky barrier structures for electrons (holes) on n^+ (p^+) substrates. Photoluminescence (PL) spectra as a function of electron charging energy at different bias voltages is shown in figure 1.6 [85].

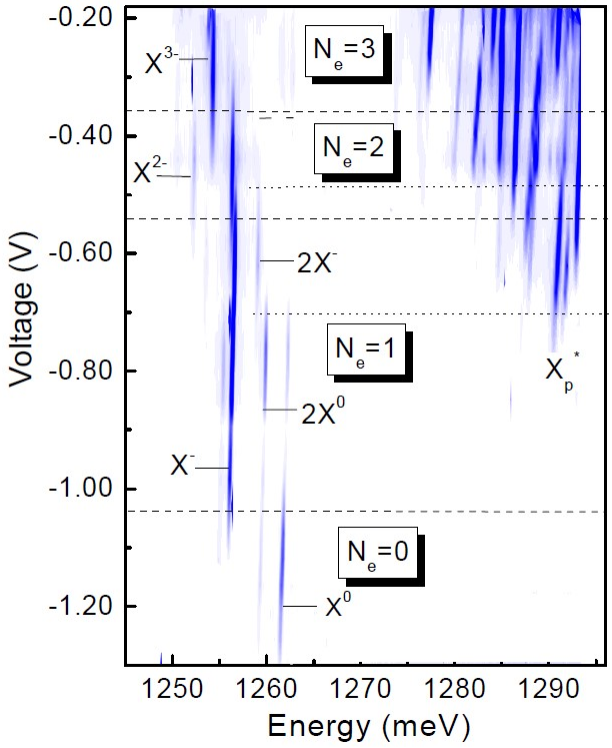

Figure 1.6: PL spectra for a single quantum dot of InGaAs as a function of electron charging [85].

The similar experiment can be performed on a p^+ substrate to find hole charging energies [84]. One notable feature deduced from these experiments is the red shifts on electron charging and the blue shifts on hole charging that can be inferred from different extents of the electron and hole wave functions which represent the dominant effects of direct Coulomb interactions for single charged excitons [86]. The critical challenges in epitaxially-grown

quantum dots are random nucleation and the island's size and composition fluctuations. Controlling the nucleation of SA quantum dots can be achieved with various degrees through surface patterning which defines the nucleation positions in a more constrained way [87–91]. Moreover, the islands size might be enhanced by diffusion and the island ripening process before capping [92].

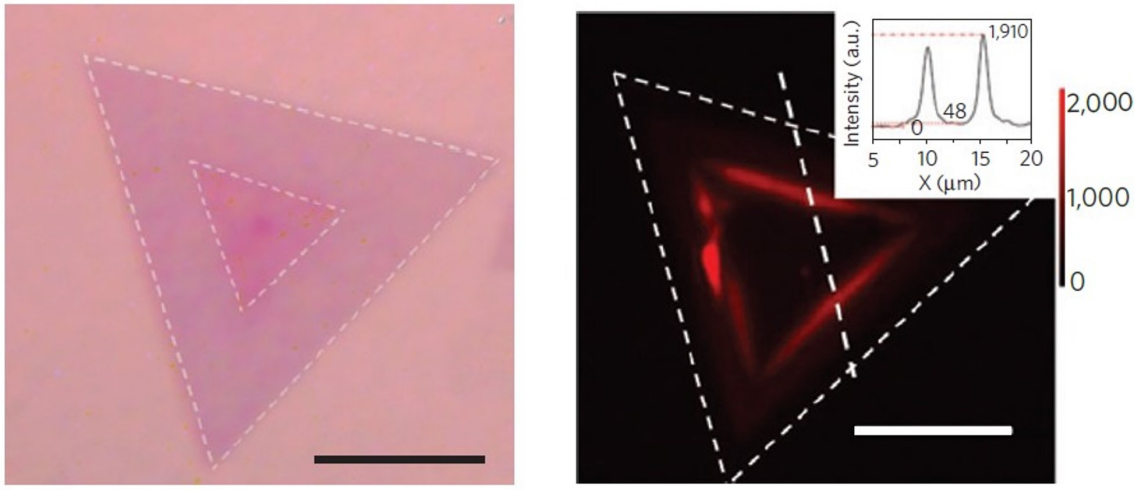

Figure 1.7: Optical microscopy of in-plane WS_2/MoS_2 heterojunction and the PL-intensity mapping that shows strong localized PL enhancement at the interface [93].

Designing nanoscale monolayer heterostructures that can localize excitons and exhibit discrete bound states using 2D materials is complementary to the traditional semiconducting materials mentioned above. In stark contrast to graphene with massless Dirac fermions, 2D TMD monolayers with electronically stable surfaces and atomic-scale thicknesses that provide perfect out-of-plane confinement, natively host massive Dirac fermions due to the band gap that reduce the probability of Klein tunneling [94–97]. Furthermore, the coherent in-plane quantum confinement can be envisioned in the lateral heterostructures of these systems due to their isostructural lattices with small variations in the lattice constant. The band offsets between different TMDs in a heterostructure can be exploited to construct a confining potential step with type II band alignment due to the sharp change in the absolute band energies at a clean interface between the two TMD materials [98]. The lateral heterostructure

architecture for quantum confinement can be obtained by lateral epitaxy [93, 99, 100] or through mechanically-transferred vdW heterojunction [27]. The lateral heterojunction quantum dots lead to enticing new physics and applications. However, the fabrication of 2D heterostructures with clean and sharp interfaces is imperative for preserving the exciton and its optoelectronic properties driven by the interlayer or intralayer coupling. So far, the mechanical stacking of the heterojunctions has remained challenging due to defects and contamination. Moreover, the stacking orientation of different 2D TMD materials using mechanical transfer techniques may not be precisely controlled [101, 102]. Moreover, due to their stochastic nature, the growing techniques are also challenging. The precise control over the growing and the lattice matching leads to chalcogen intermixing, and the in-plane control over dopant density in selective areas may be more constrained than the vertical growth counterpart [27].

1.3.2 Quantum Emitters by Defects

Single photon emitters are at the heart of solid-state quantum optic and photonic technology. Quantum emitters have been realized in zero-dimensional (0D) and three-dimensional (3D) systems such as single molecules, quantum dot formation due to the composition fluctuations in semiconductor hererostructures, and Nitrogen vacancies (color centers) in diamond where the crystal defects are properly isolated so that they can emit single photons[83, 83, 103–105]. Unlike trapped ions and atoms, the solid-state quantum emitters embedded in the bulk material benefit from long-term stability. These heterostructure devices with monolithic structures provide enhanced functionality and performance in quantum information processing and quantum networking applications by introducing the so-called localized emitters that are correlated with the internal spin structures but buried in the bulk material with a high refractive index [106]. It is no stretch of the truth to say that the high dielectric material and the internal reflection in the bulk are quite of challenge to extract single-optical mode phonons [107]. Further, photon interactions and charge and spin fluctuations within the

emitter's environment lead to dephasing [108, 109]. Nonetheless, 2D geometries of single photon emitters confined in atomically thin materials enhance the photon extraction efficiency and the integration with photonic circuits. Therefore, 2D TMD semiconductors are intriguing alternatives to host quantum emitters.

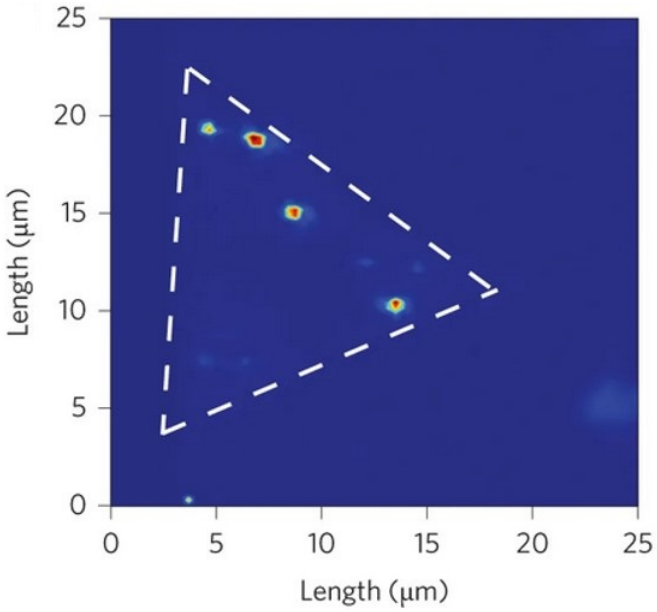

Figure 1.8: PL-intensity map of narrow emission lines of a monolayer WSe_2 sample [110].

Monolayer semiconducting TMDs with unconventional electronic bands and remarkable functionalities arising from the internal degrees of freedom of electrons such as spin and valley pseudospin can coherently interact with circularly polarized light and exhibit a variety of achievements including the optical generation of valley polarization and coherence [28, 53–55, 111], valley Hall effect [2], valley polarized light-emitting diodes [112], and valley selective optical Stark effect [113, 114]. In fact, the optical selection rule associated with the valley pseudospin of the delocalized excitons in high-quality samples can explain all of these effects. Further, the robust photoluminescence (PL) due to the quantum confinement in one-molecule-thick layer of TMDs with direct band gap semiconductor structure will be progressively quenched and red shifted as the number of layers is increased. The PL completely vanishes in sufficiently thick flakes [47]. Single photon emission has been observed from quantum

light emitters in atomically thin layers of TMDs with above band gap excitation. The origin of quantum emitters in these materials could be assigned to defects [110, 115–119]. The localized deformations in monolayer TMDs can result in the quantum confinement of the excitons. Moreover, the PL experiments have revealed excitonic states related to defects that emit remarkably below the energy of the delocalized valley excitons [28, 53–55, 111, 120]. The strong electron-hole binding in monolayer TMDs will guarantee a quantized optical excitation spectrum due to the trapped neutral excitons at anisotropic confining potential from defects [110]. Large field gradients induced by gating can also trap neutral or charged excitons where the emission properties of the single photons can be controlled by the external electric and magnetic fields owing to the close proximity of the embedded single quantum emitters [116]. At low temperatures, the structural defects in monolayer TMDs or at the edge of the thin film of the monolayer flakes exfoliated on an alien substrate, give rise to the sharp emission lines due to the formation of spatially localized excitons. The linewidth of these optical emissions are narrower than those of the delocalized valley excitons and they exhibit strong photon antibunching which unequivocally demonstrates the zero-dimensional nature of these single photon emitters. The defects are also responsible for additional recombination of electron-hole pairs which can be revealed by sub-band gap emission. Moreover, a controlled introduction of defects in these materials will significantly help utilizing these localized defect-bound excitons for quantum applications.

1.3.3 Quantum Emitters by Strain

Experiments on the defect-induced quantum emitters rely on the rare and random occurrence of these localized deformations; therefore, a general approach to deterministically obtain and isolate defects is crucial for the further development of this platform. Indeed, scalability is one of the great challenges in quantum photonics which requires deterministic engineering of the quantum emitters' locations. In the established platforms such as NV in diamond and self-assembled quantum dots, site positioning progress has been obtained, yet with compromised

coherence and optical quality [121]. Nanoscale strain engineering of the electronic band structure is viable for creating quantum confinement and deterministically achieving quantum emitters in bulk semiconductors. For example, in epitaxially grown heterostructures such as quantum wells and wires, in particular, local strain is created to laterally confine the carriers [122–125]. However, due to the small vertical propagation and limited elastic strain in these bulk systems, the robust strain-induced quantum confinement of the carriers cannot be adequately realized.

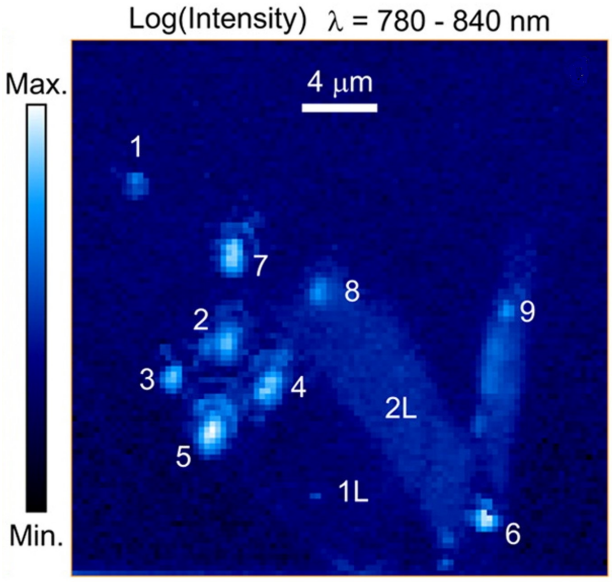

Figure 1.9: PL spectra corresponding to localized bright spots of a WSe_2 sample [106].

Optically active 2D semiconductor TMDs with high elastic (up to 11%) strain limit can be intriguing platforms for nanoscale strain-induced quantum emitters [126–131]. Strain gradients in monolayer TMDs, either unintentionally induced or engineered by substrate patterning can significantly tune the electronic band gap and result in spatially and spectrally isolated quantum emitters [106, 132, 133]. Moreover, quantum light emitters in atomically thin layers of TMDs at random locations and in low densities hinder experiments for further investigations unless they are created in precise positions with large numbers of quantum emitters which will open up the scalability and on-chip applications. Using nanopatterned

substrate, one can achieve arrays of single photon emitters in the host monolayer TMD material [134]. Massive strain gradients are possible in 2D TMDs and several approaches for both static and in-situ tuning of the strain are available [135]. Rather than suspending the flake over a hole, one can obtain periodic arrays of quantum emitters by placing the flake over a periodic array of steps, holes, or nanopillars and observe high red shifted localized exciton lines which are comb-like [121].

1.3.4 Quantum Emitters by Moiré Patterns

As mentioned before, TMDs are layered semiconducting materials with strong in-plane metal-chalcogen covalent bonds and weak out-of-plane vdW bonds which hold the thin layers of few-angstrom thicknesses together. The relatively weak vdW bonding between the constituent monolayers of a TMD crystal enables the mechanical exfoliation of the bulk material. By lifting the usual constraint of lattice matching, the weak vdW force not only beckons monolayer crystals with incommensurate lattices to stack vertically to form heterostructures but also allows arbitrary mutual rotation between the adjacent layers of the heterostructures in contrast to epitaxially grown counterparts in which the rotation is fixed between the neighboring layers by the crystals axes [136, 137]. These unique vertically stacked vdW heterostructures result in overarching periodicity in the atomic registry of the constituent TMD monolayers, which offers possibilities to modulate the electronic band structure. These vertical stacks lead to unique transport properties such as unconventional superconductivity, insulating behaviors driven by correlations, and the fractional quantum Hall effect. These also allow engineering optical properties via forming in-plane moiré superlattices [138–143]. In mechanically stacked heterobilayer of semiconducting TMDs with a twist angle between the two incommensurate monolayers, a moiré pattern is expected with three high-symmetry points of local energy extrema within each moiré supercell. These patterns can be imaged with high-resolution transmission electron microscopy (TEM) [144].

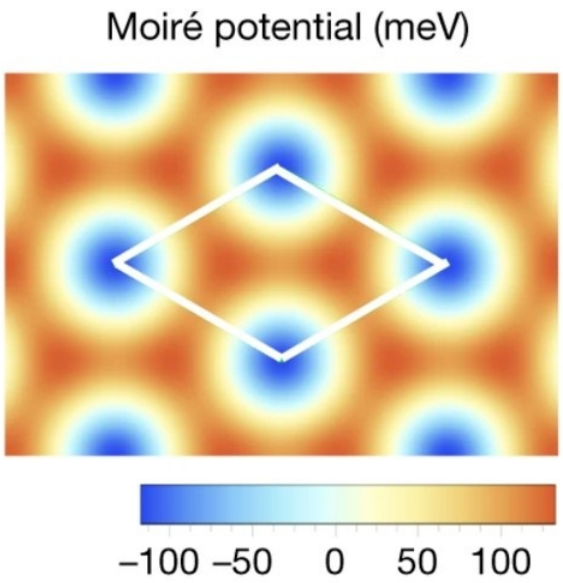

Figure 1.10: The moiré potential of the interlayer exciton transition for a $MoSe_2/WSe_2$ sample [145].

Further, the periodicity of the moiré superlattice is determined by the mismatch in the lattice constants of the constituent monolayers and the rotation angle between those monolayers. These TMD heterobilayers exhibit atomically sharp interfaces and type II band alignment that host interlayer excitons which are Coulomb-bound states between electrons and holes situated in adjacent monolayers and excited by circularly polarized optical pumping [146]. When the moiré supercell has a period larger than the exciton Bohr radius, the moiré potential localizes the interlayer excitons and gives rise to multiple interlayer exciton resonances with different optical selection rules. Thus, the moiré potential minima act as a quantum-dot-like confinement. The interlayer excitons trapped in this potential inherit the valley-contrasting physics [147–150]. At low temperatures, the twist angle between the adjacent monolayers influences the PL efficiency of these interlayer valley excitons. This could be manifested by the twist-angle dependency of the PL peaks red shift [151–153].

1.3.5 Quantum Dots by Patterned Electrodes

The strength of intervalley coupling in TMD quantum dots depends on the shape of the confinement potentials. The intervalley coupling as a function of the lateral size of the quantum dot exhibits oscillating behavior with an exponentially decaying envelope. Moreover, for a sharp confinement potential with vertical walls generated by lateral heterostructure of different monolayer TMDs, the intervalley coupling is stronger than the case for smooth confining potential generated by patterned electrodes with slopping potential walls [73]. Therefore, confinement not much greater than the lattice spacing leads to strong valley hybridization, which deteriorates coherence, so the valley is no longer a good quantum number. Further, the challenging issues of the aforementioned quantum dots have motivated the researchers to investigate more deterministic engineering of quantum dots to overcome the shortcomings. The gate-defined quantum dot not only allows electronic control and manipulation of the quantum states but also appropriates tuning of the confinement length in TMD quantum dots to achieve desired level spacing.

Coulomb blockade is transport spectroscopy of the gate-defined quantum dots. Realizing gate-controlled Coulomb blockade is associated with the confinement of electrons and demonstrating electrical control over charged carriers with tunable local confinement potential and tunnel coupling. In other words, Coulomb blockade is monotonic control of a confined electron gas known as a quantum dot which enables precise tuning of the quantum dot-reservoir-tunnel coupling. According to the orthodox Coulomb blockade theory, in the ballistic regime where the confinement size becomes smaller than the mean free path, the charged carriers experience no scattering, and the transport occurs by tunneling through an isolated electronic gas [154, 155]. A quantum dot in this context can be considered a system coupled to the source and drain contacts via tunnel barriers modeled by a tunnel resistor and a capacitor. Quantum dot is also capacitively coupled to the gate electrodes. The voltage applied to the gates allows electrostatic tuning of the dot. In the constant interaction model, which

describes the behavior of quantum dots, two basic assumptions are introduced. First, the Coulomb interactions among electrons are capacitively characterized, $C = C_S + C_D + C_G$ where C_S, C_D,and C_G are capacitances between the dot and the source, the drain, and the gate, respectively. Secondly, the single-particle energy level is independent of the number of electrons in the dot [156, 157].

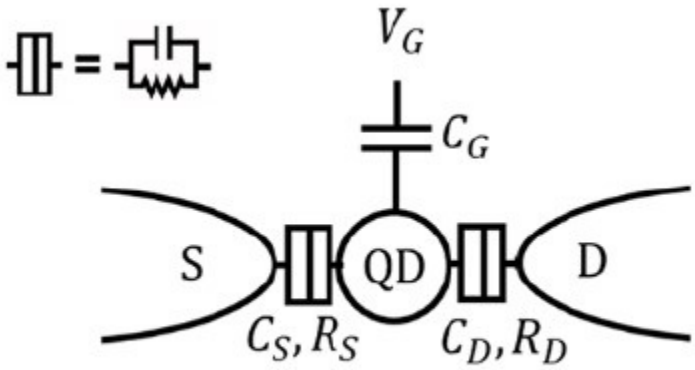

Figure 1.11: Networks of tunnel resistors and capacitors representing single quantum dot [158].

Under these assumptions, the electrochemical potential μ(N) is described as the energy cost for adding the Nth electron to the quantum dot, which contains N-1 electrons and is given by $\mu(N) = (N - N_0 - 1/2)E_C - E_C(C_S V_S + C_D V_D + C_G V_G)/e + E_N(B)$. Here, N_0 is the number of electrons responsible for the background charge. $E_C = e^2/C$ is charging energy which is the energy required to overcome the Coulomb repulsion from the existing carriers on the dot. V_S, V_D,and V_G are voltages applied to the source, the drain, and the gate, respectively. $E_N(B)$ is the single-particle energy level of the Nth electron, which can be manipulated by the magnetic field B. As the electrochemical potential relation represents, μ(N) linearly depends on the gate voltage, and the dependence is the same for all N electrons. This results in an electrochemical potential ladder.

The ladder spacing is given by $\mu(N + 1) - \mu(N) = \Delta E + E_C$, known as charge addition energy E_{add} which has two contributions. One is from the ΔE, which is the energy separation

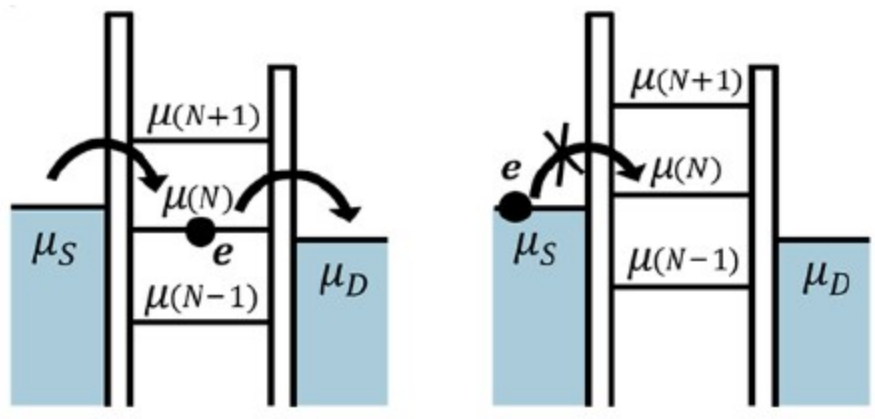

Figure 1.12: Schematic diagrams of the electrochemical potential levels of a single quantum dot. If μ(N) is tuned into the bias window set by μ(S) and μ(D), the number of electrons can vary between N - 1 and N, resulting in a single electron tunneling current (left panel). If no level is in the bias window, the electron number is fixed, and no current flows, known as Coulomb blockade (right panel) [158].

between two discrete quantum levels. ΔE represents the material quantum states and is usually much smaller than the E_C if the dot contains a large number of electrons. When the dot enters a few-electron regime at low temperatures where ΔE is greater than the thermal excitations ($k_B T$) known as the quantum regime, the contribution of ΔE is revealed, and one can access the quantum states of the material and study their properties. This is in sharp contrast with the so-called classical regime, where ΔE is smaller than $k_B T$, and the internal quantum levels are smeared together. The other contribution to E_{add} is from the charging energy E_C. A large charging energy makes the quantum dot smaller as E_C is related to the dot size $E_C = e^2/8\epsilon_0\epsilon_r r$. By changing the gate voltage, the Fermi level of the material changes, and the charging energy E_C should change if the energy band varies smoothly. For example, for an n-type semiconductor, more negative gate voltage leads to a smaller quantum dot and larger charging energy. Charge addition energy and its constituents can be obtained from transport measurements.

If a particular electrochemical potential μ(N) is tuned into the bias window $\mu_S > \mu(N) > \mu_D$ where μ_S and μ_D are the electrochemical potentials of the source and the drain reservoirs, respectively, an electron can tunnel through the dot and a current flows through the dot.

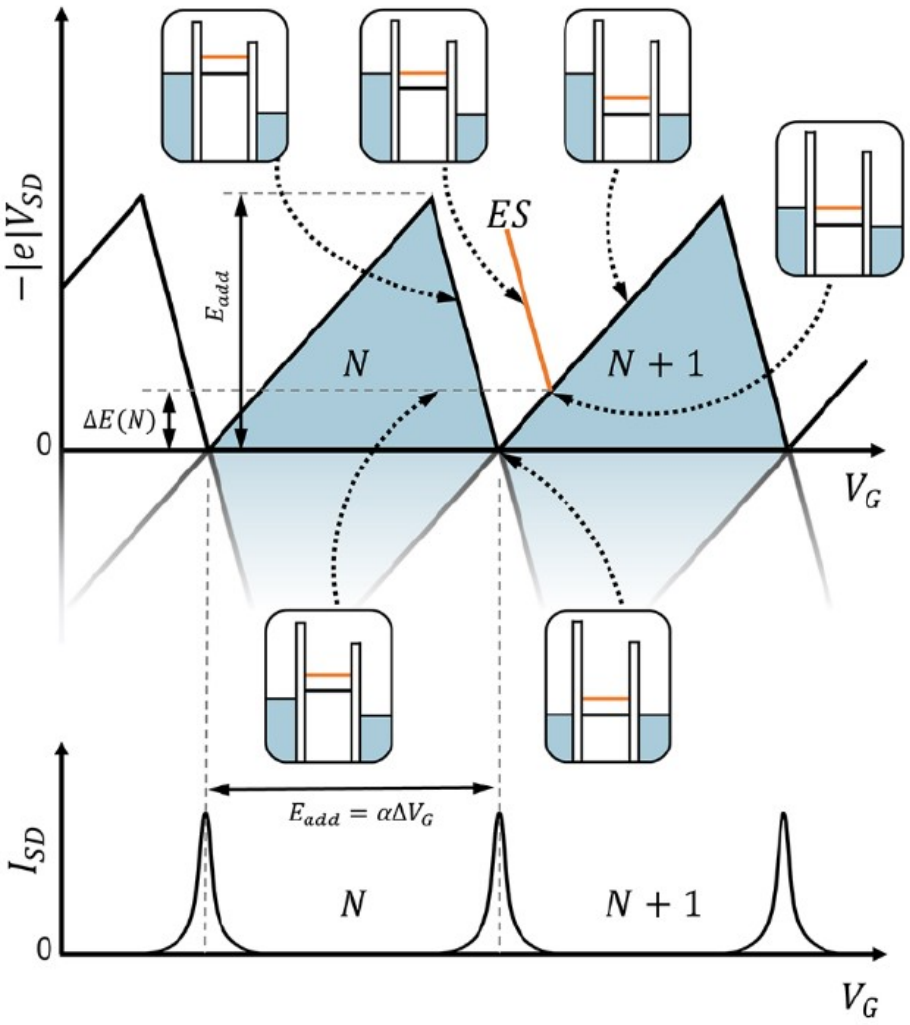

Figure 1.13: Upper panel, the schematic plot of source - drain current I_{SD} as a function of V_{SD} and V_G known as Coulomb diamonds. Insets show the level alignment. The orange level indicates a transition related to the excited state (ES). The lower panel shows I_{SD} as a function of as a function of V_G, known as Coulomb oscillations [158].

The single electron tunneling event when μ_S and μ_D, and μ(N) are aligned is referred to as resonant tunneling. Otherwise, if there is no electrochemical level of the dot available within the bias window of the reservoirs, there would be no current flow which is known as Coulomb blockade. By continuously tuning the electrochemical potential ladder via varying gate voltages, a series of current peaks can be observed, known as Coulomb oscillations. Coulomb oscillations represent conductance as a function of gate voltage associated with single electron charging phenomena and reveal the nature of the Coulomb blockade. To

observe Coulomb oscillations, the charge addition energy must be greater than the thermal excitations (k_BT). Otherwise, the thermal fluctuation effect will be dominant, and Coulomb oscillations will vanish. Coulomb oscillations consist of Coulomb peaks of conductance and suppressed conductance regions. At each peak, an electron is loaded into the dot and then tunnels out, while between the peaks, the number of electrons in the dot remains fixed. The spacing between two successive Coulomb where resonant tunneling happens is determined by the charge addition energy through a voltage energy conversion coefficient known as lever arm, $\alpha = E_{add}/\Delta V_G$. Further, the lever arm or gate coupling coefficient is conversion of gate voltage into the charging energy scale, which is essential for a quantitative understanding of the transport spectroscopy of the devices. The small lever arm could be due to the fringing field screening effect from the source and the drain electrodes wherein the channel length is smaller than the thickness of the gate dielectric, or it could be attributed to metal diffusion during the thermal annealing step, for example, which reduces the actual channel length [159]. To have a more efficient gate effect, one can use a high dielectric constant insulator to compensate for its thickness and to make the source-drain electrode screening less effective.

Another essential condition for observing Coulomb oscillations is related to the number of electrons on the quantum dot, which must be well-defined. This requires that the contact between the dot, the source, and the drain leads be resistive. Quantitatively, the contact resistance needs to be larger than the resistance of a single conductance channel h/e^2 $\sim 25.81k\Omega$ [160]. Coulomb diamonds are corresponding 2D conductance map of Coulomb oscillations as a function of the bias and the gate voltages. Coulomb diamond manifests the formation of the quantum dot. Regular closed diamond patterns indicate single electron charging on a single quantum dot under the gate biasing conditions. If the Coulomb diamond does not form, it means high conductance that could be due to the contact junctions being too transparent for single electron charging [161, 162]. The size of Coulomb diamonds is determined by E_{add}, thus contains information about quantum states. In the quantum regime at low temperatures, where $\Delta E > k_BT$, the excited states are involved in addition to the

ground-state spectrum. The existence of the excited state results in measurable current change when the related excited state potential also lies in the bias window. The orange level in the insets of the above figure indicates the excited state potential where an excited state is involved, and the orange line in the Coulomb diamond represents the excited state energy ΔE. Therefore, Coulomb diamond measurements are essential to characterize a single quantum dot. The slopes of the diamond (eC_G/C_S and $-eC_G/(C - C_S)$) represent the capacitive coupling to the quantum dot. If the separation between the diamonds and the slopes of the transitions remain constant over some consecutive charge transitions, it implies a uniform dot near the device's center. Besides, a symmetric Coulomb diamond means equivalent tunnel coupling to the source and the drain leads. Again, since the charging energy value is usually in the range of a few meV, the temperature needs to be kept low enough to reduce thermal excitation and the bias voltage should also be kept small. Further, the tunneling barriers need to be opaque enough so the energy uncertainty is much smaller than the charging energy, assuming the electrons are located either in the source and drain or in the dot.

Moreover, the temperature dependence of the Coulomb oscillations is a way to investigate the nature of the Coulomb blockade. Coulomb blockade phenomena at low temperatures ascribe the transport behavior of single electron tunneling through an isolated clean quantum dot and help understand the intrinsic electronic properties of the materials. According to the standard theory of semiconductor quantum dot [155], the line shape of the Coulomb oscillations in the weak coupling regime where the tunneling rate $h\Gamma$ is much smaller than the thermal excitations ($h\Gamma << k_BT$) manifests in different forms for various temperatures. In the so-called classical regime where ΔE is smaller than thermal fluctuations ($\Delta E < k_BT < E_C$), the peak heights of the conductance remain constant in the absence of disordered confining potential, but the full width at the half maximum (FWHM) of the Coulomb peaks increases linearly with temperature.

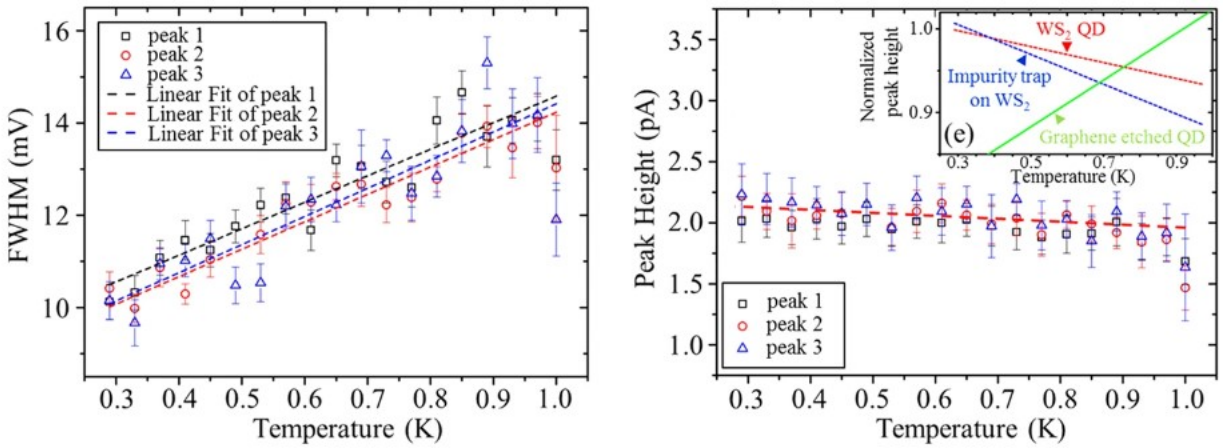

Figure 1.14: Left panel, the FWHM of the Coulomb peaks which linearly increases with temperature. Right panel, the peak height of the Coulomb peaks as a function of temperature. The peak heights are almost independent of temperature [163].

Conversely, in the quantum regime where ΔE is greater than the thermal excitations ($k_BT < \Delta E, E_C$), the peak heights of the conductance decrease linearly with temperature. Nonetheless, in the strong coupling regime where the tunneling rate is greater than the thermal excitations ($h\Gamma > k_BT$), the line shape of the Coulomb peaks is obtained from Breit-Wigner formula, and it is only related to the tunneling rate. Further, in $h\Gamma \sim k_BT$ regime, the line shape of the Coulomb peaks has a Lorentzian form [156].

In the following, some of the significant challenges regarding the confinement and the control of the electronic landscape in the TMD nanostructures are discussed. Technically, manipulation of electronic and excitonic excitations in TMD nanostructures is challenging due to the emergence of defects, edge states, and residual disorders in the material which prevents accurate experimental control of the local confinement [164]. Disordered confining potential due to the edge states formed in the narrow constrictions connecting the quantum dot and the reservoirs, which are observed in the low-frequency noise experiments, causes large potential fluctuations and results in anomalous behavior of Coulomb peaks and energy-independent tunneling behavior [72]. Quantum confined structures on TMDs with tunnel barriers defined by electric fields can decrease the influence of defects and edge states which are a major aspect limiting the performance of the graphene nanodevices [164–166]. The tunable TMD quantum

dots isolated from the edge states could be used as spin and valley qubits. The residual disorder also limits mobility and device homogeneity. The inhomogeneous 2D electron gases (2DEGs) due to the residual disorder can lead to accidental quantum dot formation with reduced controllability similar to those identified in modulation-doped Si/SiGe quantum dot [167], short MoS_2 channel [159], and graphene nanoribbons [168, 169]. The impurity potential modulates the band gap and affects the quantum dot. To overcome this challenge, one can employ high-quality heterostructures and also apply high gate voltages so the Fermi level increases; thus the influence of disorder potential decreases and the electrical control of the charged carriers becomes more efficient. One way to check this is to see whether rapid Coulomb oscillations are observed over a wide range of gate parameters. Such behavior is due to disorder-defined tunnel coupling insensitive to the applied gate voltages. However, if the conductance shows a monotonic increase as a function of gate voltage, then it would be in sharp contrast to accidental quantum dot formation due to the disorder landscape.

Achieving homogeneous 2DEG and transparent ohmic contacts becomes difficult as the thickness of a TMD flake approaches the atomic limit [59, 170–175]. When the mobility is low and the contact quality is low, there would be a significant contribution from the contact resistance. In quantum transport studies in TMDs, one of the significant hurdles lies in the large metal-semiconductor junction barrier for carrier injection. This can lead to a contact resistance-dominant charge transport which limits access to intrinsic transport behavior in TMDs [173, 176–178]. Further, electron transport study on mono- and few-layer TMDs is still challenging at low temperatures due to contact-dominant transport. One solution is to try various contact metals with different metal work functions and incorporate a thermal annealing step, which induces metal migration [159] for high performance TMD single electron transistors. For single electron transition, the contacts are coupled to the dot by tunnel barriers which requires very small Schottky barrier at the metal-semiconductor junction. When the TMD channel is weakly coupled to the metallic leads by opaque enough contact junction that forms tunnel barriers, a suitable platform to study Coulomb blockade

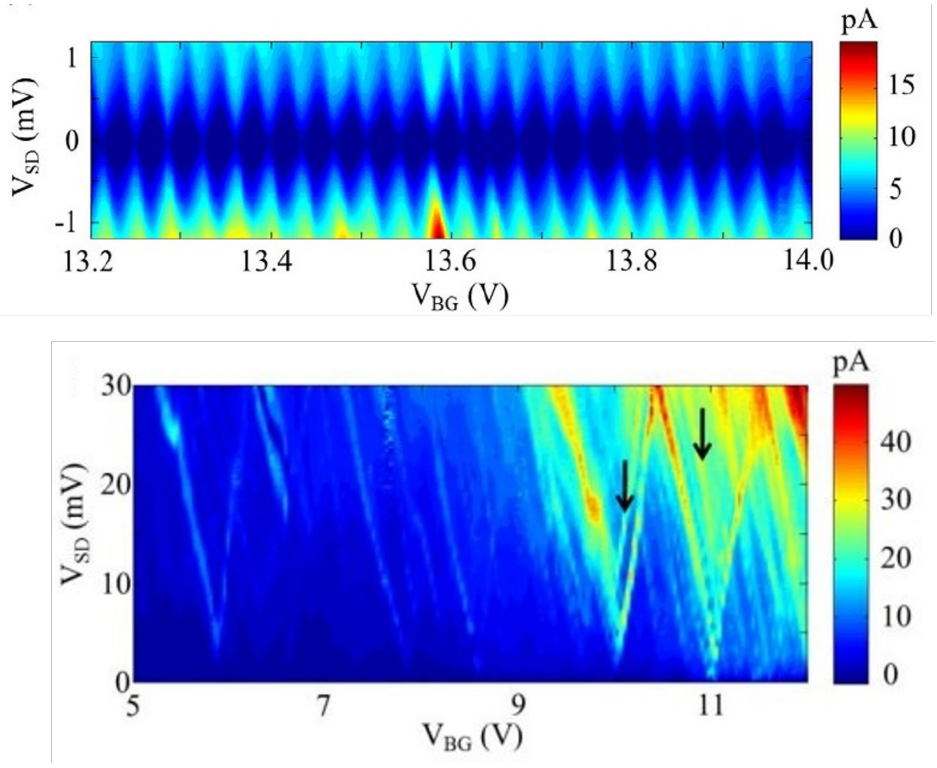

Figure 1.15: Upper panel, Coulomb diamonds of a WS_2 quantum dot. Lower panel, A series of Coulomb diamonds found at larger V_{SD} considered to be the result of an impurity trap [163].

phenomena at low temperatures is provided [179]. Otherwise, the lack of control of the metal-semiconductor barrier may lead to too transparent, contacts which should be avoided for studying single electron tunneling. A drain current versus source bias characteristics shows whether the behavior is ohmic [173] or Schottky [180] barrier-dominated.

The gate-controlled quantum dots provide promising platforms to study the quantum states of electrons at single electron transitions. Moreover, when external fields such as magnetic fields are applied, different quantum degrees of freedom including charge, spin, and valley, can be manipulated. Further, the Fermi energy with respect to the band edge and the charging energy in the quantum dot should be smaller than the spin-orbit gap in TMDs, ensuring the spin-valley locked nature of the confined carriers [58]. Due to the large exciton binding energy, 2D TMDs provide platforms for novel quantum Optoelectronic devices [182]. Similar to the charge confinement demonstrated by gate-defined nanostructures, charged excitons can also

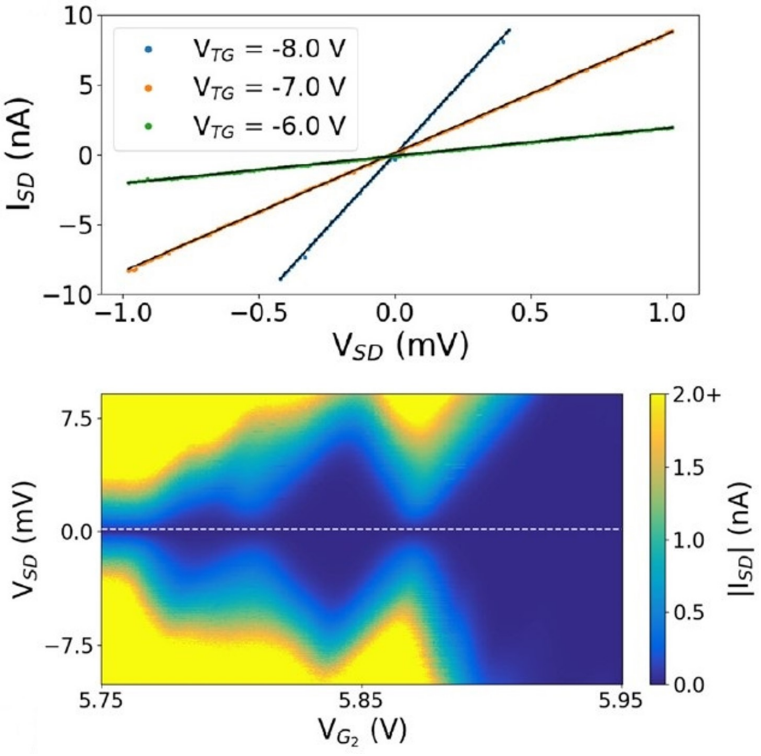

Figure 1.16: Upper panel, the drain current at various top gate voltages shows linear behavior representing ohmic contacts. Lower panel, Coulomb diamonds at 4K [181].

be manipulated by gate-defined confinement. The hallmark features of confinement effects are size-dependent electronic and optical properties [183, 184]. In the weak confinement regime with the confinement size greater than the exciton Bohr radius, optical and electronic properties become size-tunable, whereas the strong confinement with the confinement size smaller than the Bohr radius enables discrete energy levels and the formation of quantum dots in TMDs [185–187].

1.4 Dissertation Overview

In addition to this introductory chapter, this dissertation consists of three other chapters compiled based on two individual projects.

Chapter 2 discusses the gate-defined quantum dots in monolayer and bilayer WSe_2. Chapter 2 has been published in Physical Review Applied as: S. Davari et al. "Gate-Defined

Accumulation-Mode Quantum Dots in Monolayer and Bilayer WSe_2", *Physical Review Applied*, 13(5) 054058, 2020.".

Chapter 3 discusses gate-controlled tellurium nanowire quantum dots. Following a brief introduction to the tellurium crystal structure, some of the transport-related phenomena in tellurium are reviewed. Then, the fabrication and device measurements of gate-controlled Te nanowire quantum dots are discussed.

Finally, Chapter 4 concludes the dissertation with a summary reviewing all the chapters and concluding remarks.

References

[1] Xiaodong Xu, Wang Yao, Di Xiao, and Tony F Heinz. Spin and pseudospins in layered transition metal dichalcogenides. *Nature Physics*, 10(5):343–350, 2014.

[2] Kin Fai Mak, Kathryn L McGill, Jiwoong Park, and Paul L McEuen. The valley hall effect in mos2 transistors. *Science*, 344(6191):1489–1492, 2014.

[3] Zefei Wu, Benjamin T Zhou, Xiangbin Cai, Patrick Cheung, Gui-Bin Liu, Meizhen Huang, Jiangxiazi Lin, Tianyi Han, Liheng An, Yuanwei Wang, et al. Intrinsic valley hall transport in atomically thin mos2. *Nature communications*, 10(1):1–8, 2019.

[4] Zefang Wang, Jie Shan, and Kin Fai Mak. Valley-and spin-polarized landau levels in monolayer wse2. *Nature nanotechnology*, 12(2):144–149, 2017.

[5] G Dorda, I Eisele, and H Gesch. Many-valley interactions in n-type silicon inversion layers. *Physical Review B*, 17(4):1785, 1978.

[6] I Eisele. Stress and intersubband correlation in the silicon inversion layer. *Surface Science*, 73:315–337, 1978.

[7] DC Tsui and G Kaminsky. Observation of sixfold valley degeneracy in electron inversion layers on si (111). *Physical Review Letters*, 42(9):595, 1979.

[8] MJ Kelly and LM Falicov. The dependence of the electronic ground-state of n-type silicon inversion layers on stress, temperature, magnetic field and gate voltage. *Surface Science*, 73:303–314, 1978.

[9] JJ Quinn and G Kawamoto. Charge density waves in silicon inversion layers: Effect of four valley interaction terms. *Solid State Communications*, 28(9):797–801, 1978.

[10] O Gunawan, B Habib, EP De Poortere, and M Shayegan. Quantized conductance in an alas two-dimensional electron system quantum point contact. *Physical Review B*, 74(15):155436, 2006.

[11] NC Bishop, M Padmanabhan, K Vakili, YP Shkolnikov, EP De Poortere, and M Shayegan. Valley polarization and susceptibility of composite fermions around a filling factor ν= 3 2. *Physical review letters*, 98(26):266404, 2007.

[12] YP Shkolnikov, EP De Poortere, E Tutuc, and M Shayegan. Valley splitting of alas two-dimensional electrons in a perpendicular magnetic field. *Physical review letters*, 89(22):226805, 2002.

[13] Kei Takashina, Yukinori Ono, Akira Fujiwara, Yasuo Takahashi, and Yoshiro Hirayama. Valley polarization in si (100) at zero magnetic field. *Physical review letters*, 96(23):236801, 2006.

[14] J Karch, SA Tarasenko, EL Ivchenko, J Kamann, P Olbrich, M Utz, ZD Kvon, and SD Ganichev. Photoexcitation of valley-orbit currents in (111)-oriented silicon metal-oxide-semiconductor field-effect transistors. *Physical Review B*, 83(12):121312, 2011.

[15] Jan Isberg, Markus Gabrysch, Johan Hammersberg, Saman Majdi, Kiran Kumar Kovi, and Daniel J Twitchen. Generation, transport and detection of valley-polarized electrons in diamond. *Nature materials*, 12(8):760–764, 2013.

[16] Zengwei Zhu, Aurélie Collaudin, Benoît Fauqué, Woun Kang, and Kamran Behnia. Field-induced polarization of dirac valleys in bismuth. *Nature Physics*, 8(1):89–94, 2012.

[17] O Gunawan, YP Shkolnikov, K Vakili, T Gokmen, EP De Poortere, and M Shayegan. Valley susceptibility of an interacting two-dimensional electron system. *Physical review letters*, 97(18):186404, 2006.

[18] Valeria Nicolosi, Manish Chhowalla, Mercouri G Kanatzidis, Michael S Strano, and Jonathan N Coleman. Liquid exfoliation of layered materials. *Science*, 340(6139):1226419, 2013.

[19] Zhiyuan Zeng, Ting Sun, Jixin Zhu, Xiao Huang, Zongyou Yin, Gang Lu, Zhanxi Fan, Qingyu Yan, Huey Hoon Hng, and Hua Zhang. An effective method for the fabrication of few-layer-thick inorganic nanosheets. *Angewandte Chemie International Edition*, 51(36):9052–9056, 2012.

[20] Zhiyuan Zeng, Chaoliang Tan, Xiao Huang, Shuyu Bao, and Hua Zhang. Growth of noble metal nanoparticles on single-layer tis 2 and tas 2 nanosheets for hydrogen evolution reaction. *Energy & Environmental Science*, 7(2):797–803, 2014.

[21] Kostya S Novoselov, D Jiang, F Schedin, TJ Booth, VV Khotkevich, SV Morozov, and Andre K Geim. Two-dimensional atomic crystals. *Proceedings of the National Academy of Sciences*, 102(30):10451–10453, 2005.

[22] Hai Li, Gang Lu, Zongyou Yin, Qiyuan He, Hong Li, Qing Zhang, and Hua Zhang. Optical identification of single-and few-layer mos2 sheets. *Small*, 8(5):682–686, 2012.

[23] Dattatray J Late, Bin Liu, HSS Ramakrishna Matte, CNR Rao, and Vinayak P Dravid. Rapid characterization of ultrathin layers of chalcogenides on sio2/si substrates. *Advanced Functional Materials*, 22(9):1894–1905, 2012.

[24] Jian Zheng, Han Zhang, Shaohua Dong, Yanpeng Liu, Chang Tai Nai, Hyeon Suk Shin, Hu Young Jeong, Bo Liu, and Kian Ping Loh. High yield exfoliation of two-dimensional chalcogenides using sodium naphthalenide. *Nature communications*, 5(1):1–7, 2014.

[25] Xing Gu, Wei Cui, Hai Li, Zhongwei Wu, Zhiyuan Zeng, Shuit-Tong Lee, Hua Zhang, and Baoquan Sun. A solution-processed hole extraction layer made from ultrathin mos2 nanosheets for efficient organic solar cells. *Advanced Energy Materials*, 3(10):1262–1268, 2013.

[26] Manish Chhowalla, Hyeon Suk Shin, Goki Eda, Lain-Jong Li, Kian Ping Loh, and Hua Zhang. The chemistry of two-dimensional layered transition metal dichalcogenide nanosheets. *Nature chemistry*, 5(4):263–275, 2013.

[27] Deep Jariwala, Vinod K Sangwan, Lincoln J Lauhon, Tobin J Marks, and Mark C Hersam. Emerging device applications for semiconducting two-dimensional transition metal dichalcogenides. *ACS nano*, 8(2):1102–1120, 2014.

[28] Di Xiao, Gui-Bin Liu, Wanxiang Feng, Xiaodong Xu, and Wang Yao. Coupled spin and valley physics in monolayers of mos 2 and other group-vi dichalcogenides. *Physical review letters*, 108(19):196802, 2012.

[29] Gang Luo, Zhuo-Zhi Zhang, Hai-Ou Li, Xiang-Xiang Song, Guang-Wei Deng, Gang Cao, Ming Xiao, and Guo-Ping Guo. Quantum dot behavior in transition metal dichalcogenides nanostructures. *Frontiers of Physics*, 12(4):1–13, 2017.

[30] Tianshu Li and Giulia Galli. Electronic properties of mos2 nanoparticles. *The Journal of Physical Chemistry C*, 111(44):16192–16196, 2007.

[31] Yi Ding, Yanli Wang, Jun Ni, Lin Shi, Siqi Shi, and Weihua Tang. First principles study of structural, vibrational and electronic properties of graphene-like mx2 (m= mo, nb, w, ta; x= s, se, te) monolayers. *Physica B: Condensed Matter*, 406(11):2254–2260, 2011.

[32] Kin Fai Mak, Changgu Lee, James Hone, Jie Shan, and Tony F Heinz. Atomically thin mos 2: a new direct-gap semiconductor. *Physical review letters*, 105(13):136805, 2010.

[33] Kyunghee Choi, Kimoon Lee, Sanghyuck Yu, Sehoon Oh, Hyoung Joon Choi, Heesun Bae, and Seongil Im. Interband transitions in monolayer and few-layer wse2 probed using photoexcited charge collection spectroscopy. *ACS applied materials & interfaces*, 10(24):20213–20218, 2018.

[34] KK Kam and BA Parkinson. Detailed photocurrent spectroscopy of the semiconducting group vib transition metal dichalcogenides. *The Journal of Physical Chemistry*, 86(4):463–467, 1982.

[35] Terry YT Hung, Kerem Y Camsari, Shengjiao Zhang, Pramey Upadhyaya, and Zhihong Chen. Direct observation of valley-coupled topological current in mos2. *Science advances*, 5(4):eaau6478, 2019.

[36] Elyse Barré, Jean Anne C Incorvia, Suk Hyun Kim, Connor J McClellan, Eric Pop, H-S Philip Wong, and Tony F Heinz. Spatial separation of carrier spin by the valley hall effect in monolayer wse2 transistors. *Nano letters*, 19(2):770–774, 2019.

[37] Lingfei Li, Lei Shao, Xiaowei Liu, Anyuan Gao, Hao Wang, Binjie Zheng, Guozhi Hou, Khurram Shehzad, Linwei Yu, Feng Miao, et al. Room-temperature valleytronic transistor. *Nature nanotechnology*, 15(9):743–749, 2020.

[38] Jieun Lee, Kin Fai Mak, and Jie Shan. Electrical control of the valley hall effect in bilayer mos2 transistors. *Nature nanotechnology*, 11(5):421–425, 2016.

[39] Yilei Li, Jonathan Ludwig, Tony Low, Alexey Chernikov, Xu Cui, Ghidewon Arefe, Young Duck Kim, Arend M Van Der Zande, Albert Rigosi, Heather M Hill, et al. Valley splitting and polarization by the zeeman effect in monolayer mose 2. *Physical review letters*, 113(26):266804, 2014.

[40] Grant Aivazian, Zhirui Gong, Aaron M Jones, Rui-Lin Chu, Jiaqiang Yan, David G Mandrus, Chuanwei Zhang, David Cobden, Wang Yao, and Xiaodong Xu. Magnetic control of valley pseudospin in monolayer wse2. *Nature Physics*, 11(2):148–152, 2015.

[41] David MacNeill, Colin Heikes, Kin Fai Mak, Zachary Anderson, Andor Kormányos, Viktor Zólyomi, Jiwoong Park, and Daniel C Ralph. Breaking of valley degeneracy by magnetic field in monolayer mose 2. *Physical review letters*, 114(3):037401, 2015.

[42] Ajit Srivastava, Meinrad Sidler, Adrien V Allain, Dominik S Lembke, Andras Kis, and A Imamoğlu. Valley zeeman effect in elementary optical excitations of monolayer wse2. *Nature Physics*, 11(2):141–147, 2015.

[43] Gang Wang, Louis Bouet, MM Glazov, Thierry Amand, EL Ivchenko, Etienne Palleau, Xavier Marie, and B Urbaszek. Magneto-optics in transition metal diselenide monolayers. *2D Materials*, 2(3):034002, 2015.

[44] Di Xiao, Wang Yao, and Qian Niu. Valley-contrasting physics in graphene: magnetic moment and topological transport. *Physical review letters*, 99(23):236809, 2007.

[45] Wang Yao, Di Xiao, and Qian Niu. Valley-dependent optoelectronics from inversion symmetry breaking. *Physical Review B*, 77(23):235406, 2008.

[46] R Coehoorn, C Haas, and RA De Groot. Electronic structure of mose 2, mos 2, and wse 2. ii. the nature of the optical band gaps. *Physical Review B*, 35(12):6203, 1987.

[47] Weijie Zhao, Zohreh Ghorannevis, Leiqiang Chu, Minglin Toh, Christian Kloc, Ping-Heng Tan, and Goki Eda. Evolution of electronic structure in atomically thin sheets of ws2 and wse2. *ACS nano*, 7(1):791–797, 2013.

[48] Hualing Zeng, Gui-Bin Liu, Junfeng Dai, Yajun Yan, Bairen Zhu, Ruicong He, Lu Xie, Shijie Xu, Xianhui Chen, Wang Yao, et al. Optical signature of symmetry variations and spin-valley coupling in atomically thin tungsten dichalcogenides. *Scientific reports*, 3(1):1–5, 2013.

[49] Wanxiang Feng, Yugui Yao, Wenguang Zhu, Jinjian Zhou, Wang Yao, and Di Xiao. Intrinsic spin hall effect in monolayers of group-vi dichalcogenides: A first-principles study. *Physical Review B*, 86(16):165108, 2012.

[50] Sanfeng Wu, Jason S Ross, Gui-Bin Liu, Grant Aivazian, Aaron Jones, Zaiyao Fei, Wenguang Zhu, Di Xiao, Wang Yao, David Cobden, et al. Electrical tuning of valley magnetic moment through symmetry control in bilayer mos2. *Nature Physics*, 9(3):149–153, 2013.

[51] Andrea Splendiani, Liang Sun, Yuanbo Zhang, Tianshu Li, Jonghwan Kim, Chi-Yung Chim, Giulia Galli, and Feng Wang. Emerging photoluminescence in monolayer mos2. *Nano letters*, 10(4):1271–1275, 2010.

[52] Agnieszka Kuc, Nourdine Zibouche, and Thomas Heine. Influence of quantum confinement on the electronic structure of the transition metal sulfide t s 2. *Physical Review B*, 83(24):245213, 2011.

[53] Hualing Zeng, Junfeng Dai, Wang Yao, Di Xiao, and Xiaodong Cui. Valley polarization in mos2 monolayers by optical pumping. *Nature nanotechnology*, 7(8):490–493, 2012.

[54] Ting Cao, Gang Wang, Wenpeng Han, Huiqi Ye, Chuanrui Zhu, Junren Shi, Qian Niu, Pingheng Tan, Enge Wang, Baoli Liu, et al. Valley-selective circular dichroism of monolayer molybdenum disulphide. *Nature communications*, 3(1):1–5, 2012.

[55] Kin Fai Mak, Keliang He, Jie Shan, and Tony F Heinz. Control of valley polarization in monolayer mos2 by optical helicity. *Nature nanotechnology*, 7(8):494–498, 2012.

[56] R Suzuki, M Sakano, YJ Zhang, R Akashi, D Morikawa, A Harasawa, K Yaji, K Kuroda, K Miyamoto, T Okuda, et al. Valley-dependent spin polarization in bulk mos2 with broken inversion symmetry. *Nature nanotechnology*, 9(8):611–617, 2014.

[57] Kin Fai Mak, Di Xiao, and Jie Shan. Light–valley interactions in 2d semiconductors. *Nature Photonics*, 12(8):451–460, 2018.

[58] Zefei Wu, Shuigang Xu, Huanhuan Lu, Armin Khamoshi, Gui-Bin Liu, Tianyi Han, Yingying Wu, Jiangxiazi Lin, Gen Long, Yuheng He, et al. Even–odd layer-dependent magnetotransport of high-mobility q-valley electrons in transition metal disulfides. *Nature communications*, 7(1):1–8, 2016.

[59] Babak Fallahazad, Hema CP Movva, Kyounghwan Kim, Stefano Larentis, Takashi Taniguchi, Kenji Watanabe, Sanjay K Banerjee, and Emanuel Tutuc. Shubnikov–de haas oscillations of high-mobility holes in monolayer and bilayer wse 2: Landau level degeneracy, effective mass, and negative compressibility. *Physical review letters*, 116(8):086601, 2016.

[60] Hema CP Movva, Babak Fallahazad, Kyounghwan Kim, Stefano Larentis, Takashi Taniguchi, Kenji Watanabe, Sanjay K Banerjee, and Emanuel Tutuc. Density-dependent quantum hall states and zeeman splitting in monolayer and bilayer wse 2. *Physical review letters*, 118(24):247701, 2017.

[61] Shuigang Xu, Junying Shen, Gen Long, Zefei Wu, Zhi-qiang Bao, Cheng-Cheng Liu, Xiao Xiao, Tianyi Han, Jiangxiazi Lin, Yingying Wu, et al. Odd-integer quantum hall states and giant spin susceptibility in p-type few-layer wse 2. *Physical Review Letters*, 118(6):067702, 2017.

[62] QH Chen, JM Lu, Lei Liang, Oleksandr Zheliuk, A Ali, Ping Sheng, and JT Ye. Inducing and manipulating heteroelectronic states in a single mos 2 thin flake. *Physical Review Letters*, 119(14):147002, 2017.

[63] Riccardo Pisoni, Andor Kormányos, Matthew Brooks, Zijin Lei, Patrick Back, Marius Eich, Hiske Overweg, Yongjin Lee, Peter Rickhaus, Kenji Watanabe, et al. Interactions and magnetotransport through spin-valley coupled landau levels in monolayer mos 2. *Physical review letters*, 121(24):247701, 2018.

[64] Martin V Gustafsson, Matthew Yankowitz, Carlos Forsythe, Daniel Rhodes, Kenji Watanabe, Takashi Taniguchi, James Hone, Xiaoyang Zhu, and Cory R Dean. Ambipolar landau levels and strong band-selective carrier interactions in monolayer wse2. *Nature materials*, 17(5):411–415, 2018.

[65] Hema CP Movva, Timothy Lovorn, Babak Fallahazad, Stefano Larentis, Kyounghwan Kim, Takashi Taniguchi, Kenji Watanabe, Sanjay K Banerjee, Allan H MacDonald, and Emanuel Tutuc. Tunable γ- k valley populations in hole-doped trilayer wse 2. *Physical Review Letters*, 120(10):107703, 2018.

[66] Jiangxiazi Lin, Tianyi Han, Benjamin A Piot, Zefei Wu, Shuigang Xu, Gen Long, Liheng An, Patrick Cheung, Peng-Peng Zheng, Paulina Plochocka, et al. Determining interaction enhanced valley susceptibility in spin-valley-locked mos2. *Nano letters*, 19(3):1736–1742, 2019.

[67] Riccardo Pisoni, Tim Davatz, Kenji Watanabe, Takashi Taniguchi, Thomas Ihn, and Klaus Ensslin. Absence of interlayer tunnel coupling of k-valley electrons in bilayer mos 2. *Physical Review Letters*, 123(11):117702, 2019.

[68] Daniel Loss and David P DiVincenzo. Quantum computation with quantum dots. *Physical Review A*, 57(1):120, 1998.

[69] Jason R Petta, Alexander Comstock Johnson, Jacob M Taylor, Edward A Laird, Amir Yacoby, Mikhail D Lukin, Charles M Marcus, Micah P Hanson, and Arthur C Gossard. Coherent manipulation of coupled electron spins in semiconductor quantum dots. *Science*, 309(5744):2180–2184, 2005.

[70] Ronald Hanson, Leo P Kouwenhoven, Jason R Petta, Seigo Tarucha, and Lieven MK Vandersypen. Spins in few-electron quantum dots. *Reviews of modern physics*, 79(4):1217, 2007.

[71] Christopher C Price, Nathan C Frey, Deep Jariwala, and Vivek B Shenoy. Engineering zero-dimensional quantum confinement in transition-metal dichalcogenide heterostructures. *ACS nano*, 13(7):8303–8311, 2019.

[72] Xiang-Xiang Song, Di Liu, Vahid Mosallanejad, Jie You, Tian-Yi Han, Dian-Teng Chen, Hai-Ou Li, Gang Cao, Ming Xiao, Guang-Can Guo, et al. A gate defined quantum dot on the two-dimensional transition metal dichalcogenide semiconductor wse 2. *Nanoscale*, 7(40):16867–16873, 2015.

[73] Gui-Bin Liu, Hongliang Pang, Yugui Yao, and Wang Yao. Intervalley coupling by quantum dot confinement potentials in monolayer transition metal dichalcogenides. *New Journal of Physics*, 16(10):105011, 2014.

[74] Louis E Brus. Electron–electron and electron-hole interactions in small semiconductor crystallites: The size dependence of the lowest excited electronic state. *The Journal of chemical physics*, 80(9):4403–4409, 1984.

[75] Marcel Bruchez Jr, Mario Moronne, Peter Gin, Shimon Weiss, and A Paul Alivisatos. Semiconductor nanocrystals as fluorescent biological labels. *science*, 281(5385):2013–2016, 1998.

[76] Xavier Michalet, Fabien F Pinaud, Laurent A Bentolila, James M Tsay, SJJL Doose, Jack J Li, G Sundaresan, AM Wu, SS Gambhir, and S Weiss. Quantum dots for live cells, in vivo imaging, and diagnostics. *science*, 307(5709):538–544, 2005.

[77] DJ Eaglesham and M Cerullo. Dislocation-free stranski-krastanow growth of ge on si (100). *Physical review letters*, 64(16):1943, 1990.

[78] D Leonard, M Krishnamurthy, CMv Reaves, Steven P DenBaars, and Pierre M Petroff. Direct formation of quantum-sized dots from uniform coherent islands of ingaas on gaas surfaces. *Applied Physics Letters*, 63(23):3203–3205, 1993.

[79] Nir Tessler, Vlad Medvedev, Miri Kazes, ShiHai Kan, and Uri Banin. Efficient near-infrared polymer nanocrystal light-emitting diodes. *Science*, 295(5559):1506–1508, 2002.

[80] Zhiliang Yuan, Beata E Kardynal, R Mark Stevenson, Andrew J Shields, Charlene J Lobo, Ken Cooper, Neil S Beattie, David A Ritchie, and Michael Pepper. Electrically driven single-photon source. *science*, 295(5552):102–105, 2002.

[81] VI Klimov, AA Mikhailovsky, Su Xu, A Malko, JA Hollingsworth, a CA Leatherdale, H-J Eisler, and MG Bawendi. Optical gain and stimulated emission in nanocrystal quantum dots. *science*, 290(5490):314–317, 2000.

[82] N Kirstaedter, NN Ledentsov, M Grundmann, D Bimberg, VM Ustinov, SS Ruvimov, MV Maximov, and PS Kop'ev. Zh. i. alfenov, u. richter, p. werner, u. gösele and j. heydenreich. *Electron. Lett*, 30:1416, 1994.

[83] P Michler, A Imamoğlu, MD Mason, PJ Carson, GF Strouse, and SK Buratto. Quantum correlation among photons from a single quantum dot at room temperature. *Nature*, 406(6799):968–970, 2000.

[84] MS Skolnick and DJ Mowbray. Recent developments in the physics and applications of self-assembled quantum dots. *Physica E: Low-dimensional Systems and Nanostructures*, 21(2-4):155–163, 2004.

[85] JJ Finley, PW Fry, AD Ashmore, A Lemaître, AI Tartakovskii, R Oulton, DJ Mowbray, MS Skolnick, M Hopkinson, Philip Derek Buckle, et al. Observation of multicharged excitons and biexcitons in a single ingaas quantum dot. *Physical Review B*, 63(16):161305, 2001.

[86] S Rodt, R Heitz, A Schliwa, RL Sellin, F Guffarth, and D Bimberg. Repulsive exciton-exciton interaction in quantum dots. *Physical Review B*, 68(3):035331, 2003.

[87] H Lee, JA Johnson, JS Speck, and PM Petroff. Controlled ordering and positioning of inas self-assembled quantum dots. *Journal of Vacuum Science & Technology B: Microelectronics and Nanometer Structures Processing, Measurement, and Phenomena*, 18(4):2193–2196, 2000.

[88] H Lee, JA Johnson, MY He, JS Speck, and PM Petroff. Strain-engineered self-assembled semiconductor quantum dot lattices. *Applied Physics Letters*, 78(1):105–107, 2001.

[89] BD Gerardot, G Subramanian, S Minvielle, H Lee, JA Johnson, WV Schoenfeld, D Pine, JS Speck, and PM Petroff. Self-assembling quantum dot lattices through nucleation site engineering. *Journal of crystal growth*, 236(4):647–654, 2002.

[90] Jianjun Zhang, Armando Rastelli, Oliver G Schmidt, and Günther Bauer. Compositional evolution of sige islands on patterned si (001) substrates. *Applied Physics Letters*, 97(20):203103, 2010.

[91] JJ Zhang, N Hrauda, H Groiss, A Rastelli, J Stangl, F Schäffler, OG Schmidt, and G Bauer. Strain engineering in si via closely stacked, site-controlled sige islands. *Applied Physics Letters*, 96(19):193101, 2010.

[92] Pierre M Petroff. Semiconductor self-assembled quantum dots: Present status and future trends. *Advanced Materials*, 23(20):2372–2376, 2011.

[93] Yongji Gong, Junhao Lin, Xingli Wang, Gang Shi, Sidong Lei, Zhong Lin, Xiaolong Zou, Gonglan Ye, Robert Vajtai, Boris I Yakobson, et al. Vertical and in-plane heterostructures from ws2/mos2 monolayers. *Nature materials*, 13(12):1135–1142, 2014.

[94] Kostya S Novoselov, Andre K Geim, Sergei V Morozov, De-eng Jiang, Yanshui Zhang, Sergey V Dubonos, Irina V Grigorieva, and Alexandr A Firsov. Electric field effect in atomically thin carbon films. *science*, 306(5696):666–669, 2004.

[95] MI Katsnelson, KS Novoselov, and AK Geim. Chiral tunnelling and the klein paradox in graphene. *Nature physics*, 2(9):620–625, 2006.

[96] Juwon Lee, Dillon Wong, Jairo Velasco Jr, Joaquin F Rodriguez-Nieva, Salman Kahn, Hsin-Zon Tsai, Takashi Taniguchi, Kenji Watanabe, Alex Zettl, Feng Wang, et al. Imaging electrostatically confined dirac fermions in graphene quantum dots. *Nature Physics*, 12(11):1032–1036, 2016.

[97] Christopher Gutiérrez, Lola Brown, Cheol-Joo Kim, Jiwoong Park, and Abhay N Pasupathy. Klein tunnelling and electron trapping in nanometre-scale graphene quantum dots. *Nature Physics*, 12(11):1069–1075, 2016.

[98] Wei Hu and Jinlong Yang. Two-dimensional van der waals heterojunctions for functional materials and devices. *Journal of Materials Chemistry C*, 5(47):12289–12297, 2017.

[99] Saien Xie, Lijie Tu, Yimo Han, Lujie Huang, Kibum Kang, Ka Un Lao, Preeti Poddar, Chibeom Park, David A Muller, Robert A DiStasio Jr, et al. Coherent, atomically thin transition-metal dichalcogenide superlattices with engineered strain. *Science*, 359(6380):1131–1136, 2018.

[100] Zhengwei Zhang, Peng Chen, Xidong Duan, Ketao Zang, Jun Luo, and Xiangfeng Duan. Robust epitaxial growth of two-dimensional heterostructures, multiheterostructures, and superlattices. *Science*, 357(6353):788–792, 2017.

[101] Sarah J Haigh, Ali Gholinia, Rashid Jalil, Simon Romani, Liam Britnell, Daniel C Elias, Konstantin S Novoselov, Leonid A Ponomarenko, Andre K Geim, and R Gorbachev. Cross-sectional imaging of individual layers and buried interfaces of graphene-based heterostructures and superlattices. *Nature materials*, 11(9):764–767, 2012.

[102] Wei Yang, Guorui Chen, Zhiwen Shi, Cheng-Cheng Liu, Lianchang Zhang, Guibai Xie, Meng Cheng, Duoming Wang, Rong Yang, Dongxia Shi, et al. Epitaxial growth of single-domain graphene on hexagonal boron nitride. *Nature materials*, 12(9):792–797, 2013.

[103] Alexander Högele, Christophe Galland, Martin Winger, and Atac Imamoğlu. Photon antibunching in the photoluminescence spectra of a single carbon nanotube. *Physical review letters*, 100(21):217401, 2008.

[104] Brahim Lounis and William E Moerner. Single photons on demand from a single molecule at room temperature. *Nature*, 407(6803):491–493, 2000.

[105] Christian Kurtsiefer, Sonja Mayer, Patrick Zarda, and Harald Weinfurter. Stable solid-state source of single photons. *Physical review letters*, 85(2):290, 2000.

[106] Santosh Kumar, Artur Kaczmarczyk, and Brian D Gerardot. Strain-induced spatial and spectral isolation of quantum emitters in mono-and bilayer wse2. *Nano letters*, 15(11):7567–7573, 2015.

[107] Peter Lodahl, Sahand Mahmoodian, and Søren Stobbe. Interfacing single photons and single quantum dots with photonic nanostructures. *Reviews of Modern Physics*, 87(2):347, 2015.

[108] Richard J Warburton. Single spins in self-assembled quantum dots. *Nature materials*, 12(6):483–493, 2013.

[109] WB Gao, Atac Imamoglu, Hannes Bernien, and Ronald Hanson. Coherent manipulation, measurement and entanglement of individual solid-state spins using optical fields. *Nature Photonics*, 9(6):363–373, 2015.

[110] Yu-Ming He, Genevieve Clark, John R Schaibley, Yu He, Ming-Cheng Chen, Yu-Jia Wei, Xing Ding, Qiang Zhang, Wang Yao, Xiaodong Xu, et al. Single quantum emitters in monolayer semiconductors. *Nature nanotechnology*, 10(6):497–502, 2015.

[111] Aaron M Jones, Hongyi Yu, Nirmal J Ghimire, Sanfeng Wu, Grant Aivazian, Jason S Ross, Bo Zhao, Jiaqiang Yan, David G Mandrus, Di Xiao, et al. Optical generation of excitonic valley coherence in monolayer wse2. *Nature nanotechnology*, 8(9):634–638, 2013.

[112] YJ Zhang, T Oka, Ryo Suzuki, JT Ye, and Y Iwasa. Electrically switchable chiral light-emitting transistor. *Science*, 344(6185):725–728, 2014.

[113] Edbert Jarvis Sie. Valley-selective optical stark effect in monolayer ws 2. In *Coherent Light-Matter Interactions in Monolayer Transition-Metal Dichalcogenides*, pages 37–57. Springer, 2018.

[114] Jonghwan Kim, Xiaoping Hong, Chenhao Jin, Su-Fei Shi, Chih-Yuan S Chang, Ming-Hui Chiu, Lain-Jong Li, and Feng Wang. Ultrafast generation of pseudo-magnetic field for valley excitons in wse2 monolayers. *Science*, 346(6214):1205–1208, 2014.

[115] Philipp Tonndorf, Robert Schmidt, Robert Schneider, Johannes Kern, Michele Buscema, Gary A Steele, Andres Castellanos-Gomez, Herre SJ van der Zant, Steffen Michaelis de Vasconcellos, and Rudolf Bratschitsch. Single-photon emission from localized excitons in an atomically thin semiconductor. *Optica*, 2(4):347–352, 2015.

[116] Ajit Srivastava, Meinrad Sidler, Adrien V Allain, Dominik S Lembke, Andras Kis, and Atac Imamoğlu. Optically active quantum dots in monolayer wse2. *Nature nanotechnology*, 10(6):491–496, 2015.

[117] Maciej Koperski, K Nogajewski, Ashish Arora, V Cherkez, Paul Mallet, J-Y Veuillen, J Marcus, Piotr Kossacki, and M Potemski. Single photon emitters in exfoliated wse2 structures. *Nature nanotechnology*, 10(6):503–506, 2015.

[118] Chitraleema Chakraborty, Laura Kinnischtzke, Kenneth M Goodfellow, Ryan Beams, and A Nick Vamivakas. Voltage-controlled quantum light from an atomically thin semiconductor. *Nature nanotechnology*, 10(6):507–511, 2015.

[119] Toan Trong Tran, Kerem Bray, Michael J Ford, Milos Toth, and Igor Aharonovich. Quantum emission from hexagonal boron nitride monolayers. *Nature nanotechnology*, 11(1):37–41, 2016.

[120] Sefaattin Tongay, Joonki Suh, Can Ataca, Wen Fan, Alexander Luce, Jeong Seuk Kang, Jonathan Liu, Changhyun Ko, Rajamani Raghunathanan, Jian Zhou, et al. Defects activated photoluminescence in two-dimensional semiconductors: interplay between bound, charged and free excitons. *Scientific reports*, 3(1):1–5, 2013.

[121] Artur Branny, Santosh Kumar, Raphaël Proux, and Brian D Gerardot. Deterministic strain-induced arrays of quantum emitters in a two-dimensional semiconductor. *Nature communications*, 8(1):1–7, 2017.

[122] K Kash, R Bhat, Derek D Mahoney, PSD Lin, A Scherer, JM Worlock, BP Van der Gaag, M Koza, and P Grabbe. Strain-induced confinement of carriers to quantum wires and dots within an ingaas-inp quantum well. *Applied physics letters*, 55(7):681–683, 1989.

[123] C Obermüller, A Deisenrieder, G Abstreiter, K Karrai, S Grosse, S Manus, J Feldmann, Harri Lipsanen, Markku Sopanen, and Jouni Ahopelto. Pauli-blocking imaging of single strain-induced semiconductor quantum dots. *Applied physics letters*, 74(21):3200–3202, 1999.

[124] Florian JR Schülein, Arne Laucht, Juha Riikonen, Marco Mattila, Markku Sopanen, Harri Lipsanen, Jonathan J Finley, Achim Wixforth, and Hubert J Krenner. Cascaded exciton emission of an individual strain-induced quantum dot. *Applied Physics Letters*, 95(8):083122, 2009.

[125] D Gershoni, rJ S Weiner, SNG Chu, GA Baraff, JM Vandenberg, LN Pfeiffer, K West, RA Logan, and T Tanbun-Ek. Optical transitions in quantum wires with strain-induced lateral confinement. *Physical Review Letters*, 65(13):1631, 1990.

[126] Simone Bertolazzi, Jacopo Brivio, and Andras Kis. Stretching and breaking of ultrathin mos2. *ACS nano*, 5(12):9703–9709, 2011.

[127] Keliang He, Charles Poole, Kin Fai Mak, and Jie Shan. Experimental demonstration of continuous electronic structure tuning via strain in atomically thin mos2. *Nano letters*, 13(6):2931–2936, 2013.

[128] Hiram J Conley, Bin Wang, Jed I Ziegler, Richard F Haglund Jr, Sokrates T Pantelides, and Kirill I Bolotin. Bandgap engineering of strained monolayer and bilayer mos2. *Nano letters*, 13(8):3626–3630, 2013.

[129] Andres Castellanos-Gomez, Rafael Roldán, Emmanuele Cappelluti, Michele Buscema, Francisco Guinea, Herre SJ van der Zant, and Gary A Steele. Local strain engineering in atomically thin mos2. *Nano letters*, 13(11):5361–5366, 2013.

[130] CR Zhu, Gang Wang, BL Liu, Xavier Marie, XF Qiao, X Zhang, XX Wu, H Fan, PH Tan, Thierry Amand, et al. Strain tuning of optical emission energy and polarization in monolayer and bilayer mos 2. *Physical Review B*, 88(12):121301, 2013.

[131] Sujay B Desai, Gyungseon Seol, Jeong Seuk Kang, Hui Fang, Corsin Battaglia, Rehan Kapadia, Joel W Ager, Jing Guo, and Ali Javey. Strain-induced indirect to direct bandgap transition in multilayer wse2. *Nano letters*, 14(8):4592–4597, 2014.

[132] Artur Branny, Gang Wang, Santosh Kumar, Cedric Robert, Benjamin Lassagne, Xavier Marie, Brian D Gerardot, and Bernhard Urbaszek. Discrete quantum dot like emitters in monolayer mose2: Spatial mapping, magneto-optics, and charge tuning. *Applied Physics Letters*, 108(14):142101, 2016.

[133] Johannes Kern, Iris Niehues, Philipp Tonndorf, Robert Schmidt, Daniel Wigger, Robert Schneider, Torsten Stiehm, Steffen Michaelis de Vasconcellos, Doris E Reiter, Tilmann Kuhn, et al. Nanoscale positioning of single-photon emitters in atomically thin wse2. *Advanced materials*, 28(33):7101–7105, 2016.

[134] Carmen Palacios-Berraquero, Dhiren M Kara, Alejandro R-P Montblanch, Matteo Barbone, Pawel Latawiec, Duhee Yoon, Anna K Ott, Marko Loncar, Andrea C Ferrari, and Mete Atatüre. Large-scale quantum-emitter arrays in atomically thin semiconductors. *Nature communications*, 8(1):1–6, 2017.

[135] Rafael Roldán, Andrés Castellanos-Gomez, Emmanuele Cappelluti, and Francisco Guinea. Strain engineering in semiconducting two-dimensional crystals. *Journal of Physics: Condensed Matter*, 27(31):313201, 2015.

[136] Andre K Geim and Irina V Grigorieva. Van der waals heterostructures. *Nature*, 499(7459):419–425, 2013.

[137] KS Novoselov, o A Mishchenko, o A Carvalho, and AH Castro Neto. 2d materials and van der waals heterostructures. *Science*, 353(6298):aac9439, 2016.

[138] Yuan Cao, Valla Fatemi, Shiang Fang, Kenji Watanabe, Takashi Taniguchi, Efthimios Kaxiras, and Pablo Jarillo-Herrero. Unconventional superconductivity in magic-angle graphene superlattices. *Nature*, 556(7699):43–50, 2018.

[139] Benjamin Hunt, Javier D Sanchez-Yamagishi, Andrea F Young, Matthew Yankowitz, Brian J LeRoy, Kenji Watanabe, Takashi Taniguchi, Pilkyung Moon, Mikito Koshino, Pablo Jarillo-Herrero, et al. Massive dirac fermions and hofstadter butterfly in a van der waals heterostructure. *Science*, 340(6139):1427–1430, 2013.

[140] Cory R Dean, L Wang, P Maher, C Forsythe, Fereshte Ghahari, Y Gao, Jyoti Katoch, M Ishigami, P Moon, M Koshino, et al. Hofstadter's butterfly and the fractal quantum hall effect in moiré superlattices. *Nature*, 497(7451):598–602, 2013.

[141] Kyounghwan Kim, Ashley DaSilva, Shengqiang Huang, Babak Fallahazad, Stefano Larentis, Takashi Taniguchi, Kenji Watanabe, Brian J LeRoy, Allan H MacDonald, and Emanuel Tutuc. Tunable moiré bands and strong correlations in small-twist-angle bilayer graphene. *Proceedings of the National Academy of Sciences*, 114(13):3364–3369, 2017.

[142] LA Ponomarenko, RV Gorbachev, GL Yu, DC Elias, R Jalil, AA Patel, A Mishchenko, AS Mayorov, CR Woods, JR Wallbank, et al. Cloning of dirac fermions in graphene superlattices. *Nature*, 497(7451):594–597, 2013.

[143] M Kuwabara, D R_ Clarke, and DA Smith. Anomalous superperiodicity in scanning tunneling microscope images of graphite. *Applied physics letters*, 56(24):2396–2398, 1990.

[144] Arend M Van Der Zande, Jens Kunstmann, Alexey Chernikov, Daniel A Chenet, YuMeng You, XiaoXiao Zhang, Pinshane Y Huang, Timothy C Berkelbach, Lei Wang, Fan Zhang, et al. Tailoring the electronic structure in bilayer molybdenum disulfide via interlayer twist. *Nano letters*, 14(7):3869–3875, 2014.

[145] Kha Tran, Galan Moody, Fengcheng Wu, Xiaobo Lu, Junho Choi, Kyounghwan Kim, Amritesh Rai, Daniel A Sanchez, Jiamin Quan, Akshay Singh, et al. Evidence for moiré excitons in van der waals heterostructures. *Nature*, 567(7746):71–75, 2019.

[146] Kyle L Seyler, Pasqual Rivera, Hongyi Yu, Nathan P Wilson, Essance L Ray, David G Mandrus, Jiaqiang Yan, Wang Yao, and Xiaodong Xu. Signatures of moiré-trapped valley excitons in mose2/wse2 heterobilayers. *Nature*, 567(7746):66–70, 2019.

[147] Fengcheng Wu, Timothy Lovorn, and AH MacDonald. Theory of optical absorption by interlayer excitons in transition metal dichalcogenide heterobilayers. *Physical Review B*, 97(3):035306, 2018.

[148] Fengcheng Wu, Timothy Lovorn, and Allan H MacDonald. Topological exciton bands in moiré heterojunctions. *Physical review letters*, 118(14):147401, 2017.

[149] Hongyi Yu, Gui-Bin Liu, Jianju Tang, Xiaodong Xu, and Wang Yao. Moiré excitons: From programmable quantum emitter arrays to spin-orbit–coupled artificial lattices. *Science advances*, 3(11):e1701696, 2017.

[150] Roland Gillen and Janina Maultzsch. Interlayer excitons in mose 2/wse 2 heterostructures from first principles. *Physical Review B*, 97(16):165306, 2018.

[151] Pasqual Rivera, Hongyi Yu, Kyle L Seyler, Nathan P Wilson, Wang Yao, and Xiaodong Xu. Interlayer valley excitons in heterobilayers of transition metal dichalcogenides. *Nature nanotechnology*, 13(11):1004–1015, 2018.

[152] Hoseok Heo, Ji Ho Sung, Soonyoung Cha, Bo-Gyu Jang, Joo-Youn Kim, Gangtae Jin, Donghun Lee, Ji-Hoon Ahn, Myoung-Jae Lee, Ji Hoon Shim, et al. Interlayer orientation-dependent light absorption and emission in monolayer semiconductor stacks. *Nature communications*, 6(1):1–7, 2015.

[153] Pramoda K Nayak, Yevhen Horbatenko, Seongjoon Ahn, Gwangwoo Kim, Jae-Ung Lee, Kyung Yeol Ma, A-Rang Jang, Hyunseob Lim, Dogyeong Kim, Sunmin Ryu, et al. Probing evolution of twist-angle-dependent interlayer excitons in mose2/wse2 van der waals heterostructures. *ACS nano*, 11(4):4041–4050, 2017.

[154] DV Averin and KK Likharev. Coulomb blockade of single-electron tunneling, and coherent oscillations in small tunnel junctions. *Journal of low temperature physics*, 62(3):345–373, 1986.

[155] Carlo WJ Beenakker. Theory of coulomb-blockade oscillations in the conductance of a quantum dot. *Physical Review B*, 44(4):1646, 1991.

[156] Leo P Kouwenhoven, Charles M Marcus, Paul L McEuen, Seigo Tarucha, Robert M Westervelt, and Ned S Wingreen. Electron transport in quantum dots. In *Mesoscopic electron transport*, pages 105–214. Springer, 1997.

[157] R Hanson, LP Kouwenhoven, JR Petta, S Tarucha, and LMK Vandersypen. Publisher's note: Spins in few-electron quantum dots [rev. mod. phys. 79, 1217 (2007)]. *Reviews of Modern Physics*, 79(4):1455, 2007.

[158] Fang-Ming Jing, Zhuo-Zhi Zhang, Guo-Quan Qin, Gang Luo, Gang Cao, Hai-Ou Li, Xiang-Xiang Song, and Guo-Ping Guo. Gate-controlled quantum dots based on 2d materials. *Advanced Quantum Technologies*, page 2100162, 2022.

[159] Kyunghoon Lee, Girish Kulkarni, and Zhaohui Zhong. Coulomb blockade in monolayer mos 2 single electron transistor. *Nanoscale*, 8(14):7755–7760, 2016.

[160] Jiwoong Park. *Electron transport in single molecule transistors*. University of California, Berkeley, 2003.

[161] Zhaohui Zhong, Ying Fang, Wei Lu, and Charles M Lieber. Coherent single charge transport in molecular-scale silicon nanowires. *Nano letters*, 5(6):1143–1146, 2005.

[162] Amelia Barreiro, Herre SJ van der Zant, and Lieven MK Vandersypen. Quantum dots at room temperature carved out from few-layer graphene. *Nano letters*, 12(12):6096–6100, 2012.

[163] Xiang-Xiang Song, Zhuo-Zhi Zhang, Jie You, Di Liu, Hai-Ou Li, Gang Cao, Ming Xiao, and Guo-Ping Guo. Temperature dependence of coulomb oscillations in a few-layer two-dimensional ws2 quantum dot. *Scientific reports*, 5(1):1–7, 2015.

[164] Ke Wang, Kristiaan De Greve, Luis A Jauregui, Andrey Sushko, Alexander High, You Zhou, Giovanni Scuri, Takashi Taniguchi, Kenji Watanabe, Mikhail D Lukin, et al. Electrical control of charged carriers and excitons in atomically thin materials. *Nature nanotechnology*, 13(2):128–132, 2018.

[165] Jens Martin, Nitzan Akerman, G Ulbricht, T Lohmann, JH v Smet, K Von Klitzing, and Amir Yacoby. Observation of electron–hole puddles in graphene using a scanning single-electron transistor. *Nature physics*, 4(2):144–148, 2008.

[166] Xiang-Xiang Song, Hai-Ou Li, Jie You, Tian-Yi Han, Gang Cao, Tao Tu, Ming Xiao, Guang-Can Guo, Hong-Wen Jiang, and Guo-Ping Guo. Suspending effect on low-frequency charge noise in graphene quantum dot. *Scientific reports*, 5(1):1–6, 2015.

[167] C Payette, K Wang, PJ Koppinen, Y Dovzhenko, James C Sturm, and Jason R Petta. Single charge sensing and transport in double quantum dots fabricated from commercially grown si/sige heterostructures. *Applied Physics Letters*, 100(4):043508, 2012.

[168] Dominik Bischoff, Marius Eich, Oded Zilberberg, C Rossler, Thomas Ihn, and Klaus Ensslin. Measurement back-action in stacked graphene quantum dots. *Nano letters*, 15(9):6003–6008, 2015.

[169] Minsheng Wang, Emil B Song, Sejoon Lee, Jianshi Tang, Murong Lang, Caifu Zeng, Guangyu Xu, Yi Zhou, and Kang L Wang. Quantum dot behavior in bilayer graphene nanoribbons. *ACS nano*, 5(11):8769–8773, 2011.

[170] Xu Cui, Gwan-Hyoung Lee, Young Duck Kim, Ghidewon Arefe, Pinshane Y Huang, Chul-Ho Lee, Daniel A Chenet, Xian Zhang, Lei Wang, Fan Ye, et al. Multi-terminal transport measurements of mos2 using a van der waals heterostructure device platform. *Nature nanotechnology*, 10(6):534–540, 2015.

[171] Morteza Kayyalha, Jesse Maassen, Mark Lundstrom, Li Shi, and Yong P Chen. Gate-tunable and thickness-dependent electronic and thermoelectric transport in few-layer mos2. *Journal of Applied Physics*, 120(13):134305, 2016.

[172] Wei Liu, Jiahao Kang, Deblina Sarkar, Yasin Khatami, Debdeep Jena, and Kaustav Banerjee. Role of metal contacts in designing high-performance monolayer n-type wse2 field effect transistors. *Nano letters*, 13(5):1983–1990, 2013.

[173] Saptarshi Das, Hong-Yan Chen, Ashish Verma Penumatcha, and Joerg Appenzeller. High performance multilayer mos2 transistors with scandium contacts. *Nano letters*, 13(1):100–105, 2013.

[174] Han Liu, Mengwei Si, Yexin Deng, Adam T Neal, Yuchen Du, Sina Najmaei, Pulickel M Ajayan, Jun Lou, and Peide D Ye. Switching mechanism in single-layer molybdenum disulfide transistors: An insight into current flow across schottky barriers. *ACS nano*, 8(1):1031–1038, 2014.

[175] Jiahao Kang, Wei Liu, Deblina Sarkar, Debdeep Jena, and Kaustav Banerjee. Computational study of metal contacts to monolayer transition-metal dichalcogenide semiconductors. *Physical Review X*, 4(3):031005, 2014.

[176] Han Liu, Adam T Neal, and Peide D Ye. Channel length scaling of mos2 mosfets. *ACS nano*, 6(10):8563–8569, 2012.

[177] Rajesh Kappera, Damien Voiry, Sibel Ebru Yalcin, Brittany Branch, Gautam Gupta, Aditya D Mohite, and Manish Chhowalla. Phase-engineered low-resistance contacts for ultrathin mos2 transistors. *Nature materials*, 13(12):1128–1134, 2014.

[178] Lili Yu, Yi-Hsien Lee, Xi Ling, Elton JG Santos, Yong Cheol Shin, Yuxuan Lin, Madan Dubey, Efthimios Kaxiras, Jing Kong, Han Wang, et al. Graphene/mos2 hybrid

technology for large-scale two-dimensional electronics. *Nano letters*, 14(6):3055–3063, 2014.

[179] L Marty, V Bouchiat, C Naud, M Chaumont, T Fournier, and AM Bonnot. Schottky barriers and coulomb blockade in self-assembled carbon nanotube fets. *Nano Letters*, 3(8):1115–1118, 2003.

[180] Branimir Radisavljevic, Aleksandra Radenovic, Jacopo Brivio, Valentina Giacometti, and Andras Kis. Single-layer mos2 transistors. *Nature nanotechnology*, 6(3):147–150, 2011.

[181] Justin Boddison-Chouinard, Alex Bogan, Norman Fong, Kenji Watanabe, Takashi Taniguchi, Sergei Studenikin, Andrew Sachrajda, Marek Korkusinski, Abdulmenaf Altintas, Maciej Bieniek, et al. Gate-controlled quantum dots in monolayer wse2. *Applied Physics Letters*, 119(13):133104, 2021.

[182] Qing Hua Wang, Kourosh Kalantar-Zadeh, Andras Kis, Jonathan N Coleman, and Michael S Strano. Electronics and optoelectronics of two-dimensional transition metal dichalcogenides. *Nature nanotechnology*, 7(11):699–712, 2012.

[183] Galan Moody, Corey McDonald, Ari Feldman, Todd Harvey, Richard P Mirin, and Kevin L Silverman. Electronic enhancement of the exciton coherence time in charged quantum dots. *Physical review letters*, 116(3):037402, 2016.

[184] A Pioda, E Totoki, H Kiyama, T Fujita, G Allison, T Asayama, A Oiwa, and S Tarucha. Single-shot detection of electrons generated by individual photons in a tunable lateral quantum dot. *Physical Review Letters*, 106(14):146804, 2011.

[185] ZX Gan, LZ Liu, HY Wu, YL Hao, Y Shan, XL Wu, and Paul K Chu. Quantum confinement effects across two-dimensional planes in mos2 quantum dots. *Applied Physics Letters*, 106(23):233113, 2015.

[186] Deepesh Gopalakrishnan, Dijo Damien, Bo Li, Hemtej Gullappalli, Vijayamohanan K Pillai, Pulickel M Ajayan, and Manikoth M Shaijumon. Electrochemical synthesis of luminescent mos 2 quantum dots. *Chemical Communications*, 51(29):6293–6296, 2015.

[187] Ho Jin, Minji Ahn, Sohee Jeong, Jae Hyo Han, Dongwon Yoo, Dong Hee Son, and Jinwoo Cheon. Colloidal single-layer quantum dots with lateral confinement effects on 2d exciton. *Journal of the American Chemical Society*, 138(40):13253–13259, 2016.

Chapter 2

Gate-Defined Accumulation-Mode Quantum Dots in Monolayer and Bilayer Tungsten Diselenide

2.1 Abstract

We report the fabrication and characterization of gate-defined hole quantum dots in monolayer and bilayer WSe_2. The devices were operated with gates above and below the WSe_2 layer to accumulate a hole gas, which for some devices was then selectively depleted to define the dot. Temperature dependence of conductance in the Coulomb blockade regime is consistent with transport through a single level, and excited state transport through the dots was observed at temperatures up to 10 K. For adjacent charge states of a bilayer WSe_2 dot, magnetic field dependence of excited state energies was used to estimate g-factors between 0.8 and 2.4 for different states. These devices provide a platform to evaluate valley-spin states in monolayer and bilayer WSe_2 for application as qubits.

2.2 Introduction

Certain crystals possess two or more inequivalent band extrema, or valleys, that can serve as a pseudospin defining a qubit. Application of the valley and spin degrees of freedom for qubits was demonstrated in carbon nanotube quantum dots [1] and has also been investigated in Si quantum dots [2, 3]. As an alternative, coherent valleytronics using few-layer transition metal dichalcogenides (TMDs) and their heterostructures offers long-lived and coherent valley-spin states [4–14], several proposals for qubit designs [15–22], and an inherent light-matter interface for control, readout, and coupling to other quantum systems [23]. Confinement sufficient to address valley-spin states of a small number of particles is required to define a qubit in this context, and significant recent activity in this area has focused on quantum emitters localized by defects [24–27], strain [28–30], and moiré patterns [31–34]. For the valley pseudospin,

localization to length scales not significantly larger than the lattice spacing generates valley coupling that would be detrimental to the design and coherence of an eventual TMD valley-spin qubit [35]. Gate-defined quantum dots, in addition to allowing electronic probes and electrical control of devices, provide a means to tune the confinement length L in valley-based qubits to balance the competing demands of valley coupling in small dots against impractically small level spacing $\Delta \propto 1/L^2$ in large dots. TMD single quantum dots defined by gates have been reported for multi-layer WSe_2 and WS_2 [36, 37] and few-layer MoS_2 [38–40], and a double quantum dot has been reported in multilayer MoS_2 [41]. Additionally, excited states have been observed in a dot defined in a MoS_2 nanotube [42], and size-controlled dots have also been formed in etched MoS_2 [43]. All gate-defined, two-dimensional TMD quantum dot devices reported so far have operated in a so-called classical limit, $\Delta < k_B T$, in which the individual quantum states required to define an eventual qubit were not resolved [44]. We report the fabrication and characterization of gate-defined hole quantum dots using monolayer and bilayer WSe_2, which has so far been the most actively investigated and promising material for non-gate-defined quantum emitters. Our devices have $L \sim 25$ nm, small enough for the observation of discrete levels at temperatures up to 10 K. Because of the low level of unintentional doping in monolayer and bilayer WSe_2, an additional accumulation gate was required to generate a hole gas within which the dot could be defined, similar to an approach that has been used successfully for quantum dots in Si [45, 46]. Temperature dependence of a Coulomb blockade conductance peak maximum confirms single-level transport, and comparison of excited state energies at different magnetic fields provides a lower-bound on the g-factors of excited states of adjacent charge states in a bilayer WSe_2 quantum dot ranging from $g = 0.8$ to 2.4.

2.3 Experimental Methods

Because of the relatively large band gap and heavy effective mass in WSe_2 compared to most other materials used for gate-defined quantum dots, two principles guided the design of our

devices: first, gate dimensions were made as small as possible to maximize Δ, and second, metal contacts were brought as close as possible to the entrance and exit of the dot to avoid the creation of multiple accidental dots in the contact region.

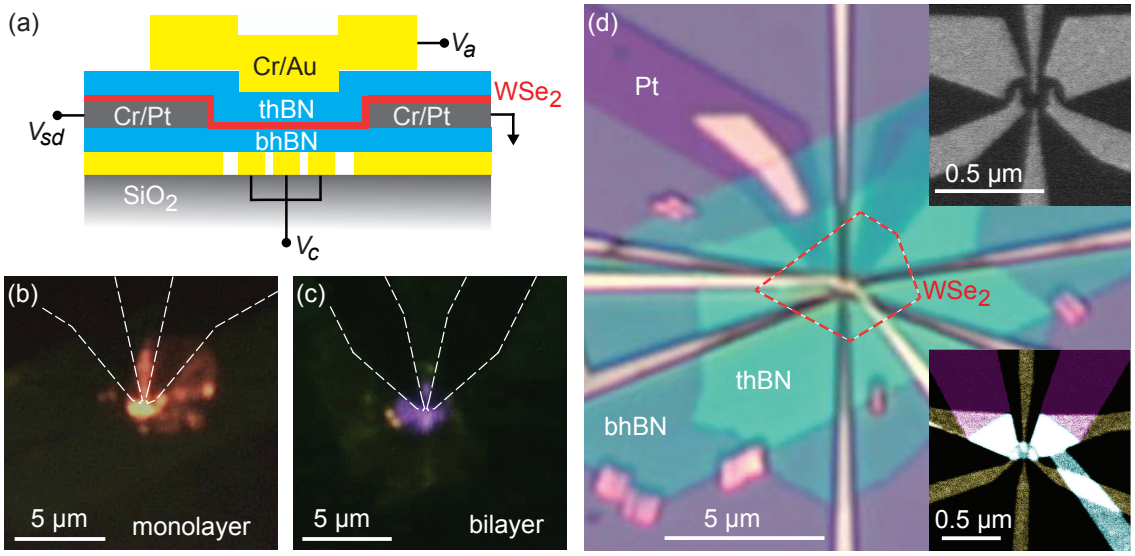

Figure 2.1: (a) Schematic of monolayer or bilayer WSe_2 quantum dot devices, contacted on bottom by Pt, encapsulated by top (thBN) and bottom (bhBN) layers, and with bottom confining gates and a top accumulation gate. (b) Photoluminescence images of a monolayer and (c) bilayer WSe_2 device with contacts outlined in white. (d) Optical image of a complete device (location of the WSe_2 outlined with red dashed line). Upper inset: scanning electron micrograph of the confining gates. Lower inset: false-color scanning electron micrograph of a complete device showing alignment of the confining gates (yellow), hBN-support gates (green), contacts (purple), and accumulation gate (blue).

A schematic of the WSe_2 quantum dot devices we fabricated is shown in Fig. 1(a), in which monolayer or bilayer WSe_2 was encapsulated by two hBN layers and contacted from below with Pt. The devices were gated on top with a single accumulation gate and on bottom with four confining gates. In detail, fabrication began with lithography and evaporation (5/15 nm Cr/Au) of bottom confining gates defining a quantum dot with a lithographic diameter of ∼80-100 nm [upper right inset to Fig. 1(d)]. We note that the larger gates under the contact region of the device [colored green in the lower right inset to Fig. 1(d)] were not used electrically, but were present to promote flatness of the final hBN/WSe_2/hBN stack (without these features, the bottom hBN layer invariably wrinkled in the dot region).

Next, the confining gates were insulated by polycarbonate-based dry transfer of the bottom hBN layer (∼10 nm thick), which was tacked in place around the perimeter [Fig. 1(d)] to prevent lateral movement during the second transfer. Bottom contacts for the WSe_2 were then patterned on the bottom hBN layer using 2/8 nm of Cr/Pt deposited by electron beam evaporation [47]. To remove processing residue from the bottom hBN, the devices were then annealed for 3 hours at 200 °C in forming gas (3% H_2 in Ar). Bulk WSe_2 grown by chemical vapor transport was mechanically exfoliated to obtain monolayer and bilayer flakes, which were identified and confirmed using photoluminescence imaging and spectroscopy [48]. hBN flakes were also obtained by exfoliation of bulk crystals, and the top hBN layer (∼10 nm thick) and monolayer or bilayer WSe_2 were then picked up and transferred onto the contacts and bottom hBN.Photoluminescence images for monolayer and bilayer WSe_2 at this stage of the fabrication process are shown in Figs. 1(b) and 1(c), respectively. The top accumulation gate and bond pads (5 nm Cr and 40-65 nm Au) were then defined in a final lithography step. The accumulation gate is shaped such that holes accumulate only in the dot and contact regions of the WSe_2 flake. The overlay of all three metal layers is shown in the lower right inset to Fig. 1(d) [1]. Finally, a second forming gas anneal identical to the first one was necessary to achieve adequate contact transparency for low-temperature, low-frequency transport measurements. An optical image of a completed device is shown in Fig. 1(d) with the location of the monolayer WSe_2 outlined in red. Devices were measured using standard DC transport and lock-in techniques in a pumped ^{4}He cryostat (2 K) or a dilution refrigerator (50 mK).

2.4 Results and Discussion

Six devices (two monolayers and four bilayers) were measured, and we focus on electronic transport data for three of them, one monolayer device (denoted ML) and two bilayer devices (BL1 and BL2). First, DC current at fixed source-drain bias V_{sd} was measured as a function of

[1]To promote adhesion the accumulation gate was extended in later designs across the entire width of the top and bottom hBN layers, but this feature is not present in the lower right inset to Fig. 1(d).

the voltage applied to the accumulation gate, V_a. Both monolayer devices displayed ambipolar transport characteristics as shown in Fig. 2(a) for device ML at a temperature of 55 mK and $V_{sd} = 12$ mV. Current strongly favored hole conduction, as expected for the high work function Pt contacts [47]. Bilayer devices were similar but with generally lower resistance, and in contrast to the monolayer devices, no measurable n-type current reliably distinct from leakage current was observed, even at a relatively high $V_{sd} = 0.3$ V and higher temperature (2.3 K), as shown in Fig. 2(b).

In measurements of differential conductance as a function of V_{sd} and gate voltage (V_a, confining gate voltage V_c, or both), all six devices showed diamond-shaped conductance features indicative of Coulomb blockade. Devices with higher resistance formed quantum dots when only V_a was swept (accumulation mode), presumably because of sufficiently high contact resistance to form tunnel barriers at the contacts. One example of accumulation mode operation is shown in Fig. 2(c) for device ML, in which we note a transition from well-defined though somewhat irregular Coulomb diamonds for $V_a >$ -3.5 V to a more open regime for lower V_a. Upward- and downward-moving features in Fig. 2(c) have slopes with similar magnitudes (+0.21 and -0.19 V/V). Defining contributions to the dot capacitance from the source, drain, accumulation gate, and all confining gates as C_s, C_d, C_a, and C_c, respectively, we expect features with slope magnitudes of C_a/C_s and $C_a/(C_d + C_c)$ [49]. Because $C_d \gg C_c$, near-equality of slope magnitudes implies $C_s \simeq C_d$ and locates the dot approximately equidistant from each lead.

In lower resistance devices such as BL1 [Fig. 2(b)], activation of the confining gates was required to form a dot by depleting charge accumulated by V_a. Coulomb diamonds for this device as a function of V_{sd} and V_c at V_a = -3 V are shown in Fig. 2(d). Here V_c is the voltage applied to all confining gates simultaneously. In this case the Coulomb diamonds are tilted with unequal slopes for positively- and negatively-sloped features. In a Coulomb diamond measured as a function of V_c, the slopes are C_c/C_s and $C_c/(C_d + C_a)$ [49]. Because $C_a \gg C_c$,

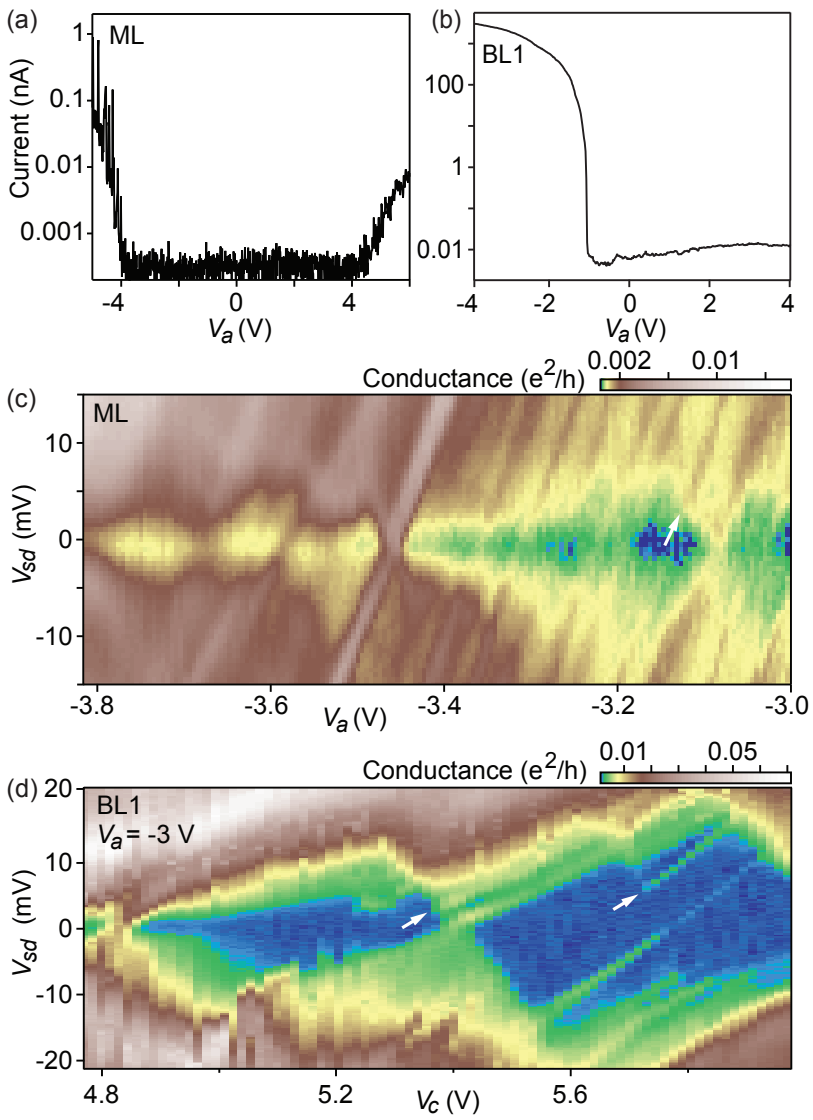

Figure 2.2: (a) Current as a function of V_a for monolayer device ML at a temperature of 50 mK. (b) Current as a function of V_a for bilayer device BL1 at a temperature of 2.1 K. (c) Conductance as a function of V_{sd} and V_a for device ML. (d) Conductance as a function of V_{sd} and V_c with V_a = -3 V.

C_a cannot be neglected in the denominator of the latter slope; therefore, diamonds as a function of V_c are expected to be tilted even for $C_s = C_d$.

We also note the appearance of clear finite-bias resonances in the Coulomb diamonds of both devices ML and BL1, marked with white arrows in Figs. 2(c) and (d). For example, these resonances appear most prominently in Fig. 2(d) at positive bias for the charge transitions near V_c = 5.4 and 5.7 V. Such features may arise from excited valley, spin, and/or orbital

states in the limit $\Delta > k_B T$, but various extrinsic mechanisms such as quasi-one-dimensional density of states fluctuations in the leads could also give rise to finite-bias conductance resonances even for $\Delta < k_B T$, particularly for devices such as ours with narrow leads [50–52].

We now examine two scenarios for the observed finite-bias conductance resonances, one involving single-level transport only and one involving multi-level transport combined with some extrinsic mechanism giving rise to the finite-bias resonances. The temperature dependence of the Coulomb blockade peak height is a standard method to distinguish between single- and multi-level transport through a quantum dot: the peak resistance is linear in T in the single-level case and independent of T in the multi-level case [44, 53]. For example, Song *et al.* demonstrated the multi-level, temperature-independent regime for a WS_2 quantum dot [37]. In Fig. 3(a) we show the evolution of a Coulomb blockade peak at zero bias for temperatures from 2.1 to 10 K for a second bilayer WSe_2 device, BL2. The resistance at the peak increases approximately linearly [Fig. 3(b)], consistent with single-level transport. We therefore conclude that device BL2 and all our other devices, which are lithographically identical to BL2, are small enough that $\Delta > k_B T$, and we associate the finite-bias conductance resonances with excited states of the quantum dots. Additionally, given our accumulation gate geometry in which V_a modulates the carrier density in the dot as well as the WSe_2 covering the contacts, we would not expect density of states resonances in the leads to be parallel to the Coulomb diamond edges.

Next we investigate the magnetic field dependence of excited state energies for two adjacent charge states in device BL2 (Fig. 4). We applied a field perpendicular to the WSe_2 because the large out-of-plane Zeeman-like spin splitting due to spin-orbit coupling [54] suppresses in-plane moments of valley-spin states in monolayer TMDs [55]. This situation also applies to bilayer TMDs because of weak interlayer coupling [15] and "hidden spin polarization" [**?** **?**]. At zero field an excited state, denoted α, is visible at 0.4 meV above the ground state of the charge state labeled N in Fig. 4(a). In a perpendicular magnetic field of 8 T, this state

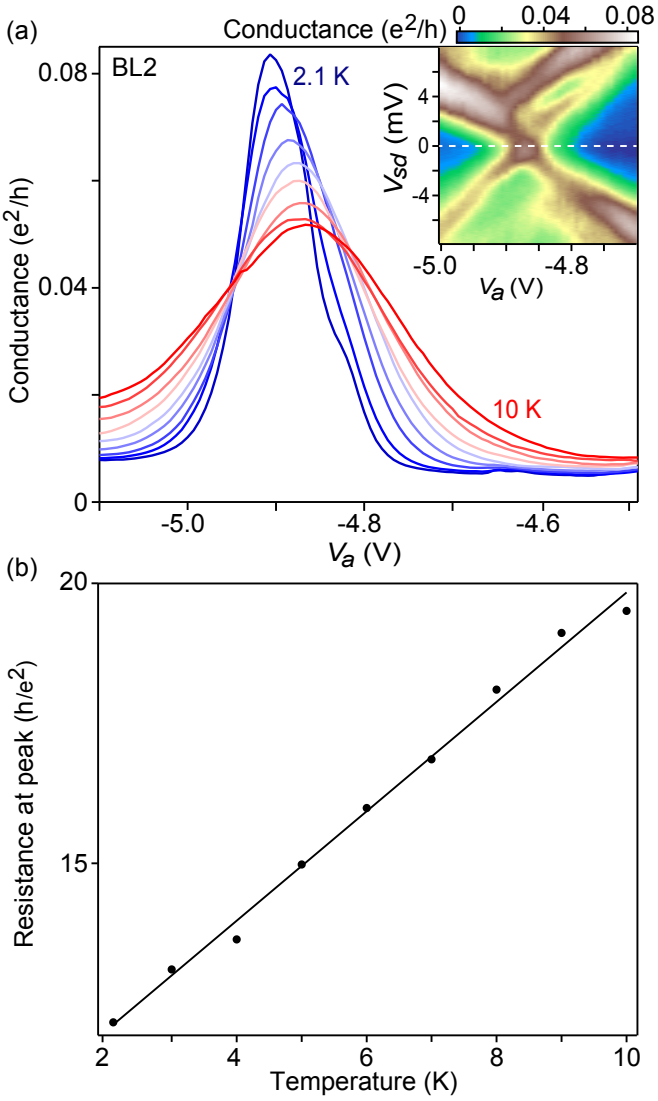

Figure 2.3: (a) Conductance at zero bias and zero magnetic field as a function of V_a at temperatures from 2.1 (blue) to 10 K (red) for device BL2. Inset: Coulomb diamond associated with the data shown in (a), taken in a magnetic field of 8 T and at a temperature of 2.3 K. (b) Peak resistance of the curves in (a) as a function of temperature. The solid black line is a linear fit.

moves up to an energy of 0.8 meV without splitting, and for the N-1 charge state, an excited state, β, appears at 0.9 meV while the ground state conductance is suppressed [Fig. 4(b)]. Additionally, the state labeled γ in Fig. 4(a) splits by 1.1 meV, as indicated by the dashed black lines in Fig. 4(b). Based on these energy shifts of $E_Z = g\mu_B B$, we calculate g-factors of 0.8, 1.9, and 2.4 for α, β, and γ, respectively. These estimates represent lower bounds on the g-factors because this method of measurement is insensitive to intermediate level

crossings that may occur between 0 and 8 T. We emphasize that these g-factors, which are significantly smaller than those observed for confined WSe_2 excitons [24–27], are not expected to be generic to all WSe_2 quantum dots, different even/odd charge state pairs within the same dot, or even different levels of the same charge state. First, in addition to dot orbital effects in perpendicular field, the Zeeman energy in WSe_2 hole quantum dots has contributions from spin, valley, and atomic orbital magnetic moments [56] which in a simple model could individually combine to add or subtract from the total moment of a given state [57], or that may each be coupled in complicated ways through device-specific parameters. Second, while the dominant contribution to spin-orbit coupling in TMDs is Zeeman-like, Rashba spin-orbit coupling is expected to be non-negligible in aggressively gated devices [58], and g-factors may therefore be dependent on device geometry and electric fields as well [59, 60].

Given the expected importance of dot size to valley coupling strength and the performance of eventual coherent valleytronic devices, we roughly estimate the diameter of our dots using the gate capacitance. The change in gate voltage required to add one hole to the dot is

$$\Delta V_a = \frac{e}{C_a}\left(1 + \frac{\Delta}{E_C}\right),$$

where C_a is the accumulation gate capacitance and E_C is the charging energy [61]. For the charge state labeled N-1 in Fig. 4(b), the addition energy is $E_{add} \equiv E_C + \Delta = 4.8$ meV. To obtain Δ, we note that the (N-1)-hole excited state γ at V_a = -4.9 V in Fig. 4(a) moves with V_a at the same slope as the boundaries of the diamond and that γ splits in a magnetic field. These observations strongly suggest that γ is an orbital excited state of the dot with $\Delta = 2$ meV [52]. Using these parameters and with $\Delta V_a = 0.32$ V, we obtain $C_a \sim 0.9$ aF. The planar geometry of the device in which the accumulation gate covers the entire area of the dot permits us to model the accumulation gate and dot as a parallel plate capacitor with the relative permittivity of hBN assumed to be in the range of $2.5 < \epsilon_{hBN} < 3.5$ [62, 63]. The top hBN thickness for device BL2 was 7 nm, which yields a dot diameter $L \sim$ 15-20 nm depending on the value of ϵ_{hBN}. A similar analysis for device BL1 yields a slightly

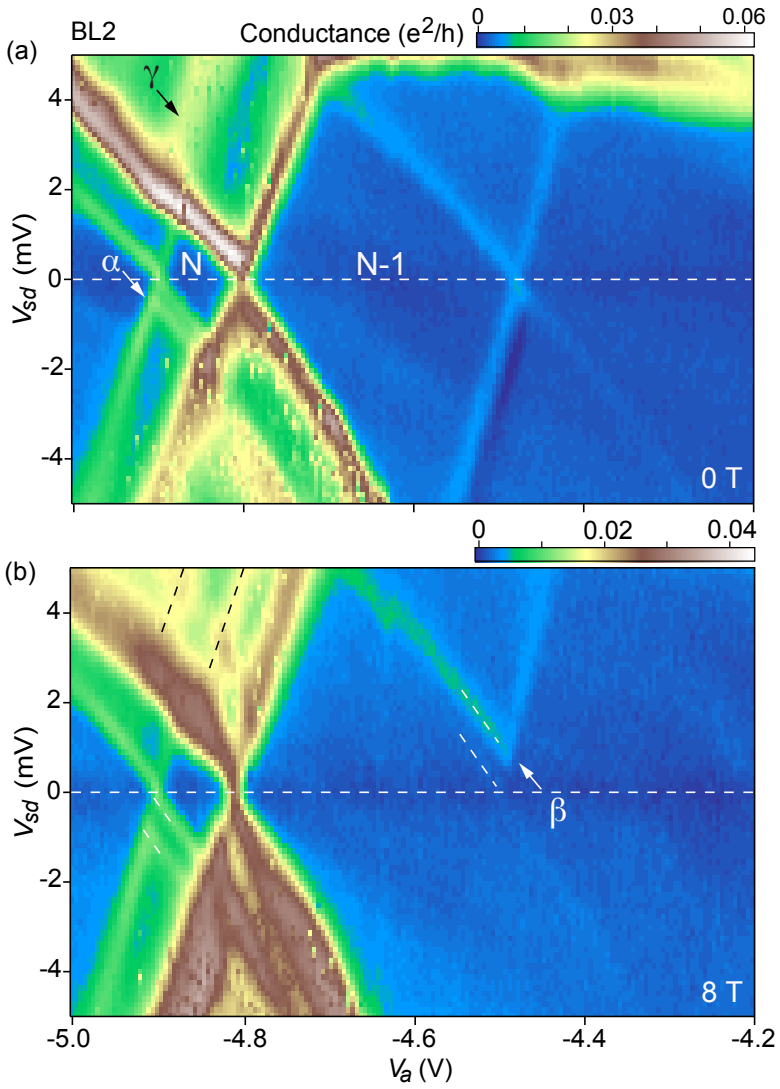

Figure 2.4: (a) Conductance as a function of V_{sd} and V_a at zero magnetic field and a temperature of 50 mK for device BL2. (b) Same as (a) in a perpendicular magnetic field of 8 T. Pairs of dashed lines highlight the levels used to calculate E_Z and g-factors. For the ground state below β, the position is inferred by extension from negative bias.

larger dot size in the range 20-25 nm [2]. These sizes are a factor of 3-5 larger than defect- or strain-bound quantum dots in TMDs [64] and are comparable to the size of the moiré supercell in moiré-defined dots [31–34]. We also note that a particle-in-a-box estimate for $\Delta \sim \hbar^2/mL^2$ is on the order of 1 meV assuming a hole mass of $0.45m_0$ [65], which roughly agrees with the zero-field energy of state γ. Finally, we estimate the number of holes in our dots. Hole conduction turns on at room temperature in our devices at electric fields from the

[2]Here we used the V_a-dependence of the charge state at $V_c = 5.6$ V in Fig. 2(d)

accumulation gate of approximately 0.2 V/nm, and a typical operating point for the dots at low temperature is 0.4 V/nm. In a parallel-plate approximation, the difference in threshold and operating electric fields, ΔE, yields a hole density $n = \epsilon_0 \epsilon_{hBN} \Delta E / e \sim 3 \times 10^{12}$ cm^{-2}, and multiplying by the dot area estimated above yields a hole number that could be expected to lie between 10 and 20. Here the uncertainty is dominated by the use of room-temperature threshold voltage to estimate the location in gate voltage of zero density.

2.5 Conclusion

We have fabricated small monolayer and bilayer WSe_2 quantum dots using a combination of accumulation and confining gates. Six devices showed Coulomb blockade at temperatures below 10 K, and three devices (one monolayer and two bilayers) showed conductance resonances consistent with single-level transport, as confirmed by temperature dependence of the peak height for one of the devices. Magnetic field dependence of peak positions implied g-factors ranging from 0.8 to 2.4 in one bilayer device. In addition to satisfying essential prerequisites for the development of future electronic and/or optoelectronic qubits based on valley-spin states in few-layer TMDs, these devices also provide a platform for high-resolution, fundamental investigations of those states using Coulomb blockade spectroscopy and other techniques.

2.6 acknowledgments

We acknowledge support from AFOSR award number FA9550-16-1-0203. WSe_2 single crystal growth is supported by the US Department of Energy, Office of Science, Basic Energy Sciences program under award DE-SC0019467. Growth of hexagonal boron nitride crystals was supported by the MEXT Element Strategy Initiative to Form Core Research Center, Grant Number JPMXP0112101001 and the CREST(JPMJCR15F3), JST.

References

[1] Edward A Laird, Fei Pei, and LP Kouwenhoven. A valley–spin qubit in a carbon nanotube. *Nature Nanotechnology*, 8(8):565, 2013.

[2] X Mi, S Kohler, and Jason R Petta. Landau-Zener interferometry of valley-orbit states in Si/SiGe double quantum dots. *Physical Review B*, 98(16):161404, 2018.

[3] Nicholas E Penthorn, Joshua S Schoenfield, John D Rooney, Lisa F Edge, and HongWen Jiang. Two-axis quantum control of a fast valley qubit in silicon. *npj Quantum Information*, 5(1):1–6, 2019.

[4] Xiaodong Xu, Wang Yao, Di Xiao, and Tony F Heinz. Spin and pseudospins in layered transition metal dichalcogenides. *Nature Physics*, 10(5):343–350, 2014.

[5] Kai Hao, Galan Moody, Fengcheng Wu, Chandriker Kavir Dass, Lixiang Xu, Chang-Hsiao Chen, Liuyang Sun, Ming-Yang Li, Lain-Jong Li, and Allan H MacDonald. Direct measurement of exciton valley coherence in monolayer WSe_2. *Nature Physics*, 12(7):677–682, 2016.

[6] Aaron M Jones, Hongyi Yu, Nirmal J Ghimire, Sanfeng Wu, Grant Aivazian, Jason S Ross, Bo Zhao, Jiaqiang Yan, David G Mandrus, Di Xiao, Wu Yao, and X Xu. Optical generation of excitonic valley coherence in monolayer WSe_2. *Nature Nanotechnology*, 8(9):634, 2013.

[7] Yanhao Tang, Kin Fai Mak, and Jie Shan. Long valley lifetime of dark excitons in single-layer WSe_2. *Nature Communications*, 10, 2019.

[8] Xin Lu, Xiaotong Chen, Sudipta Dubey, Qiang Yao, Weijie Li, Xingzhi Wang, Qihua Xiong, and Ajit Srivastava. Optical initialization of a single spin-valley in charged WSe_2 quantum dots. *Nature Nanotechnology*, 14(5):426–431, 2019.

[9] Luyi Yang, Nikolai A Sinitsyn, Weibing Chen, Jiangtan Yuan, Jing Zhang, Jun Lou, and Scott A Crooker. Long-lived nanosecond spin relaxation and spin coherence of electrons in monolayer MoS_2 and WS_2. *Nature Physics*, 11(10):830–834, 2015.

[10] Xinlin Song, Saien Xie, Kibum Kang, Jiwoong Park, and Vanessa Sih. Long-lived hole spin/valley polarization probed by Kerr rotation in monolayer WSe_2. *Nano Letters*, 16(8):5010–5014, 2016.

[11] Prasenjit Dey, Luyi Yang, Cedric Robert, Gang Wang, Bernhard Urbaszek, Xavier Marie, and SA Crooker. Gate-controlled spin-valley locking of resident carriers in WSe_2 monolayers. *Physical Review Letters*, 119(13):137401, 2017.

[12] Jonghwan Kim, Chenhao Jin, Bin Chen, Hui Cai, Tao Zhao, Puiyee Lee, Salman Kahn, Kenji Watanabe, Takashi Taniguchi, Sefaattin Tongay, Michael F. Crommie, and Feng wang. Observation of ultralong valley lifetime in WSe_2/MoS_2 heterostructures. *Science Advances*, 3(7):e1700518, 2017.

[13] Chenhao Jin, Jonghwan Kim, M Iqbal Bakti Utama, Emma C Regan, Hans Kleemann, Hui Cai, Yuxia Shen, Matthew James Shinner, Arjun Sengupta, Kenji Watanabe, Takashi Taniguchi, Sefaattin Tongay, Alex Zettl, and Feng Wang. Imaging of pure spin-valley diffusion current in WS_2-WSe_2 heterostructures. *Science*, 360(6391):893–896, 2018.

[14] Pasqual Rivera, Kyle L Seyler, Hongyi Yu, John R Schaibley, Jiaqiang Yan, David G Mandrus, Wang Yao, and Xiaodong Xu. Valley-polarized exciton dynamics in a 2D semiconductor heterostructure. *Science*, 351(6274):688–691, 2016.

[15] Zhirui Gong, Gui-Bin Liu, Hongyi Yu, Di Xiao, Xiaodong Cui, Xiaodong Xu, and Wang Yao. Magnetoelectric effects and valley-controlled spin quantum gates in transition metal dichalcogenide bilayers. *Nature Communications*, 4(1):1–6, 2013.

[16] Yue Wu, Qingjun Tong, Gui-Bin Liu, Hongyi Yu, and Wang Yao. Spin-valley qubit in nanostructures of monolayer semiconductors: Optical control and hyperfine interaction. *Physical Review B*, 93(4):045313, 2016.

[17] Matthew Brooks and Guido Burkard. Spin-degenerate regimes for single quantum dots in transition metal dichalcogenide monolayers. *Physical Review B*, 95(24):245411, 2017.

[18] G Széchenyi, L Chirolli, and A Pályi. Impurity-assisted electric control of spin-valley qubits in monolayer MoS_2. *2D Materials*, 5(3):035004, 2018.

[19] J Pawłowski, D Żebrowski, and S Bednarek. Valley qubit in a gated MoS_2 monolayer quantum dot. *Physical Review B*, 97(15):155412, 2018.

[20] Alessandro David, Guido Burkard, and Andor Kormányos. Effective theory of monolayer TMDC double quantum dots. *2D Materials*, 5(3):035031, 2018.

[21] J Pawłowski. Spin-valley system in a gated MoS_2-monolayer quantum dot. *New Journal of Physics*, 21(12):123029, 2019.

[22] Feng-Wu Chen and Yu-Shu G Wu. Theory of field-modulated spin valley orbital pseudospin physics. *Physical Review Research*, 2(1):013076, 2020.

[23] Kin Fai Mak and Jie Shan. Photonics and optoelectronics of 2D semiconductor transition metal dichalcogenides. *Nature Photonics*, 10(4):216, 2016.

[24] Chitraleema Chakraborty, Laura Kinnischtzke, Kenneth M Goodfellow, Ryan Beams, and A Nick Vamivakas. Voltage-controlled quantum light from an atomically thin semiconductor. *Nature Nanotechnology*, 10(6):507, 2015.

[25] M Koperski, K Nogajewski, A Arora, V Cherkez, P Mallet, J-Y Veuillen, J Marcus, P Kossacki, and M Potemski. Single photon emitters in exfoliated WSe_2 structures. *Nature Nanotechnology*, 10(6):503, 2015.

[26] Yu-Ming He, Genevieve Clark, John R Schaibley, Yu He, Ming-Cheng Chen, Yu-Jia Wei, Xing Ding, Qiang Zhang, Wang Yao, Xiaodong Xu, Chao-Yang Lu, and Pan Jian-Wei. Single quantum emitters in monolayer semiconductors. *Nature Nanotechnology*, 10(6):497–502, 2015.

[27] Ajit Srivastava, Meinrad Sidler, Adrien V Allain, Dominik S Lembke, Andras Kis, and A Imamoğlu. Optically active quantum dots in monolayer WSe_2. *Nature Nanotechnology*, 10(6):491, 2015.

[28] Santosh Kumar, Artur Kaczmarczyk, and Brian D Gerardot. Strain-induced spatial and spectral isolation of quantum emitters in mono-and bilayer WSe_2. *Nano Letters*, 15(11):7567–7573, 2015.

[29] Carmen Palacios-Berraquero, Dhiren M Kara, Alejandro R-P Montblanch, Matteo Barbone, Pawel Latawiec, Duhee Yoon, Anna K Ott, Marko Loncar, Andrea C Ferrari, and Mete Atatüre. Large-scale quantum-emitter arrays in atomically thin semiconductors. *Nature Communications*, 8(1):1–6, 2017.

[30] Artur Branny, Santosh Kumar, Raphaël Proux, and Brian D Gerardot. Deterministic strain-induced arrays of quantum emitters in a two-dimensional semiconductor. *Nature Communications*, 8(1):1–7, 2017.

[31] Kha Tran, Galan Moody, Fengcheng Wu, Xiaobo Lu, Junho Choi, Kyounghwan Kim, Amritesh Rai, Daniel A Sanchez, Jiamin Quan, Akshay Singh, Jacob Embley, André Zepeda, Marshall Campbell, Travis Autry, Takashi Taniguchi, Kenji Watanabe, Nanshu Lu, Sanjay K Banerjee, Kevin L Silverman, Suenne Kim, Emanuel Tutuc, Li Yang, Allan H MacDonald, and Xiaoqin Li. Evidence for moiré excitons in van der Waals heterostructures. *Nature*, 567(7746):71–75, 2019.

[32] Kyle L Seyler, Pasqual Rivera, Hongyi Yu, Nathan P Wilson, Essance L Ray, David G Mandrus, Jiaqiang Yan, Wang Yao, and Xiaodong Xu. Signatures of moiré-trapped valley excitons in $MoSe_2/WSe_2$ heterobilayers. *Nature*, 567(7746):66–70, 2019.

[33] Evgeny M Alexeev, David A Ruiz-Tijerina, Mark Danovich, Matthew J Hamer, Daniel J Terry, Pramoda K Nayak, Seongjoon Ahn, Sangyeon Pak, Juwon Lee, Jung Inn Sohn, Maciej R. Molas, Maciej Koperski, Kenji Watanabe, Takashi Taniguchi, Kostya S. Novoselov, Roman V. Gorbachev, Hyeon Suk Shin, Vladimir I. Fal'ko, and Alexander I. Tartakovskii. Resonantly hybridized excitons in moiré superlattices in van der Waals heterostructures. *Nature*, 567(7746):81–86, 2019.

[34] Chenhao Jin, Emma C Regan, Aiming Yan, M Iqbal Bakti Utama, Danqing Wang, Sihan Zhao, Ying Qin, Sijie Yang, Zhiren Zheng, Shenyang Shi, Kenji Watanabe, Takashi Taniguchi, Sefaattin Tongay, Alex Zettl, and Feng Wang. Observation of moiré excitons in WSe_2/WS_2 heterostructure superlattices. *Nature*, 567(7746):76–80, 2019.

[35] Gui-Bin Liu, Hongliang Pang, Yugui Yao, and Wang Yao. Intervalley coupling by quantum dot confinement potentials in monolayer transition metal dichalcogenides. *New Journal of Physics*, 16(10):105011, 2014.

[36] Xiang-Xiang Song, Di Liu, Vahid Mosallanejad, Jie You, Tian-Yi Han, Dian-Teng Chen, Hai-Ou Li, Gang Cao, Ming Xiao, Guang-Can Guo, and Guo-Ping Guo. A gate defined quantum dot on the two-dimensional transition metal dichalcogenide semiconductor WSe_2. *Nanoscale*, 7(40):16867–16873, 2015.

[37] Xiang-Xiang Song, Zhuo-Zhi Zhang, Jie You, Di Liu, Hai-Ou Li, Gang Cao, Ming Xiao, and Guo-Ping Guo. Temperature dependence of coulomb oscillations in a few-layer two-dimensional WS_2 quantum dot. *Scientific Reports*, 5:16113, 2015.

[38] Kyunghoon Lee, Girish Kulkarni, and Zhaohui Zhong. Coulomb blockade in monolayer MoS_2 single electron transistor. *Nanoscale*, 8(14):7755–7760, 2016.

[39] Ke Wang, Kristiaan De Greve, Luis A Jauregui, Andrey Sushko, Alexander High, You Zhou, Giovanni Scuri, Takashi Taniguchi, Kenji Watanabe, Mikhail D Lukin, Hongkun Park, and Philip Kimothers. Electrical control of charged carriers and excitons in atomically thin materials. *Nature Nanotechnology*, 13(2):128–132, 2018.

[40] Riccardo Pisoni, Zijin Lei, Patrick Back, Marius Eich, Hiske Overweg, Yongjin Lee, Kenji Watanabe, Takashi Taniguchi, Thomas Ihn, and Klaus Ensslin. Gate-tunable quantum dot in a high quality single layer MoS_2 van der Waals heterostructure. *Applied Physics Letters*, 112(12):123101, 2018.

[41] Zhuo-Zhi Zhang, Xiang-Xiang Song, Gang Luo, Guang-Wei Deng, Vahid Mosallanejad, Takashi Taniguchi, Kenji Watanabe, Hai-Ou Li, Gang Cao, Guang-Can Guo, Franco Nori, and Guo-Ping Guo. Electrotunable artificial molecules based on van der Waals heterostructures. *Science Advances*, 3(10):e1701699, 2017.

[42] Simon Reinhardt, Luka Pirker, Christian Bäuml, Maja Remškar, and Andreas K Hüttel. Coulomb blockade spectroscopy of a MoS_2 nanotube. *physica status solidi (RRL)–Rapid Research Letters*, 13(11):1900251, 2019.

[43] Guohua Wei, David A Czaplewski, Erik J Lenferink, Teodor K Stanev, Il Woong Jung, and Nathaniel P Stern. Size-tunable lateral confinement in monolayer semiconductors. *Scientific Reports*, 7(1):1–8, 2017.

[44] Leo P Kouwenhoven, Charles M Marcus, Paul L McEuen, Seigo Tarucha, Robert M Westervelt, and Ned S Wingreen. Electron transport in quantum dots. In *Mesoscopic electron transport*, pages 105–214. Springer, 1997.

[45] Floris A Zwanenburg, Andrew S Dzurak, Andrea Morello, Michelle Y Simmons, Lloyd CL Hollenberg, Gerhard Klimeck, Sven Rogge, Susan N Coppersmith, and Mark A Eriksson. Silicon quantum electronics. *Reviews of Modern Physics*, 85(3):961, 2013.

[46] Erika Kawakami, P Scarlino, Daniel R Ward, FR Braakman, DE Savage, MG Lagally, Mark Friesen, Susan N Coppersmith, Mark A Eriksson, and LMK Vandersypen. Electrical control of a long-lived spin qubit in a Si/SiGe quantum dot. *Nature Nanotechnology*, 9(9):666, 2014.

[47] Hema C. P. Movva, Amritesh Rai, Sangwoo Kang, Kyounghwan Kim, Babak Fallahazad, Takashi Taniguchi, Kenji Watanabe, Emanuel Tutuc, and Sanjay K. Banerjee. High-mobility holes in dual-gated WSe_2 field-effect transistors. *ACS Nano*, 9(10):10402–10410, 2015.

[48] Weijie Zhao, Zohreh Ghorannevis, Leiqiang Chu, Minglin Toh, Christian Kloc, Ping-Heng Tan, and Goki Eda. Evolution of electronic structure in atomically thin sheets of WS_2 and WSe_2. *ACS Nano*, 7(1):791–797, 2013.

[49] Ronald Hanson, Leo P Kouwenhoven, Jason R Petta, Seigo Tarucha, and Lieven MK Vandersypen. Spins in few-electron quantum dots. *Reviews of Modern Physics*, 79(4):1217, 2007.

[50] T Schmidt, Rolf J Haug, K v Klitzing, A Förster, and H Lüth. Spectroscopy of the single-particle states of a quantum-dot molecule. *Physical Review Letters*, 78(8):1544, 1997.

[51] M Möttönen, KY Tan, KW Chan, FA Zwanenburg, WH Lim, CC Escott, J-M Pirkkalainen, A Morello, C Yang, JA Van Donkelaar, A. D. C. Alves, D. N. Jamieson, L. C. L. Hollenberg, and A. S. Dzurak. Probe and control of the reservoir density of states in single-electron devices. *Physical Review B*, 81(16):161304, 2010.

[52] CC Escott, FA Zwanenburg, and A Morello. Resonant tunnelling features in quantum dots. *Nanotechnology*, 21(27):274018, 2010.

[53] CWJ Beenakker. Theory of coulomb-blockade oscillations in the conductance of a quantum dot. *Physical Review B*, 44(4):1646, 1991.

[54] ZY Zhu, YC Cheng, and Udo Schwingenschlögl. Giant spin-orbit-induced spin splitting in two-dimensional transition-metal dichalcogenide semiconductors. *Physical Review B*, 84(15):153402, 2011.

[55] Xiao-Xiao Zhang, Ting Cao, Zhengguang Lu, Yu-Chuan Lin, Fan Zhang, Ying Wang, Zhiqiang Li, James C Hone, Joshua A Robinson, Dmitry Smirnov, Steven G. Louie, and Tony F. Heinz. Magnetic brightening and control of dark excitons in monolayer WSe_2. *Nature Nanotechnology*, 12(9):883, 2017.

[56] Di Xiao, Gui-Bin Liu, Wanxiang Feng, Xiaodong Xu, and Wang Yao. Coupled spin and valley physics in monolayers of $MoS_2$2 and other group-VI dichalcogenides. *Physical Review Letters*, 108(19):196802, 2012.

[57] Maciej Koperski, Maciej R Molas, Ashish Arora, Karol Nogajewski, Miroslav Bartos, Jan Wyzula, Diana Vaclavkova, Piotr Kossacki, and Marek Potemski. Orbital, spin and valley contributions to Zeeman splitting of excitonic resonances in MoS_2, WSe_2 and WS_2 monolayers. *2D Materials*, 6(1):015001, 2018.

[58] Andor Kormányos, Viktor Zólyomi, Neil D Drummond, and Guido Burkard. Spin-orbit coupling, quantum dots, and qubits in monolayer transition metal dichalcogenides. *Physical Review X*, 4(1):011034, 2014.

[59] MT Björk, Andreas Fuhrer, AE Hansen, MW Larsson, LE Fröberg, and Lars Samuelson. Tunable effective g factor in InAs nanowire quantum dots. *Physical Review B*, 72(20):201307, 2005.

[60] S Csonka, L Hofstetter, F Freitag, S Oberholzer, C Schonenberger, Thomas Sand Jespersen, Martin Aagesen, and Jesper Nygård. Giant fluctuations and gate control of the g-factor in InAs nanowire quantum dots. *Nano Letters*, 8(11):3932–3935, 2008.

[61] LP Kouwenhoven, NC Van der Vaart, AT Johnson, W Kool, CJPM Harmans, JG Williamson, AAM Staring, and CT Foxon. Single electron charging effects in semiconductor quantum dots. *Zeitschrift für Physik B Condensed Matter*, 85(3):367–373, 1991.

[62] B Hunt, JD Sanchez-Yamagishi, AF Young, M Yankowitz, Brian J LeRoy, K Watanabe, T Taniguchi, Pilkyung Moon, M Koshino, P Jarillo-Herrero, and R. C. Ashoori. Massive Dirac fermions and Hofstadter butterfly in a van der Waals heterostructure. *Science*, 340(6139):1427–1430, 2013.

[63] Faisal Ahmed, Sunwoo Heo, Zheng Yang, Fida Ali, Chang Ho Ra, Ho-In Lee, Takashi Taniguchi, James Hone, Byoung Hun Lee, and Won Jong Yoo. Dielectric dispersion and high field response of multilayer hexagonal boron nitride. *Advanced Functional Materials*, 28(40):1804235, 2018.

[64] Weijie Li, Xin Lu, Sudipta Dubey, Luka Devenica, and Ajit Srivastava. Dipolar interactions between field-tuneable, localized emitters in van der Waals heterostructures. *arXiv preprint arXiv:1910.08139*, 2019.

[65] Babak Fallahazad, Hema CP Movva, Kyounghwan Kim, Stefano Larentis, Takashi Taniguchi, Kenji Watanabe, Sanjay K Banerjee, and Emanuel Tutuc. Shubnikov–de haas oscillations of high-mobility holes in monolayer and bilayer WSe_2: Landau level degeneracy, effective mass, and negative compressibility. *Physical Review Letters*, 116(8):086601, 2016.

Chapter 3

Gate-controlled Tellurium Nanowire Quantum Dots

3.1 Introduction

Topological band theory has revolutionized our understanding of possible quantum states in materials and therefore has led to experimental realization of many of these states including topological insulators, Dirac, Weyl, and Majorana fermions. While these quantum states have been investigated over the years, the development of devices based on quantum materials has remained in its infancy particularly for the Weyl and Majorana systems up until recent years. Elemental tellurium as a narrow band gap semiconductor featuring one-dimensional (1D) chiral atomic structure is a step towards implementing next generation electronic, optoelectronic, and piezoelectric applications. In this project we are motivated to investigate the helical crystal of 1D tellurium (Te) as a quantum material by investigating quantum transport in the 1D limit by fabricating gate-defined Te nanowire quantum dots as a sensitive probe of the electronic structure of Te.

3.2 Te Crystal Structure

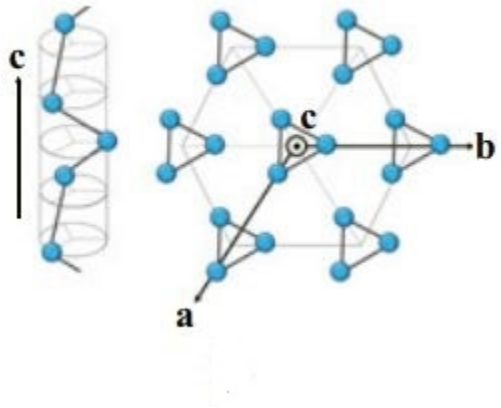

Figure 3.1: Crystal structure of trigonal Te [1].

Group VI elemental chalcogen Te crystalizes as quasi 1D helical chains that have three atoms per turn along the c-axis. The chains are ordered in hexagonal arrays in the a-b plane. Chemical bonds in Te are anisotropic, which means strong covalent bonds within the chains and weak van der Waals (vdW) bonds between the chains that permit the synthesis of 1D nanowires and 2D flakes as well as mechanical exfoliation of the bulk crystals [2–19].

Te has a narrow, almost direct band gap of 0.35 eV formed at the H points of the Brillouin zone (BZ). The conduction band minimum is doubly degenerate at the H_6 point. The Fermi level happens to be located close to the valence band. A zoomed-in examination at the valence band edge suggests a camel-back hump feature [20].

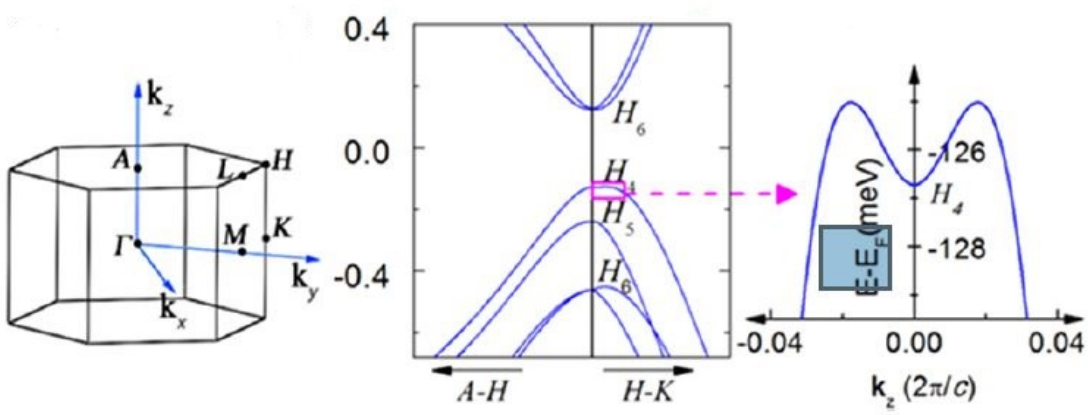

Figure 3.2: First Brillouin zone of Te and the band structure around H along the HK line [20].

The bulk crystal has a room temperature mobility of 2000 $cm^2/V.s$ (Ref), which makes this material ideal for quantum transport experiments[21].

The screw symmetry of the chains breaks the inversion and mirror symmetries. The helical chains with three-fold screw symmetry that form Te crystal by parallel assembly have different chiralities, giving rise to chirality-dependent properties such as opposite spin texture,

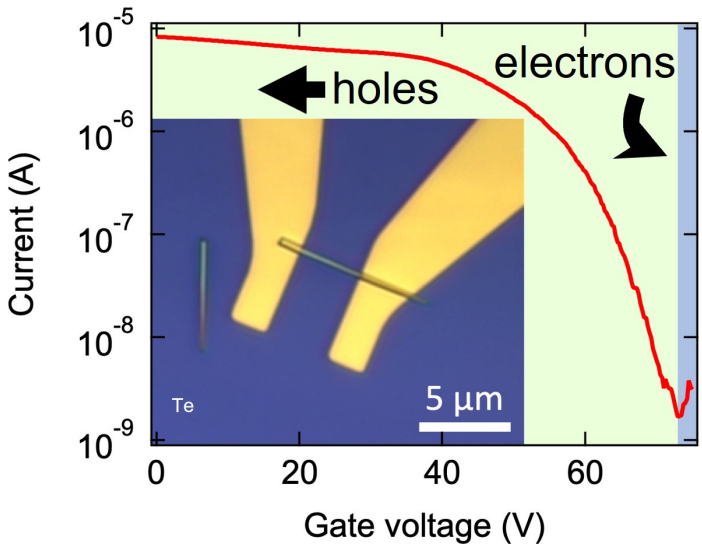

Figure 3.3: Two-terminal Te nanowire device current at 50 mV source–drain bias and 10 K. Inset: Micrograph of a device [21]

current-induced spin polarization, and circular photon drag effect [22–24]. Further, inversion asymmetric trigonal Te supports the Weyl node, and the Weyl states could be probed in transport for Te.

3.3 Thermoelectric Performance of Tellurium

In the following sections, some transport-related phenomena in Te including thermoelectric effect, angle-resolved photoemission spectroscopy, circular photogalvanic effect, Shubnikov-de Haas oscillations, quantum Hall effect,and weak antilocalization are reviewed. Further, the transport hallmarks of the Weyl states in Te which are negative longitudinal magneto-resistance, angle-narrowing in anisotropic magneto-resistance, and the planar Hall effect are discussed.

Tellurium allows efficient thermoelectricity generation. The paradigm of a superior thermoelectric material should be a heavily doped narrow band gap semiconductor where the finite band gap separates electrons and holes to avoid the opposite contribution to the Seebeck coefficient.The thermoelectrical figure of merit which evaluates the efficiency of converting

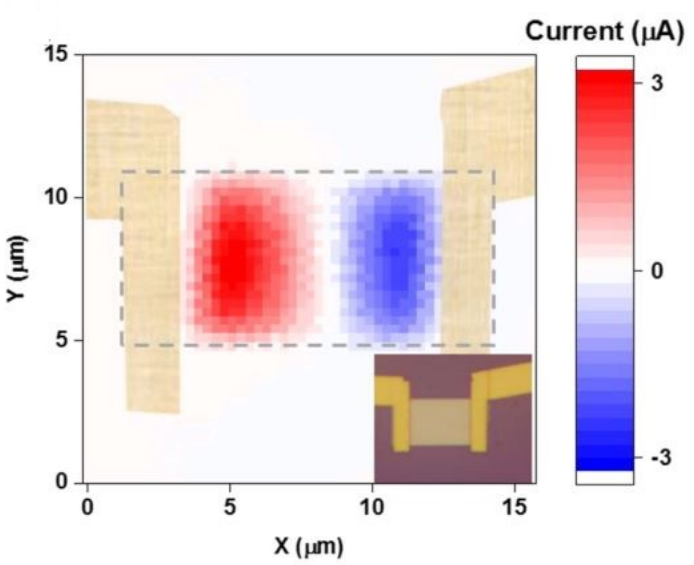

Figure 3.4: The LITE current mapping of a real device represented in the inset the optical [25].

heat to electricity increases with the electrical conductivity and the Seebeck coefficient. The thermoelectrical figure of merit decreases with the thermal conductivity. These parameters are usually correlated through the Wiedemann-Franz law [26, 27]. Pristine Te is a p-type narrow band gap semiconductor with excellent electrical and low thermal conductivity making this material an outstanding thermoelectric candidate with a high thermoelectrical figure of merit, that can be used for energy harvesting applications as well as Peltier coolers [25]. Moreover, the heavy atoms of Te contribute to lower thermal conductivity by providing effective phonon scattering centers where the difference of mean free paths between electrons and phonons disentangles the correlation between the electrical conductivity and thermal conductivity. Besides, the strong spin-orbit coupling which leads to band splitting and band degeneracy near the valence band edge, can provide multiple carriers conducting channels without compromising the Seebeck coefficient and affecting thermal conductivity [28, 29]. The bulk Te exhibits high thermoelectric performance because of meeting the aforementioned criteria but Te nanostructures due to the quantum confinement also have imperative effects. In the Te nanostructures, the quantum confinement of the charged carriers leads to an increase

in the effective band gap of the material. It also evolves the density of states (DoS) into the sharp shapes at the band edge which boosts the Seebeck coefficient because it is related to how fast DoS varies near the Fermi energy. Low-dimensional nanostructures, also, prevent acoustic phonon propagation more so the charged carriers can transmit less interrupted [20, 30–32]. As figure 3.4 shows, the laser-induced thermoelectrical (LITE) current mapping technique helps enhance the efficiency of harvesting the thermoelectric current across the 2D Te device with a laser as a heating source [25].

3.4 Angle-resolved Photoemission Spectroscopy

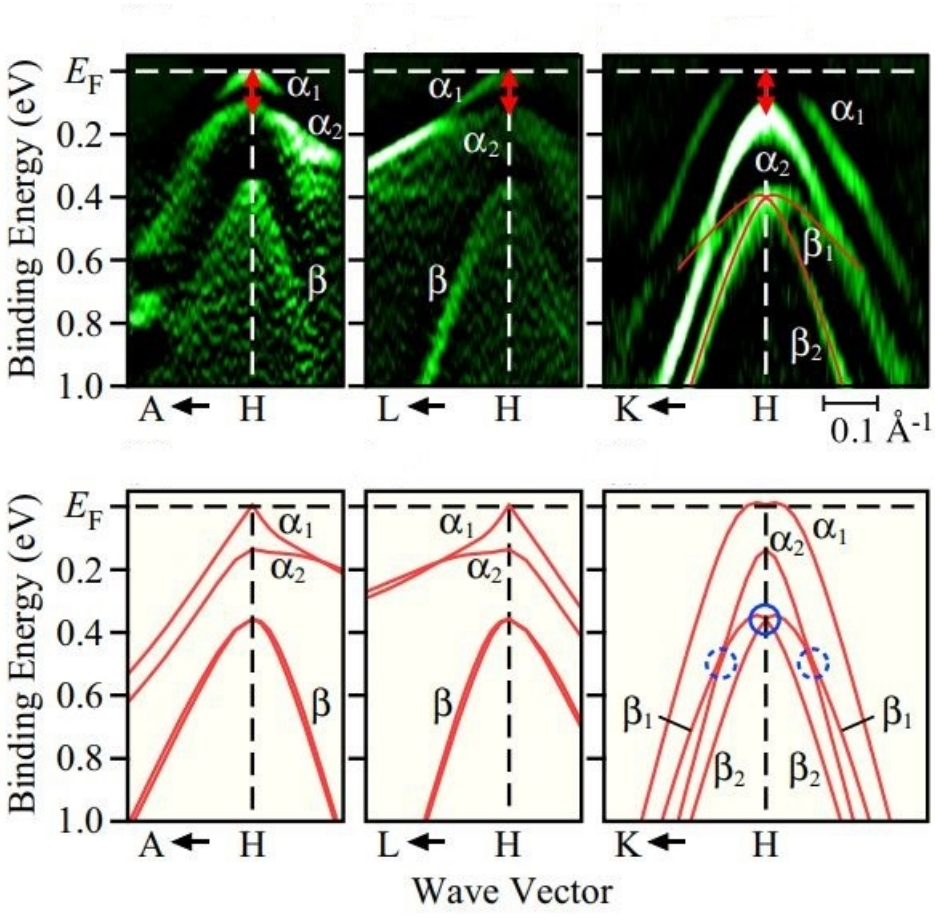

Figure 3.5: Second derivative of the near-E_F ARPES intensity crossing the H point, compared with the calculated band dispersions incorporating the spin-orbit coupling [33].

High-resolution angle-resolved photoemission spectroscopy (ARPES) by utilizing energy-tunable photons from synchrotron radiation on trigonal Te crystal consisting of helical chains in the crystal structure, is experimental band structure outputs of trigonal Te which is required to establish its fundamental electronic states.Through band structure mapping in the entire bulk Brillouin zone (BZ), intriguing spectral evidence such as energy splittings of bulk bands at several locations in the BZ originating from the broken inversion symmetry of the Te chiral crystal are elucidated [33].As figure 3.5 represents, by comparing the band dispersions between the first principle band structure calculations and the experimental valence band dispersion ARPES results which are in good agreement, the presence of Weyl nodes at the valence band around the H point protected by the nonsymmorphic screw symmetry is revealed.

3.5 Circular Photogalvanic Effect

Circular photogalvanic effect (CPGE), which is the part of a photocurrent that switches depending on the sense of the circular polarization of the incident light has been observed in systems without inversion and mirror symmetries. Moreover, there are two types of photocurrent namely, the injection current which is generated by photoelectric excitation of optical transition with an anisotropic transition rate, and the shift current which is due to the real space displacement that electrons undergo an optical transition. The contribution from the injection current diverges in the absence of a relaxation mechanism; thus, the injection current grows linear in time. However, the shift current is always finite and therefore subleading for long relaxation times. In other words, CPGE occurs when the light of specific helicity is absorbed via interband and intraband scattering processes [34, 34–38]. When impurity scattering is treated in the constant relaxation time approximation, it becomes possible to identify a contribution to the intraband CPGE associated with the Berry curvature of the free carriers. This intrinsic contribution to the photocurrent density is related to the divergence of the Berry curvature and is zero unless at isolated chiral band crossings known as

Weyl nodes [39–41]. At low temperatures, trigonal Te's transport and low-frequency optical properties are governed by the upper valence band and the lower conduction subbands which have an anisotropic Rashba-like spin-orbit splitting around H point. Besides, the Weyl node at H point between the conduction subbands has positive chirality in the right-handed structure which means it acts as a source(sink) of Berry curvature in the lower(upper) subband [42]. The photocurrent starts positive at low temperature, and becomes negative at around room temperature. Thus, an indirect evidence for the Weyl node at the H point near the conduction band minimum is provided by a sign change in circular photogalvanic effect in Te as a function of temperature for different acceptor concentrations in p-doped trigonal Te as shown in figure 3.6 [43].

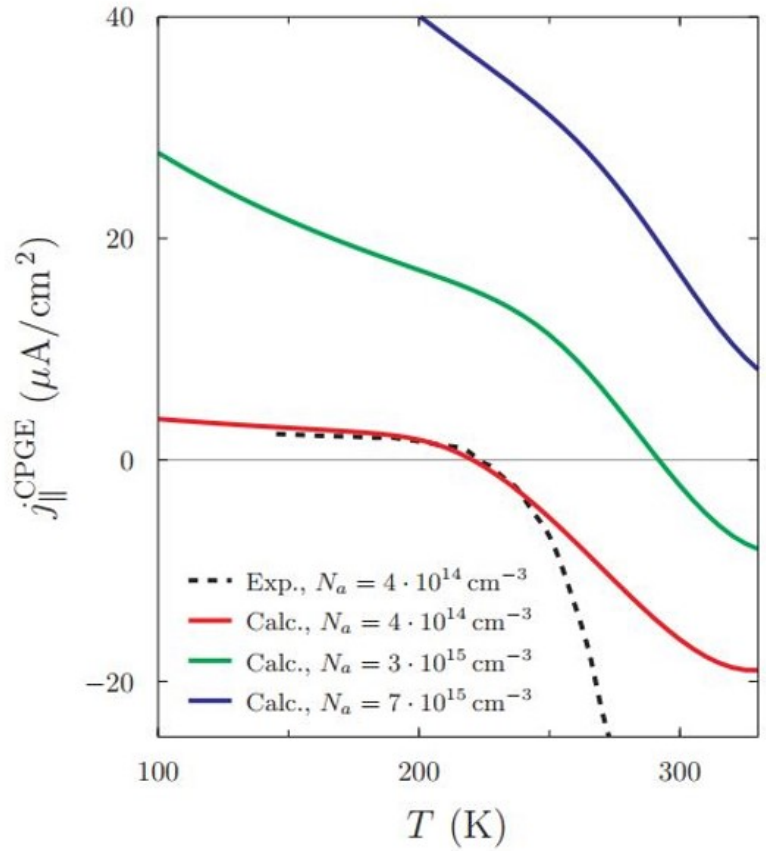

Figure 3.6: Temperature dependence for different acceptor concentrations of the intraband photocurrent density induced in right-handed Te by circularly polarized light [43].

Furthermore, it has been shown that the injection contribution to the CPGE is effectively quantized in terms of the fundamental constants of e, h, c, and ϵ_0 which are elementary charge, Planck constant, speed of light, and the vacuum permittivity, respectively, with no material-dependent parameters because that CPGE directly measures the topological charge of the Weyl nodes [44].

3.6 Shubnikov-de Haas Oscillations and Quantum Hall Effect in p-type and n-type Tellurium

Novel physical properties have been observed in Te through powerful techniques such as Shubnikov-de Haas (SdH) oscillations and quantum Hall effect (QHE). At low temperatures and under strong magnetic fields, the conductivity of Te exhibits oscillations owing to Landau quantization that leads to discrete energy levels in the electronic band structure of Te. According to Onsager rule, the oscillation frequency is associated with the Fermi surface; therefore, SdH oscillations portray the Fermi surface of the material. For the p-type Te sample, this technique obtains the carrier densities of the top of the valence band known as the camel back feature [45–50]. The SdH oscillations are preliminary to the QHE in the two-dimensional confinement regime where the Hall resistance is quantized as integer numbers of h/e^2 where h is the Planck constant and e is the elementary charge. The longitudinal resistance (R_{XX}) disappears due to back-scattering at the free edge channels as represented in figure 3.7 for a p-type device.

For the p-type Te, QHE reveals four-fold degeneracy for the Landau levels which is associated with the spin and the valley pseudospin. Further, angle-dependent measurements of the SdH oscillations have been carried out that reveal that the Landau quantization only happens at the perpendicular magnetic field which manifests the Fermi surface in the 2D limit which is different than the bulk SdH measurements [51]. With n-type doping of Te, one can access the conduction band of Te. The atomic layer deposited dielectric (ALD) technique is an effective and controllable doping method that renders Te n-type which can be confirmed by transport

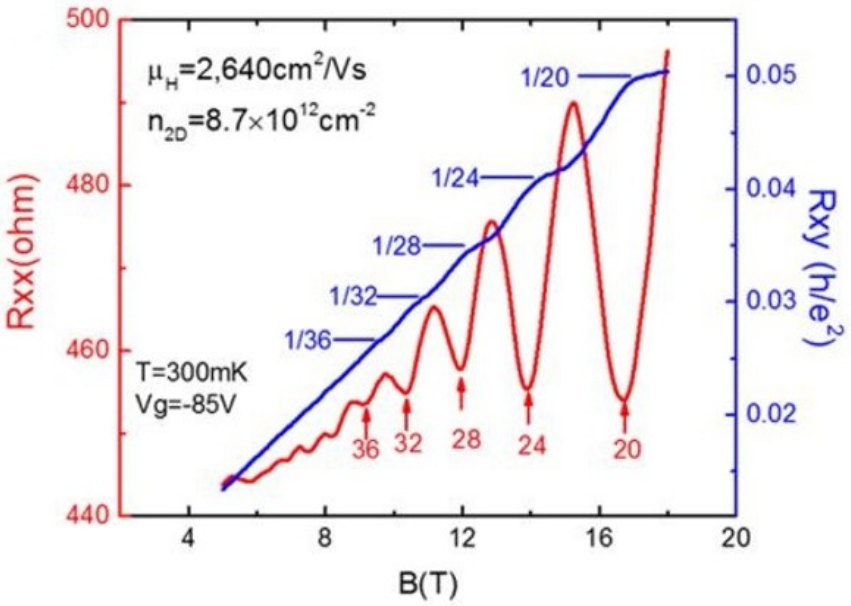

Figure 3.7: SdH oscillations in p-type 2D Te with four-fold degeneracy [51].

measurements or scanning micro-wave microscopy techniques [52, 53]. The reason behind the doping effect might be related to the presence of fixed charges in the dielectric media [54] or due to the occurrence of charge transfer, according to Wang et al. [55]. This doping strategy enables the investigation of the quantum transport of the electrons in the conduction band. At the quantum Hall regime in 2DEGs in the conduction band of n-type Te where all degeneracies are lifted under a high magnetic field, the SdH oscillations and quantum Hall states are mapped out in a Landau fan diagram, shown in figure 3.8, which implies a non-trivial π Berry phase due to the Kramers-Weyl nodes at the bottom of the conduction band. These Kramers-Weyl nodes originate from the chiral crystal structure of Te [56, 57].

As mentioned before, Te has a chiral crystal structure that leads to breaking the spatial inversion symmetry. Broken inversion symmetry in tandem with the strong spin-orbit coupling leads to large spin splitting in the valence bands of Te which ARPES has observed. Of essential features in the band structure of Te is the formation of Kramers-Weyl nodes at the

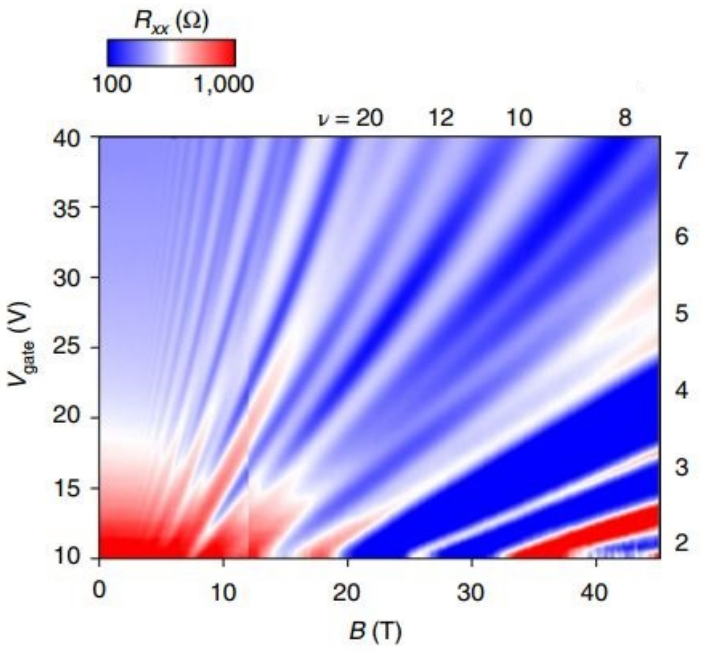

Figure 3.8: Landau fan mapping of SdH and quantum Hall effect in n-type Te in the gate voltage-B field parameter space [57].

high symmetry points due to the chiral symmetry of the crystal structure. In the n-type Te, the Kramers-Weyl node in the conduction band becomes available since it is several meV away from the bottom of the conduction band minimum. By tunung the electrochemical potential of Te via gate voltages, the Weyl node can be accessed. The non-trivial π Berry phase detected in the quantum Hall sequences proves the existence of the Weyl nodes in the n-type Te [57, 58].

3.7 Weak Antilocalization

The crystal chirality along with the strong spin-orbit coupling give rise to many intriguing phenomena in Te including weak antilocalization (WAL) induced by spin-orbit interaction. In n-type Te, electron motions are rather diffusive than ballistic which means electrons do not move along a straight line but instead experience a series of random scatterings. In systems with strong spin-orbit coupling (SOC), the spin of electrons is coupled to the orbital magnetic momentum. The electron spin rotates as it revolves around self-intersecting

paths. If the quantum interference between the counterclockwise and clockwise directions around a loop is destructive, the net resistivity decreases and vice versa. At low-density regime, the conductivity is suppressed by increasing magnetic field, the phenomenon known as weak antilocalization. As shown in the figure below, by tuning the gate voltage to reach to the low-density regime, one can see the transition from weal localization (WL) to weak antilocalization (WAL) with increasing the magnetic field. WAL is found in material systems with a non-trivial Berry phase [56].

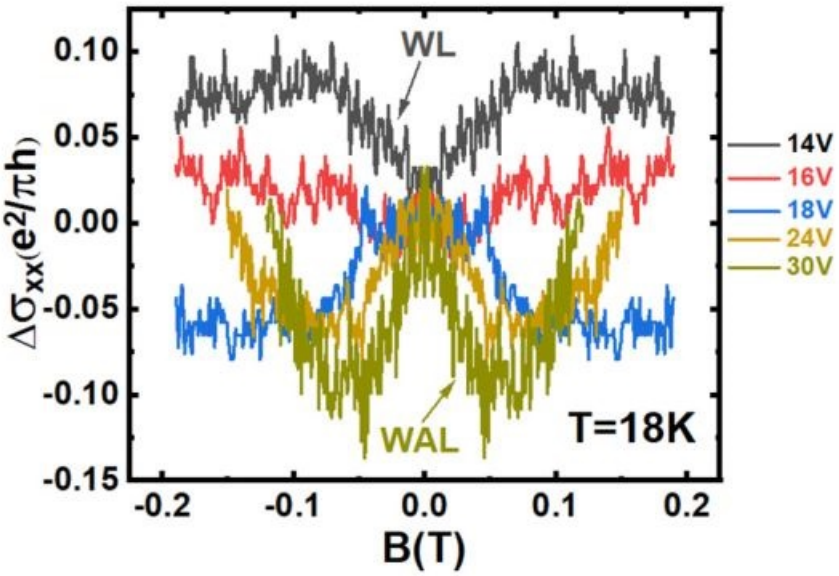

Figure 3.9: Transition from WL to WAL with at diggerent gate voltages[56].

3.8 Transport Hallmarks of the Weyl States in Te

In the context of transport theories, the unique features related to the Weyl state and its associated chiral anomaly are negative longitudinal magneto-resistance (NLMR), angle-narrowing in anisotropic magneto-resistance, and the planar Hall effect. In the spin-polarized valence band, Weyl nodes form with two different origins.

The Kramers-Weyl node, owing to the chiral symmetry of the crystal at the high symmetry point and the accidental band crossing, form a pair of Weyl nodes. The pumping of electrons

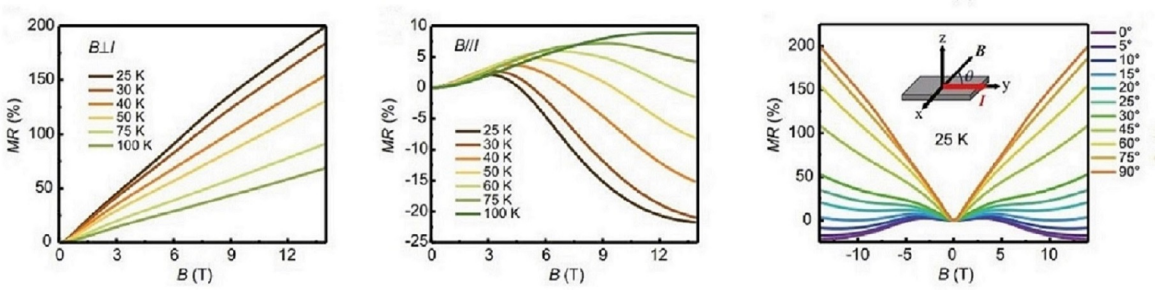

Figure 3.10: MR is proportional to magnetic field (B) when the magnetic and the electric (E) fields are parallel and it drops as B^{-}2 when B is perpendicular to E[1].

between this Weyl pair of opposite chirality gives rise to unique features such as NLMR, angle-narrowing in anisotropic magneto-resistance, and the planar Hall effect (PHE). However, direct transport evidence of Weyl nodes in the valence band is challenging because these Weyl nodes are deeply embedded in the valence band and are far away from the Fermi surface, thus have little contribution to carrier transport [1, 54].

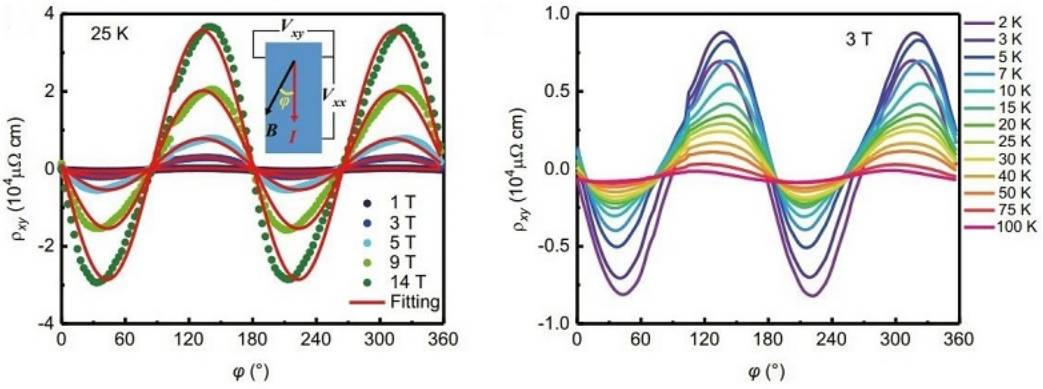

Figure 3.11: PHE, the appearance of in-plane transverse voltages when the in-plane magnetic field is not exactly parallel or perpendicular to the longitudinal current which, is a signature of Weyl nodes [1].

3.9 Growth of Te Nanostructures

In the following sections, our work on this topic is discussed. As mentioned before, scaling the Te dimension down to the quantum limit is required to explore the material's physical properties and improve the device's performance in different device architectures. Te is a

van der Waals (vdW) material, but it cannot be easily exfoliated with the conventional mechanical method using Scotch tape. However, other practical routes to acquire ultra-scaled Te have been pursued including a tape-free exfoliation method to obtain quasi-1D Te films by directly scratching bulk Te onto the silicon substrate [19]. While the mainstream technique of growing ultrathin Te is based on the solution-based hydrothermal synthesis, and the quantum transport properties of these ultrathin Te films have been explored [4, 59], an approach based on low-pressure physical vapor deposition (LP-PVD) grown material has been pursued in this project.

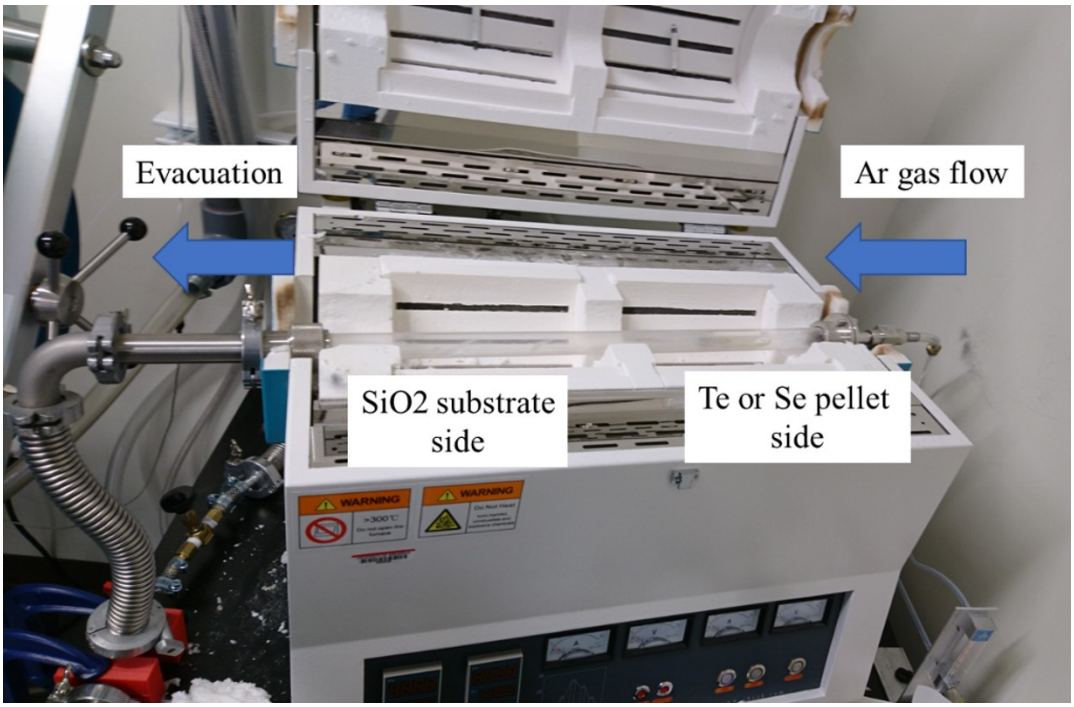

Figure 3.12: The schematic low-pressure physical vapor deposition growth of Te nanostructures in a quartz tube two-zone furnace

The one-dimensional vdW crystal structure of Te and its viable melting temperature of 450°C suggests the easy formation of 1D morphologies via LP-PVD deposition. In a two-zone furnace, the hot zone at 450°C, the bulk material source vaporizes while the substrate is kept in the cold zone at 200°C. By introducing Argon gas into the growth medium, the size, the aspect ratio, and the morphology, i.e., nanowires, nanorods, nanotubes, etc., can be tuned by carefully tweaking the gas flow rate or the pressure during the growth.

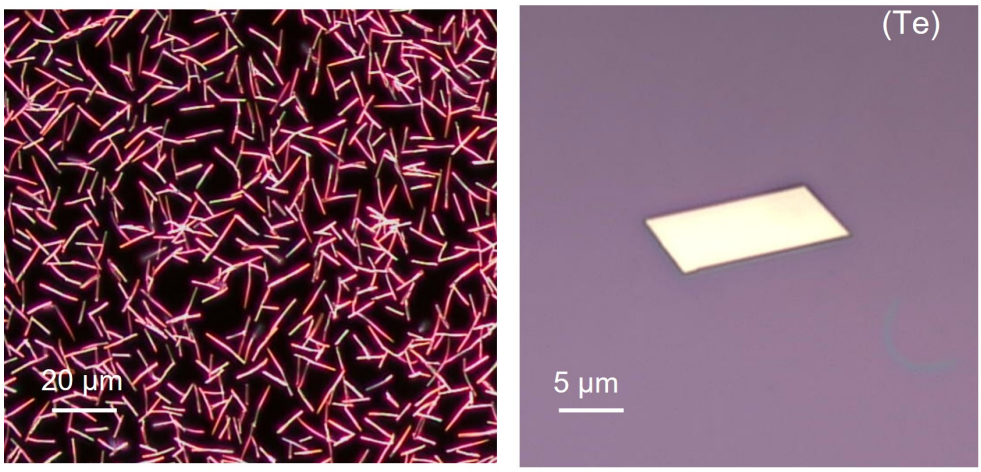

Figure 3.13: growth outcomes in different morphologies

With TEM imaging and Raman scattering, the crystallinity of the material can be verified. This bulk physical vapor growth technique results in Te structures that are theoretically slightly different from those obtained through the solution-grown method [60]. One interesting experimental observation of a potential difference between solution-grown and vapor-grown Te is that the solution-grown monolayer tellurene does not oxidize under ambient conditions. In contrast, vapor-grown Te forms a thin native oxide, and it cannot be contacted successfully unless the native oxide is removed prior to metal deposition [4, 61].The 1D nanowires can then be assembled onto the desired substrate with a transfer technique to harvest their electric properties. Moreover, Qin et al. have reported few-chain and single-chain Te nanowires isolated and stabilized inside carbon nanotubes and boron nitride nanotubes through a vapor trapping growth approach with promising electrical and optical performance [62]. Inspired by the work done by Yang et al.[63], we have also tried growing Te nanowires by LP-PVD deposition on the silicon substrate on which distributed the hexagonal boron nitride (hBN) flakes were obtained by mechanical exfoliation.

3.10 Gate-defined Te Quantum Dot and Device Design Strategy

Coulomb spectroscopy of quantum dots is a well-established technique to determine the basic properties of quantum materials by directly measuring the energies of individual quantum

levels when both gate voltages and the source-drain bias are varied. This type of measurement on a Te-based quantum dot with individually resolved quantum states provides information about the spin-orbit length in Te nanostructures, g-tensors of the spin and valley states, the strength of the exchange interaction in dots and more. Gate tuning of Fermi level allows us to compare the properties of the confined electrons in the bands that are either topologically trivial in bulk, i.e., the valence band maximum, or potentially nontrivial in the bulk, i.e., the conduction band minimum.

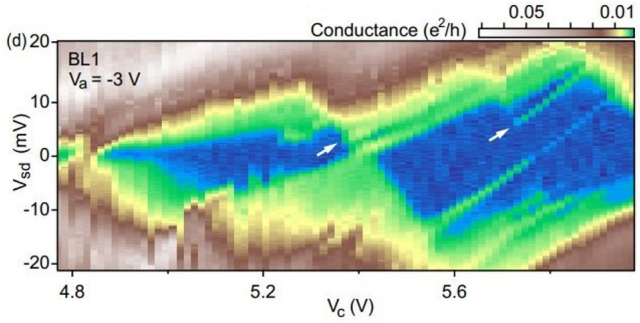

Figure 3.14: WSe_2 quantum dot device, conductance as a function of source-drain and gate voltages [64].

We fabricate devices that seek to balance the competing demands of retaining bulk-like Weyl states in Te while also maintaining electrical control through the full cross-section of Te nanowire. The electrons residing on the dot occupy quantized energy levels. The energy level spacing should be much greater than the thermal excitations to resolve these levels. The level spacing in a dot increases as the dot becomes smaller, but because our nanowires have a relatively large diameter of 100 nm, we keep the gate's width and separation to roughly that length scale. Figure 3.15 represents the SEM images of the local back gates as well as a contacted Te nanowire on the gates.

3.11 Device Fabrication

Fabrication starts with the electron beam lithography (EBL) and the metal coating of the local back gates with 2nm of chrome used as the adhesive layer and 30nm of gold followed by

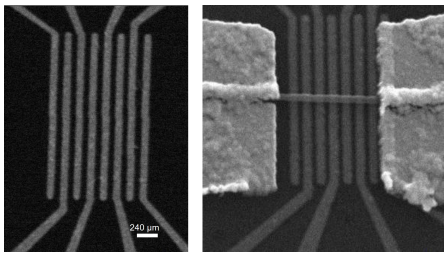

Figure 3.15: SEM image of the local bach gates and a contacted Te device.

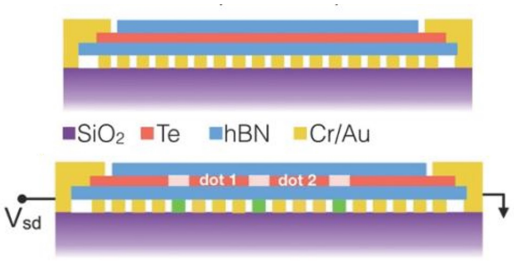

Figure 3.16: The side-view of the device design

the alignment and transferring hBN as the gate's dielectric material and Te nanowire using a dry transfer technique. A schematic of the device side-view is shown in figure 3.16.

The Te nanowire should be etched to remove its native oxide prior to the metal deposition for the source-drain contacts. Hydrochloric acid of 25% is used for two minutes followed by rinsing in DI water and IPA. To make the global top gate the Te nanowire needs to be isolated with another hBN flake. Finally, a thermal processing step in a vacuum at a temperature of 100°C for two hours is performed to achieve adequate contact transparency for low-temperature and low-frequency transport measurements.The thickness of the two hBN flakes is measured by atomic force microscopy (AFM), and the electrodes are wired before loading the device into the cryogenic system. The full fabrication process in detail is represented in figure 3.17.

The isolation of the local back gates is challenging. Using hBN as an insulator for the local back gates proved problematic because it is not stable on the gates; the challenge is referred to as mesa in the community; thus, the bottom hBN flake is clamped. Besides, the Te nanowire slides away when it's transferred on hBN, so EBL patterned a pair of chromium

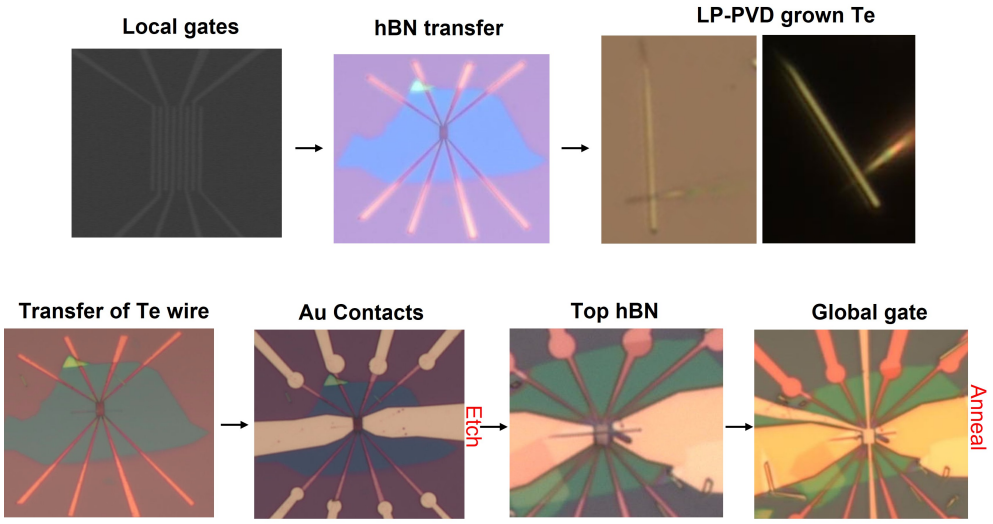

Figure 3.17: The full fabrication process in detail.

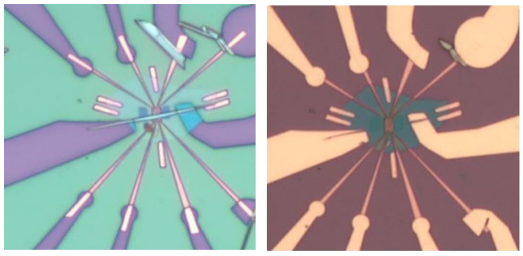

Figure 3.18: Clamped hBN and padded Te nanowire.

landing pads to fix the nanowire position. Chromium acts as an adhesive tape to the Te nanowire. We also tried different transfer techniques, including using a microneedle to pick up and transfer Te nanowire. Further, we used other materials as the gate dielectric like cadmium chalcogenide phosphate ($CdPS_3$) and zinc chalcogenide phosphate ($ZnPS_3$) and ALD aluminum oxide (Al_2O_3).

Given the difficulties associated with multiple transfers and lithography steps, the device configuration underwent a few iterations. For example, we investigated whether a more straightforward process with no additional gate dielectric could be more successful. Figure 3.19 represents a side gates strategy for a Te device in which six side gates are defined following contact deposition.

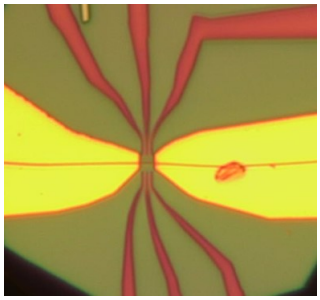

Figure 3.19: The side-gates Te nanowire device.

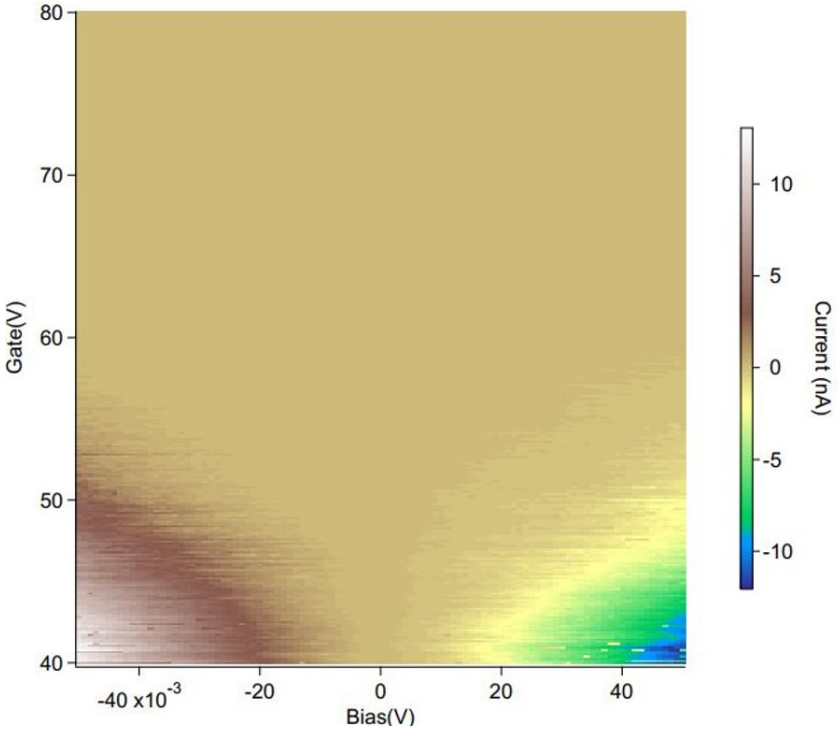

Figure 3.20: The side-gates Te nanowire device.

The current through this device was measured as a function of the source-drain bias and the gate voltage applied to all gates simultaneously. This particular device has a relatively low mobility, and there is no evidence of Coulomb blockade and just diffusive transport. The gates are effective but maybe too far from the nanowire to form a well-controlled dot, even if the mobility was higher.

The last but not the least challenge is the electrostatic discharge (ESD) as a potential threat to 1D Te nanowires, even more than other 1D devices, most likely because of the very low melting point of Te.

3.12 Conclusion

Chiral crystals of elemental Te are Weyl semiconductors with the intriguing property of combining Weyl physics with a small semiconducting band gap, which enables the creation of gate-tunable devices to probe and utilize the topological properties of Te. The formation of gate-defined quantum dots in Te would allow Coulomb blockade spectroscopy that provides information about the Weyl states with very high energy resolution, the strength of exchange interaction, spin-orbit coupling, and g-factors associated with discrete quantum states in Te nanostructures. Using low-pressure physical vapor deposition, Te nanowires are grown and transferred to the pre-patterned local gates. While atomically flat hexagonal boron nitride (hBN) gate dielectrics have been widely used for high quality layered material devices, the relatively weak adhesion to Te nanowires makes hBN-insulated Te device assembly challenging. Therefore, the configuration of the device underwent a few iterations. Different gate electrode designs and insulating strategies compare different methods involving more traditional dielectrics and a hybrid approach that uses a global Si backgate and hBN-insulated local top gates for these Weyl semiconductor devices. Early measurements of Te devices demonstrate density control in these devices. Future work must be aimed at quantum transport measurements in Te dots, noting that to minimize the influence of interfaces and defects in tellurium heterostructures using hBN as an insulator is preferred.

References

[1] Nan Zhang, Gan Zhao, Lin Li, Pengdong Wang, Lin Xie, Bin Cheng, Hui Li, Zhiyong Lin, Chuanying Xi, Jiezun Ke, et al. Magnetotransport signatures of weyl physics and discrete scale invariance in the elemental semiconductor tellurium. *Proceedings of the National Academy of Sciences*, 117(21):11337–11343, 2020.

[2] AJ Bradley. L. the crystal structures of the rhombohedral forms of selenium and tellurium. *The London, Edinburgh, and Dublin Philosophical Magazine and Journal of Science*, 48(285):477–496, 1924.

[3] Gowoon Cheon, Karel-Alexander N Duerloo, Austin D Sendek, Chase Porter, Yuan Chen, and Evan J Reed. Data mining for new two-and one-dimensional weakly bonded solids and lattice-commensurate heterostructures. *Nano letters*, 17(3):1915–1923, 2017.

[4] Yuchen Du, Gang Qiu, Yixiu Wang, Mengwei Si, Xianfan Xu, Wenzhuo Wu, and Peide D Ye. One-dimensional van der waals material tellurium: Raman spectroscopy under strain and magneto-transport. *Nano letters*, 17(6):3965–3973, 2017.

[5] Jingkai Qin, Gang Qiu, Jie Jian, Hong Zhou, Lingming Yang, Adam Charnas, Dmitry Y Zemlyanov, Cheng-Yan Xu, Xianfan Xu, Wenzhuo Wu, et al. Controlled growth of a large-size 2d selenium nanosheet and its electronic and optoelectronic applications. *ACS nano*, 11(10):10222–10229, 2017.

[6] Shengjie Gao, Yixiu Wang, Ruoxing Wang, and Wenzhuo Wu. Piezotronic effect in 1d van der waals solid of elemental tellurium nanobelt for smart adaptive electronics. *Semiconductor Science and Technology*, 32(10):104004, 2017.

[7] Lei Ren, Hongzhou Zhang, Pingheng Tan, Yaofeng Chen, Zhensheng Zhang, Yongqin Chang, Jun Xu, Fuhua Yang, and Dapeng Yu. Hexagonal selenium nanowires synthesized via vapor-phase growth. *The Journal of Physical Chemistry B*, 108(15):4627–4630, 2004.

[8] Sheng-Yi Zhang, Yi Liu, Xiang Ma, and Hong-Yuan Chen. Rapid, large-scale synthesis and electrochemical behavior of faceted single-crystalline selenium nanotubes. *The Journal of Physical Chemistry B*, 110(18):9041–9047, 2006.

[9] Bin Zhang, Wei Dai, Xingchen Ye, Fan Zuo, and Yi Xie. Photothermally assisted solution-phase synthesis of microscale tubes, rods, shuttles, and an urchin-like assembly of single-crystalline trigonal selenium. *Angewandte Chemie*, 118(16):2633–2636, 2006.

[10] Yuan Yang, Kai Wang, Hai-Wei Liang, Guo-Qiang Liu, Mei Feng, Liang Xu, Jian-Wei Liu, Jin-Long Wang, and Shu-Hong Yu. A new generation of alloyed/multimetal chalcogenide nanowires by chemical transformation. *Science advances*, 1(10):e1500714, 2015.

[11] Fengxia Liang and Haisheng Qian. Synthesis of tellurium nanowires and their transport property. *Materials Chemistry and Physics*, 113(2-3):523–526, 2009.

[12] Wen-Jie Lan, Shu-Hong Yu, Hai-Sheng Qian, and Yong Wan. Dispersibility, stabilization, and chemical stability of ultrathin tellurium nanowires in acetone: morphology change, crystallization, and transformation into teo2 in different solvents. *Langmuir*, 23(6):3409–3417, 2007.

[13] Byron Gates, Brian Mayers, Bryan Cattle, and Younan Xia. Synthesis and characterization of uniform nanowires of trigonal selenium. *Advanced Functional Materials*, 12(3):219–227, 2002.

[14] Qingyi Lu, Feng Gao, and Sridhar Komarneni. Cellulose-directed growth of selenium nanobelts in solution. *Chemistry of materials*, 18(1):159–163, 2006.

[15] Zhili Zhu, Xiaolin Cai, Seho Yi, Jinglei Chen, Yawei Dai, Chunyao Niu, Zhengxiao Guo, Maohai Xie, Feng Liu, Jun-Hyung Cho, et al. Multivalency-driven formation of te-based monolayer materials: a combined first-principles and experimental study. *Physical review letters*, 119(10):106101, 2017.

[16] Xiaochun Huang, Jiaqi Guan, Zijian Lin, Bing Liu, Shuya Xing, Weihua Wang, and Jiandong Guo. Epitaxial growth and band structure of te film on graphene. *Nano letters*, 17(8):4619–4623, 2017.

[17] Yixiu Wang, Gang Qiu, Ruoxing Wang, Shouyuan Huang, Qingxiao Wang, Yuanyue Liu, Yuchen Du, William A Goddard, Moon J Kim, Xianfan Xu, et al. Field-effect transistors made from solution-grown two-dimensional tellurene. *Nature Electronics*, 1(4):228–236, 2018.

[18] Ujjal K Gautam and CNR Rao. Controlled synthesis of crystalline tellurium nanorods, nanowires, nanobelts and related structures by a self-seeding solution process. *Journal of Materials Chemistry*, 14(16):2530–2535, 2004.

[19] Hugh OH Churchill, Gregory J Salamo, Shui-Qing Yu, Takayuki Hironaka, Xian Hu, Jeb Stacy, and Ishiang Shih. Toward single atom chains with exfoliated tellurium. *Nanoscale research letters*, 12(1):1–6, 2017.

[20] Hua Peng, Nicholas Kioussis, and G Jeffrey Snyder. Elemental tellurium as a chiral p-type thermoelectric material. *Physical Review B*, 89(19):195206, 2014.

[21] Rabindra Basnet, M Hasan Doha, Takayuki Hironaka, Krishna Pandey, Shiva Davari, Katie M Welch, Hugh OH Churchill, and Jin Hu. Growth and strain engineering of trigonal te for topological quantum phases in non-symmorphic chiral crystals. *Crystals*, 9(10):486, 2019.

[22] Masato Sakano, Motoaki Hirayama, Takanari Takahashi, Shuntaro Akebi, Mitsuhiro Nakayama, Kenta Kuroda, Kazuaki Taguchi, Tomoki Yoshikawa, Koji Miyamoto, Taichi Okuda, et al. Radial spin texture in elemental tellurium with chiral crystal structure. *Physical review letters*, 124(13):136404, 2020.

[23] VA Shalygin, AN Sofronov, LE Vorob'ev, and II Farbshtein. Current-induced spin polarization of holes in tellurium. *Physics of the Solid State*, 54(12):2362–2373, 2012.

[24] VA Shalygin, MD Moldavskaya, SN Danilov, II Farbshtein, and LE Golub. Circular photon drag effect in bulk tellurium. *Physical Review B*, 93(4):045207, 2016.

[25] Gang Qiu, Shouyuan Huang, Mauricio Segovia, Prabhu K Venuthurumilli, Yixiu Wang, Wenzhuo Wu, Xianfan Xu, and Peide D Ye. Thermoelectric performance of 2d tellurium with accumulation contacts. *Nano letters*, 19(3):1955–1962, 2019.

[26] Charles Kittel. Introduction to solid state physics, (wiley, new york, 1996). *K. Balasubramanian, Chem. Rev*, 35:90–93, 1990.

[27] Adrian Bejan and Allan D Kraus. Heat transfer handbook, 2003 john wiley & sons. *Hoboken New Jersey*, 2003.

[28] CM Bhandari and David M Rowe. Crc handbook of thermoelectrics. *CRC Press, Boca Raton, FL*, page 49, 1995.

[29] Francis J DiSalvo. Thermoelectric cooling and power generation. *Science*, 285(5428):703–706, 1999.

[30] Mildred S Dresselhaus, Gang Chen, Ming Y Tang, RG Yang, Hohyun Lee, DZ Wang, ZF Ren, J-P Fleurial, and Pawan Gogna. New directions for low-dimensional thermoelectric materials. *Advanced materials*, 19(8):1043–1053, 2007.

[31] Junwen Zeng, Xin He, Shi-Jun Liang, Erfu Liu, Yuanhui Sun, Chen Pan, Yu Wang, Tianjun Cao, Xiaowei Liu, Chenyu Wang, et al. Experimental identification of critical condition for drastically enhancing thermoelectric power factor of two-dimensional layered materials. *Nano Letters*, 18(12):7538–7545, 2018.

[32] Siqi Lin, Wen Li, Zhiwei Chen, Jiawen Shen, Binghui Ge, and Yanzhong Pei. Tellurium as a high-performance elemental thermoelectric. *Nature communications*, 7(1):1–6, 2016.

[33] K Nakayama, M Kuno, K Yamauchi, S Souma, K Sugawara, T Oguchi, T Sato, and T Takahashi. Band splitting and weyl nodes in trigonal tellurium studied by angle-resolved photoemission spectroscopy and density functional theory. *Physical Review B*, 95(12):125204, 2017.

[34] Eougenious L Ivchenko and Grigory Pikus. *Superlattices and other heterostructures: symmetry and optical phenomena*, volume 110. Springer Science & Business Media, 2012.

[35] Viktor Iosifovich Belinicher and Boris Itskhakovich Sturman. The photogalvanic effect in media lacking a center of symmetry. *Soviet Physics Uspekhi*, 23(3):199, 1980.

[36] VM Asnin, AA Bakun, AM Danishevskii, EL Ivchenko, GE Pikus, and AA Rogachev. Observation of a photo-emf that depends on the sign of the circular polarization of the light. *ZhETF Pisma Redaktsiiu*, 28:80–84, 1978.

[37] VM Asnin, AA Bakun, AM Danishevskii, EL Ivchenko, GE Pikus, and AA Rogachev. "circular" photogalvanic effect in optically active crystals. *Solid State Communications*, 30(9):565–570, 1979.

[38] Boris I Sturman and Vladimir M Fridkin. *The photovoltaic and photorefractive effects in noncentrosymmetric materials*. Routledge, 2021.

[39] E Deyo, LE Golub, EL Ivchenko, and B Spivak. Semiclassical theory of the photogalvanic effect in non-centrosymmetric systems. *arXiv preprint arXiv:0904.1917*, 2009.

[40] Joel E Moore and J Orenstein. Confinement-induced berry phase and helicity-dependent photocurrents. *Physical review letters*, 105(2):026805, 2010.

[41] Inti Sodemann and Liang Fu. Quantum nonlinear hall effect induced by berry curvature dipole in time-reversal invariant materials. *Physical review letters*, 115(21):216806, 2015.

[42] Motoaki Hirayama, Ryo Okugawa, Shoji Ishibashi, Shuichi Murakami, and Takashi Miyake. Weyl node and spin texture in trigonal tellurium and selenium. *Physical review letters*, 114(20):206401, 2015.

[43] Stepan S Tsirkin, Pablo Aguado Puente, and Ivo Souza. Gyrotropic effects in trigonal tellurium studied from first principles. *Physical Review B*, 97(3):035158, 2018.

[44] Fernando de Juan, Adolfo G Grushin, Takahiro Morimoto, and Joel E Moore. Quantized circular photogalvanic effect in weyl semimetals. *Nature communications*, 8(1):1–7, 2017.

[45] C Guthmann and JM Thuillier. Fermi surface of tellurium. *physica status solidi (b)*, 38(2):635–642, 1970.

[46] C Guthmann and JM Thuillier. Shubnikov de haas effect in tellurium. *Solid State Communications*, 6(11):835–838, 1968.

[47] MS Bresler, II Farbstein, DV Mashovets, Yu V Kosichkin, and VG Veselago. Experimental determination of the shape of the hole fermi surface in tellurium. *Physics Letters A*, 29(1):23–24, 1969.

[48] Kenneth J Button, G Landwehr, CC Bradley, P Grosse, and Benjamin Lax. Quantum effects in cyclotron resonance in p-type tellurium. *Physical Review Letters*, 23(1):14, 1969.

[49] VB Anzin, Yu V Kosichkin, VG Veselago, MS Bresler, II Farbstein, ES Itskevich, and VA Sukhoparov. Inversion asymmetry splitting of landau levels in tellurium. *Solid State Communications*, 8(21):1773–1777, 1970.

[50] K Von Klitzing and G Landwehr. Surface quantum states in tellurium. *Solid State Communications*, 9(24):2201–2205, 1971.

[51] Gang Qiu, Yixiu Wang, Yifan Nie, Yongping Zheng, Kyeongjae Cho, Wenzhuo Wu, and Peide D Ye. Quantum transport and band structure evolution under high magnetic field in few-layer tellurene. *Nano letters*, 18(9):5760–5767, 2018.

[52] Gang Qiu, Mengwei Si, Yixiu Wang, Xiao Lyu, Wenzhuo Wu, and D Ye Peide. High-performance few-layer tellurium cmos devices enabled by atomic layer deposited dielectric doping technique. In *2018 76th Device Research Conference (DRC)*, pages 1–2. IEEE, 2018.

[53] Samuel Berweger, Gang Qiu, Yixiu Wang, Benjamin Pollard, Kristen L Genter, Robert Tyrrell-Ead, T Mitch Wallis, Wenzhuo Wu, Peide D Ye, and Pavel Kabos. Imaging carrier inhomogeneities in ambipolar tellurene field effect transistors. *Nano letters*, 19(2):1289–1294, 2019.

[54] Gang Qiu, Adam Charnas, Chang Niu, Yixiu Wang, Wenzhuo Wu, and Peide D Ye. The resurrection of tellurium as an elemental two-dimensional semiconductor. *npj 2D Materials and Applications*, 6(1):1–10, 2022.

[55] Lijuan Wang, Armando Rastelli, Suwit Kiravittaya, Mohamed Benyoucef, and Oliver G Schmidt. Self-assembled quantum dot molecules. *Advanced Materials*, 21(25-26):2601–2618, 2009.

[56] Chang Niu, Gang Qiu, Yixiu Wang, Zhuocheng Zhang, Mengwei Si, Wenzhuo Wu, and D Ye Peide. Gate-tunable strong spin-orbit interaction in two-dimensional tellurium probed by weak antilocalization. *Physical Review B*, 101(20):205414, 2020.

[57] Gang Qiu, Chang Niu, Yixiu Wang, Mengwei Si, Zhuocheng Zhang, Wenzhuo Wu, and Peide D Ye. Quantum hall effect of weyl fermions in n-type semiconducting tellurene. *Nature Nanotechnology*, 15(7):585–591, 2020.

[58] Guoqing Chang, Benjamin J Wieder, Frank Schindler, Daniel S Sanchez, Ilya Belopolski, Shin-Ming Huang, Bahadur Singh, Di Wu, Tay-Rong Chang, Titus Neupert, et al. Topological quantum properties of chiral crystals. *Nature materials*, 17(11):978–985, 2018.

[59] Brian Mayers and Younan Xia. One-dimensional nanostructures of trigonal tellurium with various morphologies can be synthesized using a solution-phase approach. *Journal of Materials Chemistry*, 12(6):1875–1881, 2002.

[60] Dan Liu and David Tomanek. Microscopic mechanism of the helix-to-layer transformation in elemental selenium. In *APS March Meeting Abstracts*, volume 2018, pages P17–013, 2018.

[61] S Ades and CH Champness. Intermediate infrared optical absorption in intrinsic tellurium. *Journal of Applied Physics*, 49(8):4543–4548, 1978.

[62] Jing-Kai Qin, Pai-Ying Liao, Mengwei Si, Shiyuan Gao, Gang Qiu, Jie Jian, Qingxiao Wang, Si-Qi Zhang, Shouyuan Huang, Adam Charnas, et al. Raman response and transport properties of tellurium atomic chains encapsulated in nanotubes. *Nature electronics*, 3(3):141–147, 2020.

[63] Peng Yang, Jiajia Zha, Guoyun Gao, Long Zheng, Haoxin Huang, Yunpeng Xia, Songcen Xu, Tengfei Xiong, Zhuomin Zhang, Zhengbao Yang, et al. Growth of tellurium nanobelts on h-bn for p-type transistors with ultrahigh hole mobility. *Nano-micro letters*, 14(1):1–12, 2022.

[64] S Davari, J Stacy, AM Mercado, JD Tull, R Basnet, K Pandey, K Watanabe, T Taniguchi, J Hu, and HOH Churchill. Gate-defined accumulation-mode quantum dots in monolayer and bilayer w se 2. *Physical Review Applied*, 13(5):054058, 2020.

Chapter 4

Conclusion

4.1 Conclusion

This dissertation focuses on the investigation of gate-defined quantum dots in two-dimensional transition metal dichalcogenide tungsten diselenide (WSe_2) as a means to unravel mesoscopic physical phenomena such as valley-contrasting physics in WSe_2 flakes and its potential application for quantum information, as well as realizing gate-controlled quantum dots based on elemental tellurium nanostructures which may unlock the topological nature of the carriers such as Weyl states in tellurium nanowires.

Chapter 1 titled "Introduction" discusses the remarkable properties of two-dimensional transition metal dichalcogenides (TMDs) such as the presence of a band gap that undergoes a transition from indirect in multilayers to direct band gap in monolayer TMDs which has opened up possibilities in transport and optoelectronic measurements. Additional modalities are discussed including strong spin-orbit coupling which is necessary for spintronics and the valley-dependent optical selection rules. These effects provide a means to access the valley degree of freedom via optical pumping of circularly polarized light in TMDs. Different confinement methods in TMDs including self-assembled quantum dots, quantum emitters by defects, strain, and by moiré patterns are addressed. In addition to the valley Hall effect and Shubnikov-de Haas oscillations which are alternative ways for electrical investigation of valley degree of freedom, quantum dots by patterned electrodes provide information about valley states with high energy resolution. Coulomb blockade spectroscopy of quantum dots is discussed as a well-stablished technique which determines the basic properties of quantum materials by directly measuring the energies of individual quantum levels. This chapter concludes with a discussion of some of the main challenges associated with the gate-defined quantum dots based on two-dimensional TMDs.

Chapter 2 titled "Gate-Defined Accumulation-Mode Quantum Dots in Monolayer and Bilayer Tungsten Diselenide" focuses on the use of quantum dots in gated heterostructures to evaluate valley-spin states in monolayer and bilayer WSe_2 for application as qubits. Conductance resonances consistent with Coulomb blockade were seen in both monolayer and bilayer quantum dot devices. In addition, transport through single levels is confirmed with temperature dependence of Coulomb blockade peak heights. Notably, the number of the holes confined in the single quantum dot is approaching to few-carrier regime which allows observation of excited states in the Coulomb diamond measurements. Further, magnetic field dependence of the excited states in the bilayer devices provides a lower bound for g factors.

Chapter 3 titled "Gate-controlled Tellurium Nanowires Quantum Dots" discusses the crystal structure and the basic properties of elemental tellurium. Some of the most important transport-related phenomena in p-type tellurium are reviewed, including thermoelectric current mapping, ARPES spectra and circular photogalvanic effect, followed by a quick discussion of Shubnikov-de Haas oscillations and quantum Hall effect in both p- and n-type tellurium samples. Additionally, weak antilocalization due to the strong spin-orbit coupling in Te is discussed. The unique features related to the Weyl state and its associated chiral anomaly in tellurium which are negative longitudinal magnetoresistance, angle-narrowing in anisotropic magnetoresisrance and the planar Hall effect are briefly explained. Finally, our work on this topic which is the fabrication and characterization of gate-defined tellurium quantum dot including LP-PDV growth of tellurium nanostructures, the device design strategy, the sorted fabrication steps, and the measurement are explained. Some of the exclusive challenges for the Te nanowire device fabrication are mentioned. Initial measurements in these devices are shown but further work must be pursued.

4.2 Outlook

Beside quantum computation applications, 2D TMD quantum dots provide a powerful platform for the mesoscopic physics studies at the single-particle level, which has been the

main focus of this work. Likewise, realizing quantum dots based on topological materials, in particular elemental tellurium nanostructures, may also be helpful to unlock the exotic properties of the host material such as the Weyl states. However, there are some obstacles yet to be overcome. To name a few, the first one is the crystal quality as well as the interfaces which should be improved to reduce the influence of defects and disorders. Another significant hurdle to conquer is the electrical contact to the semiconducting material which is required to be opaque enough to form a dot, particularly at low temperatures. Last but not least is the challenge associated with the gate electrode geometry to be reconsidered. Particularly in the systems with large effective mass like elemental tellurium and WSe_2, small confinement is required to resolve quantized energy levels. Besides, due to the large spin-orbit coupling in these systems it seems that electrical manipulation of the spin and valley degrees of freedom, rather than magnetic, should be pursued.

Vitae

Education

2022 Ph.D. in Physics, University of Arkansas, Fayetteville.

2009 M.Sc. in Photonics, Shahid Beheshti University, Iran.

2005 B.Sc. in Physics, University of Isfahan, Iran, Iran.

Publications

Selected Peer-reviewed Publications

2. **S. Davari**, J. Stacy, A. M. Mercado, J. D. Hull, R. Basnet, K. Pandey, K. Watanabe, T. Taniguchi, M., J. Hu, and H. O. H. Churchill, "Gate-Defined Accumulation-Mode Quantum Dots in Monolayer and Bilayer WS_2", *Physical Review Applied* **13**, 054058 (2020)

1. R. Basnet, MH. Doha, T. Hironaka, K. Pandey, **S. Davari**, K. Welch, H. O. H. Churchill, J. Hu, "Growth and strain engineering of trigonal Te for topological quantum phases in non-symmorphic chiral crystals", *Crystals* **9**, 10 , 486 (20197),

Selected Conference Presentations

5. **S. Davari**, K. Watanabe, T. Taniguchi, and H. O. H. Churchill, "Gate-Defined Tellurium Nanowire Quantum Dots", *MRS Spring Meeting Exhibit.* (2022)

4. **S. Davari**, J. Stacy, A.M. Mercado, J. Tull, R. Basnet, K. Pandey, R. Un Nabi, K. Watanabe, T. Taniguchi, J. Hu, and H. O. H. Churchill, "Gate-defined quantum dots in monolayer and bilayer WSe2: Part II, Measurement", *APS March Meeting.* (2021)

3. **S. Davari**, K. Watanabe, T. Taniguchi, and H. O. H. Churchill, "Gate-Defined Tellurium Nanowire Quantum Dots", *APS March Meeting.* (2022)

2. J. Stacy, **S. Davari**, A.M. Mercado, J. Tull, R. Basnet, K. Pandey, R. Un Nabi, K. Watanabe, T. Taniguchi, J. Hu, and H. O. H. Churchill, "Gate-defined quantum dots in monolayer and bilayer WSe2: Part I, Fabrication", *APS March Meeting*. (2021)

1. K. Welch, **S. Davari**, J. Stacy, R. Basnet, M. Benamara, J. Hu, and H. O. H. Churchill, "Fabrication of Gate Defined Quantum Dots in Tellurium Nanowires", *Bulletin of American Physical Society* **65**, (2020)